TWO-PATCH MODEL FOR TRANSPORT PROPERTIES OF OPTIMALLY AND OVERDOPED CUPRATES

BY MICHAEL SINDEL

A thesis submitted to the
Graduate School—New Brunswick
Rutgers, The State University of New Jersey
in partial fulfillment of the requirements
for the degree of
Master of Science
Graduate Program in Physics and Astronomy
Written under the direction of
Professor Gabriel B. Kotliar
and approved by

New Brunswick, New Jersey
October, 2001

ABSTRACT OF THE THESIS

Two-patch model for transport properties of optimally

and overdoped cuprates

by Michael Sindel

Thesis Director: Professor Gabriel B. Kotliar

We compute transport properties of the normal state of BSCCO cuprates using a model

that divides the first Brillouin-zone into hot and cold regions. Within this framework

a collision operator is constructed. A phenomenological temperature dependence is as-

signed to each possible scattering mechanism of the model. This allows us to study the

temperature dependence of transport quantities.

The starting point of our analysis is a Boltzmann equation which is valid in the nor-

mal state of cuprates. DC-conductivity, Hall-angle, magnetoresistance, thermoelectric

power and thermal Hall-conductivity are calculated within our approach and compared

with experimental data. The model is able to give a reasonable fit of experimental data

of the mentioned quantities.

ii

Acknowledgements

I owe my adviser, Gabriel Kotliar big gratitude. In spite of his enormous amount of students, PostDocs and scientists working with him he always found time to discuss with me and knew how to go on. Thanks!

My friend Andrea Perali who was working with me on this project was of biggest importance for me in this project. His quick mind and his way of discussing physics (and other stuff) with me was very pleasant. I really enjoyed the work a lot with him. It is a request to me to mention our common discussions in Gabi's office. The way Gabi and Andrea doing physics was one of the greatest experiences during my stay at Rutgers. For sure I'm going to miss this discussions.

Dedication

This work dedicated to my brother MARKUS who underwent a complicated heart operation during my stay here. I'm happy that it worked out so well.

Table of Contents

Αl	bstra	${f ct}$	ii			
A	cknov	wledgements	iii			
D	edica	tion	iv			
1.	Intr	$\mathbf{oduction} \dots $	1			
2.	Reasoning for the use of a Boltzmann-equation to describe transport					
pr	oper	ties of cuprates	3			
3.	The	description of the transport process using the BE	7			
	3.1.	The BE of free (noninteracting) particles	7			
	3.2.	Considering interactions between quasiparticles - Landau's Fermi-liquid				
		theory (FLT)	10			
	3.3.	The transport equation of interacting particles in an electromagnetic field	13			
4.	Exp	perimental results for $BSCCO$				
Va	ariati	on of $ au$ over the FS	18			
	4.1.	DC-conductivity σ^{xx}	19			
		4.1.1. Experimental results: Resistivity ρ^{xx} in $BSCCO$	20			
	4.2.	Hall-conductivity σ^{xy}	22			
		4.2.1. Experimental results: Hall-angle $tan(\theta_H)$ in cuprates	23			
	4.3.	Thermoelectric power (TEP) of BSCCO	24			
	4.4.	Magnetoresistance MR in $BSCCO$	25			
	4.5.	Thermal Hall-conductivity κ^{xy}	26			
5	Twe	natch model for the collision operator	28			

	5.1.	How t	o describe the idea of hot and cold regions?	30
		5.1.1.	Description with step-function	30
		5.1.2.	Description with a smooth function	36
	5.2.	Consti	ructing the Fermi-surface	40
		5.2.1.	Velocities in the cold and in the hot regions	41
		5.2.2.	Density of energy states in cold and hot region	42
		5.2.3.	Van-Hove singularities (VHS)	45
	5.3.	The di	ifferent types of transport	46
	5.4.	Electri	ical Conductivity $\sigma^{\mu\nu}$	47
		5.4.1.	DC-conductivity σ^{xx}	49
		5.4.2.	Hall-conductivity σ^{xy}	52
			Hall-angle $\tan \theta_H(T)$	55
		5.4.3.	Magnetoresistance MR	55
			Kohler-Plot	60
	5.5.	Therm	nal transport - conductivity tensor $\kappa^{\mu\nu}$	60
		5.5.1.	Longitudinal thermal conductivity κ^{xx}	63
		5.5.2.	Thermal Hall-conductivity κ^{xy}	64
	5.6.	Therm	noelectric power TEP	66
6.	The	used	Program	70
	6.1.	The Ir	nput	70
		6.1.1.	The FS of $Bi2212$	71
		6.1.2.	The geometry of the model	71
		6.1.3.	External data	72
		6.1.4.	Parameters of the model	73
	6.2.	amming	74	
		6.2.1.	Temperature-Loop	7 4
		6.2.2.	k-Loop	75
		6.2.3.	Converting in suitable quantities	76

6.3.	subroutines	77
	6.3.1. "phipsi"	77
	6.3.2. "dphi"	77
	6.3.3. "sdphi"	77
7. Res	ults and Discussion	78
7.1.	Parameters of the TPM	78
	7.1.1. DC-resistivity ρ^{xx}	79
	7.1.2. Thermoelectric power (TEP)	32
	7.1.3. Hall-angle	83
	7.1.4. Magnetoresistance MR	85
	7.1.5. Thermal Hall-conductivity	88
7.2.	Fitting experimental data	92
	7.2.1. Lorenz-number and Kohler-plot	96
7.3.	Problems of the model	97
7.4.	How to go on?	98
Appen	dix A. Abbreviations)0
Appen	dix B. Constants)1
Appen	dix C. Properties of $\frac{\partial \Phi_{\mathbf{k}}}{\partial k_x}$ and $\frac{\partial \Psi_{\mathbf{k}}}{\partial k_x}$)2
Appen	dix D. Derivatives of the smooth function $\Phi_{\mathbf{k}}$)5
Appen	dix E. The tetrahedron method)9
E.1.	Numerical integration in 2D	10
	E.1.1. Possible situations for the triangle	11
	E.1.2. An easy root-finder and an easy integration	12
E.2.	The algorithm	14
E.3.	The mathematical background - formulas for the program	14
E.4	Estimating the contributing region	15

E.4.1.	Triangles outside FS1 - SELECT1	115
E.4.2.	Triangles inside FS2	120
E.4.3.	Integration over a triangle	121
References .		127

Chapter 1

Introduction

The explanation of the physics of high temperature superconductors (HTSC), discovered by Bednorz and Mueller in 1986, is one of the biggest challenge of the current physics. It seems that the mechanism that leads to superconductivity takes place in CuO_2 planes.¹ A good understanding of the 2D-system of the CuO_2 -planes seems to be enough to discover the mechanism that finally leads to superconductivity. But still a microscopic theory of this materials is missing.

We are concentrating on transport properties, i.e. on the temperature dependence of different transport quantities (in the normal state), of cuprates in this work. It seems fundamental to have a good knowledge of the normal state of the HTSC-materials to be able to explain the superconducting state of this materials.

A phenomenological two-patch model is introduced that is able to describe experimental results of the temperature dependence of the DC-resistivity, the Hall-angle, the magnetoresistance, the thermal Hall-conductivity and the thermoelectric power. The influence of the different regions of the model on the transport properties is studied.

We start our analysis with a reasoning that the Boltzmann-equation (BE) can be used to describe the transport process in the normal state of cuprates (chapter 2). Once we established the validity of the BE we introduce it. Chapter 3 introduces the BE for free and for interacting particles (Fermi liquid theory). Finally we derive a BE which is valid for an electromagnetic field.

Our interest in a comparison with experimental values forces us to compare our results with experimental ones. Experimental results are summarized in chapter 4.

_

¹As this HTSC have Cu^{++} atoms in common this materials are called cuprates.

The two-patch model (TPM) is introduced in chapter 5. A reasonable construction of the collision operator which governs the BE is the main idea of the TPM. Within the framework of this model the transport properties of our interest are calculated. We study the temperature dependence of the mentioned transport properties by a numerical program that is described in chapter 6. Using this program we discuss the influence of the different parameters of our model on the quantities of our interest. Furthermore a give a set of parameters that is able to fit all(!) considered quantities in a reasonable way. The effect of the different regions of our model on the different transport quantities is also studied there.

In the appendix we show analytical calculations that were used in the program mentioned in chapter 6. Furthermore we introduce the tetrahedron-method which is able to calculate the transport quantities in the low-temperature limit.

The most fascinating thing about the described model is that it is able to describe different transport experiments of cuprates within a quite easy, vivid and reasonable way. It doesn't use fancy constructions to get a good agreement with experiment. So the model is somehow ideal to study the transport behavior in the normal state of cuprates on a macroscopic level. Some insight what we expect to happen on a microscopic level can be obtained from the TPM.

Chapter 2

Reasoning for the use of a Boltzmann-equation to describe transport properties of cuprates

It is not obvious that we can use a Boltzmann-equation (BE) to describe the transport properties of cuprates in the normal state (NS). Pines & Nozieres [35] argue that it is necessary to have a Fermi-Surface (FS) inside a compound to describe transport within the framework of this equation. The reason is that a BE-treatment requires quasiparticles with a finite lifetime (bigger than the average scattering time) in (or around) the neighborhood of the FS. A description of the transport-process within the framework of the BE is applicable when this conditions are accomplished.

The NS of cuprates is the space in the phase diagram, where the compound is neither superconducting nor in the pseudogap-region. Figure 2.1 [37] shows a (possible) phase-diagram of cuprates. In the diagram temperature is plotted vs. hole-doping. Varma [37] divides the NS into a marginal Fermi-liquid (MFL) and a Fermi-liquid (FL) state. The lifetime τ_{MFL} in the MFL-state is $\propto T^{-1}$, where $\tau_{FL} \propto T^{-2}$. The reason for the phenomenological introduction of the MFL- and the FL-state is due to discrepancies with transport data.

In this report our main interest is the NS of $Bi_2Sr_2CaCu_2O_8$ (Bi2212) compounds. Thus our first question is whether this material has a FS or not. The reason why we choose Bi2212 for our studies is that this materials have no chains so we have an almost 2D-system. When we look at other cuprates, like YBCO, we also have to consider the hopping between the CuO_2 -planes. The geometry of the CuO_2 -planes is shown in figure 2.2.

Quijada [15] measured a slightly anisotropy in the in-plane-resistivity of cuprates. But

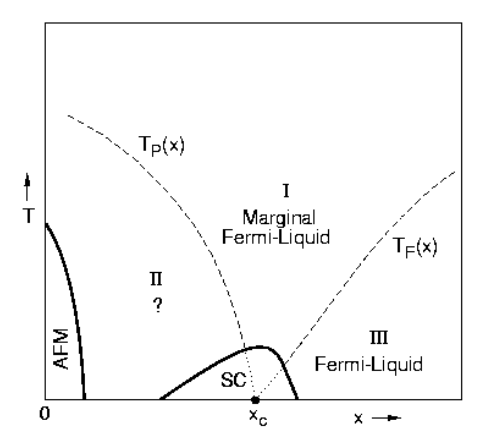


Figure 2.1: [37] The phase diagram, T vs. hole-doping, of cuprates can be splitted into several pieces. The NS is divided into marginal Fermi-liquid and a Fermi-liquid.

this effect is very small so we are dealing with the CuO_2 -planes assuming that they have fourfold symmetry as shown in figure 2.2.

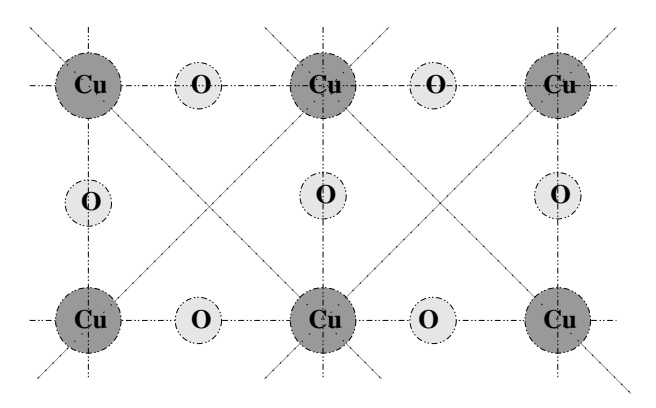


Figure 2.2: The figure shows the geometry of the CuO_2 -planes that govern the transport properties of high T_c -superconductors. Note that the planes have fourfold symmetry.

Angle resolved photo-emission spectroscopy (ARPES) [9] provides a possibility to figure out whether the compound of our interest has a FS. ARPES-experiments can even tell us something about the lifetime of the quasiparticles around the FS. It is possible to measure the spectral-function $A(\omega, \mathbf{k})$ of a material by this technique. The

spectral-function is obtained from the imaginary part of the Greens-function $G(\omega, \mathbf{k}) = \frac{1}{\omega - \epsilon_{\mathbf{k}} - \Sigma(\omega, \mathbf{k})}$, where $\Sigma(\omega, \mathbf{k})$ is the self energy of the system.¹

$$A(\omega, \mathbf{k}) = -\frac{1}{\pi} \Im[G(\omega, \mathbf{k})]$$
 (2.1)

Thus the width of the peak of the spectral-function is connected to the lifetime of quasiparticles (that means that the imaginary part of the self-energy governs the lifetime of quasiparticle).

ARPES-experiments scan the reciprocal space and measure the energy distribution curves (EDC) for different polarization of the incoming wavevector \mathbf{k} . Figure 2.3 shows the different directions of the scan of the reciprocal space of the CuO_2 -planes of Bi2212. Our interest in the NS transport-properties of Bi2212 forces us to make this experiment above the critical temperature ($T_c = 87K$) for optimally doped materials. The experiments in [9] were done at T = 95K.

The points inside the first BZ, shown in figure 2.3, are named in the following way: $\Gamma = (0,0), \bar{M} = (\pi,0), X = (\pi,-\pi), Y = (\pi,\pi).$

The upper part of figure 2.3 explains the direction of the scan, where the lower part gives the results of the ARPES-experiment, which is equivalent with the spectral-function of the CuO_2 -planes.

Depending on the measured direction the peaks in the spectral-function appear at different momenta. It can also been recognized in figure 2.3 that the width of the peak (in the spectral-function), which describes the lifetime of the quasiparticles, is smaller in (π, π) -direction. The lifetime in this regions is bigger. This observation suggests that we don't have a single lifetime in the CuO_2 -planes. The lifetime τ of a reasonable model should change around the FS.

The experiments [9] allow us to construct a FS with the shape given in figure 2.4. The electronic structure suggested by Ding et al. was recently reexaminated by Chuang [25].

¹To get the imaginary part of the Greens-function we make use of the equation: $\frac{1}{x\pm i\delta} = P(1/x) \mp i\pi\delta(x)$ which is valid in the limit $\delta \to 0$ (P denotes the principal value).

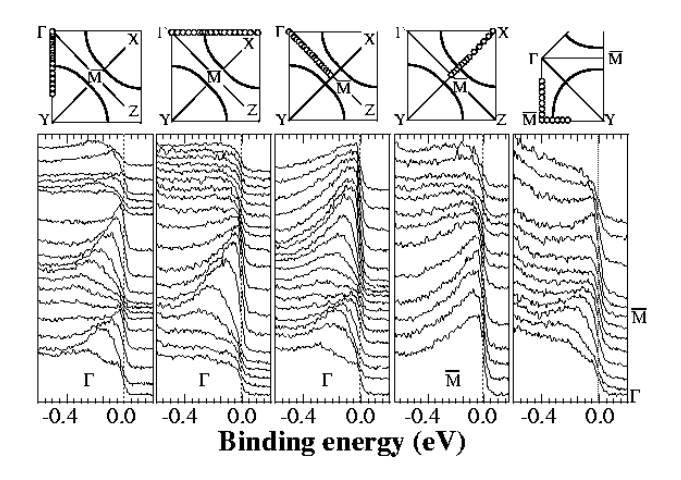


Figure 2.3: The FS is scanned over the **k**-space. Dependent on the polarization of the wavevector we get peaks in the Binding energy that contain information about the lifetime [9].

With reasons given above we can start to describe the transport properties of cuprates

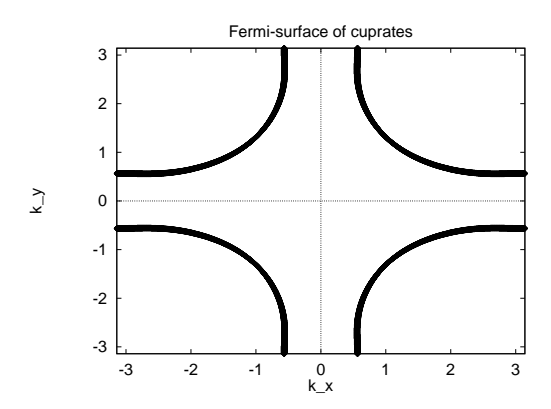


Figure 2.4: The FS of the NS of BSCCO showed above was constructed by a fit that contains hopping up to the fifth nearest neighbor given in [16], obtained from band-structure calculations. Figure 2.3 justifies a FS like it is shown in this figure.

(in the NS) with a BE-treatment that will be explained in the next chapter.

Chapter 3

The description of the transport process using the BE

Transport properties of systems with (quasi)particles (with long lifetime) around the FS can be described with a BE as showed in chapter 2. An external force, given by an electric field \mathbf{E} or a temperature gradient $\nabla_{\mathbf{r}}T$, is able to excite particles inside the Fermi-sea to generate some free, unbounded particles. A weak external field can only excite particles around the FS and make them to free particles due to the Pauli principle.

When we apply a weak force on free particles we can treat the free-particle-regime within the framework of the theory of linear response. This is equivalent with the idea to linearize the BE, which is a partial differential equation.

In section 3.1 we introduce the BE for noninteracting (free) particles. A linearized form of the BE is derived. We have to consider interactions between particles¹ when we deal with excitations of several particles. This proceeding is shown in section 3.2. The last section, section 3.3, of this chapter deals with transport in electromagnetic fields. A linearized transport equation, valid in electromagnetic fields, is derived there.

We follow the derivation of the BE given in [35].

3.1 The BE of free (noninteracting) particles

A kinetic equation describes the space and time dependence of the distribution function $n_{\mathbf{k}}(\mathbf{r},t)$ of a system of (in this case noninteracting) particles. For a system without collisions the kinetic equation has the form of the continuity equation, $\nabla_{\mathbf{r}}\mathbf{j} + \frac{\partial \rho}{\partial t} = 0$ with the current \mathbf{j} and the particle density ρ . The continuity equation conserves the particle number as the flow inwards and the flow outwards of a certain volume element

¹They are called quasiparticles in the case where interaction between them is considered.

is the same.

The question **why** particles are moving is due to forces that are acting on the particles. External fields, **E**, **B** and thermal gradients $\nabla_{\mathbf{r}}T$ are the reasons why free particles start moving or change their direction (neglecting motion due to Brownian motion). These moving particles contribute to transport. Scattering between particles is especially important in the process of transport as this models the obstacles in the transport process. Combining the idea of scattering between particles with the continuity equation, mentioned before, forces us to generalize this equation.

The distribution function $n_{\mathbf{k}}(\mathbf{r},t)$ of particles represents the number of particles at position \mathbf{r} at time t with momentum \mathbf{k} . The current is defined as $\mathbf{j} = \sum_{\mathbf{k}} n_{\mathbf{k}}(\mathbf{r},t) \mathbf{v}_{\mathbf{k}}(\mathbf{r},t)$, so it follows from the continuity equation (neglecting collisions)²

$$\frac{\partial n_{\mathbf{k}}(\mathbf{r},t)}{\partial t} + \left[\mathbf{v}_{\mathbf{k}}(\mathbf{r},t)\nabla_{\mathbf{r}}n_{\mathbf{k}}(\mathbf{r},t)\right] + \left[-\nabla_{\mathbf{r}}\epsilon_{\mathbf{k}}(\mathbf{r},t)\nabla_{\mathbf{k}}n_{\mathbf{k}}(\mathbf{r},t)\right] = 0 \tag{3.1}$$

where the last term on the l.h.s. was obtained using integration by parts and the fact that $n_{\mathbf{k}}(\mathbf{r},t)$ vanishes at the boundaries. Note that we can replace $-\nabla_{\mathbf{r}}\epsilon_{\mathbf{k}}(\mathbf{r},t)$ by the external force $\mathbf{F}(\mathbf{r},t)$.

Equation (3.1) can easily be derived from Liouville's theorem. We only calculate the total differential of $n_{\mathbf{k}}(\mathbf{r},t)$ and obtain the same result, namely $\frac{dn_{\mathbf{k}}(\mathbf{r},t)}{dt} = \frac{\partial n_{\mathbf{k}}(\mathbf{r},t)}{\partial t} + \frac{\partial n_{\mathbf{k}}(\mathbf{r},t)}{\partial \mathbf{k}} \frac{d\mathbf{r}}{dt} + \frac{\partial n_{\mathbf{k}}(\mathbf{r},t)}{\partial \mathbf{k}} \frac{d\mathbf{k}}{dt} = 0$, with $\mathbf{F}(\mathbf{r},t) = \frac{d\mathbf{k}}{dt}$.

The first term on the l.h.s. of equation (3.1) is important in the case of a dynamic distribution, the second term represents diffusion and the third is due to an applied external field. The force due to an applied electromagnetic field is given by $\mathbf{F} = \hbar \frac{d}{dt} \mathbf{k} = e \left(\mathbf{E} + \frac{1}{\hbar c} \mathbf{v}_k \times \mathbf{B} \right)$.

Note that we can express the group velocity of free particles just by $\nabla_{\mathbf{k}} \epsilon_{\mathbf{k}}(\mathbf{r}, t)$. When we have no more free particles we get the group velocity of "quasiparticles" by replacing ϵ with $\tilde{\epsilon}$, which is explained in section 3.2 (also the force has to be replaced by an effective force in the interacting case!). In a non-equilibrium system the gradient of the chemical

²Note that the density at point **r** is given by $\rho(\mathbf{r}) = \sum_{\mathbf{k}} n_{\mathbf{k}}(\mathbf{r}, t)$.

potential acts as an effective force on the system.

So far we neglected collisions between particles, which plays the dissipative (irreversible) role in the BE. In case of collisions between particles we have to add an operator, the collision operator $C_{\mathbf{k}}$, to the right hand side of (3.1). $C_{\mathbf{k}}$ takes the scattering "in" the state \mathbf{k} and "out" of the state \mathbf{k} into consideration. The modeling of the collision-operator is of special importance to describe the transport process well. It is common to use a transition probability from a state \mathbf{k} to a state \mathbf{k}' , given by a matrix $C_{\mathbf{k}\mathbf{k}'}$, to model the collision operator $C_{\mathbf{k}}$.

Physical interesting phenomena happen in the neighborhood of the FS, as only in this region particles can be excited easily. The distribution function $n_{\mathbf{k}}(\mathbf{r},t)$ is expanded around the Fermi energy (linear response theory)

$$n_{\mathbf{k}}(\mathbf{r},t) = f_{\mathbf{k}}^{0} + g_{\mathbf{k}}(\mathbf{r},t) \tag{3.2}$$

with the equilibrium distribution, the Fermi distribution $f_{\mathbf{k}}^{0}$ and the deviation from equilibrium $g_{\mathbf{k}}(\mathbf{r},t)$, which labels the free particles. As we stop the Taylor expansion of $n_{\mathbf{k}}(\mathbf{r},t)$ at first order (3.2) is only a good description in the vicinity of the FS for small external fields. Inserting (3.2) into (3.1) gives us the linearized form of the BE.

$$\frac{\partial}{\partial t} g_{\mathbf{k}}(\mathbf{r}, t) + \mathbf{v}_{k} \nabla_{r} \left(f_{\mathbf{k}}^{0} + g_{\mathbf{k}}(\mathbf{r}, t) \right) + \mathbf{v}_{k} \mathbf{F}_{k} \left[\frac{\partial f_{\mathbf{k}}^{0}}{\partial \epsilon_{\mathbf{k}}} + \frac{\partial g_{\mathbf{k}}(\mathbf{r}, t)}{\partial \epsilon_{\mathbf{k}}} \right] = C_{\mathbf{k}}$$
(3.3)

with the equilibrium distribution $f_{\mathbf{k}}^0$ that is independent of time. Note that we only take first order terms in (3.3), which means that we have to look carefully which term inside the brackets contributes in the lowest order.

Equation (3.3) allows us to calculate the number of "free" particles $g_{\mathbf{k}}(\mathbf{r}, t)$ that contribute to the current \mathbf{j} , $\mathbf{j} = \sum_{\mathbf{k}} g_{\mathbf{k}}(\mathbf{r}, t) \mathbf{v}_{\mathbf{k}}$.

We conclude this section with writing down the explicit form of the BE including the scattering operator when also a temperature gradient is applied. One driving term is due to an electromagnetic field, $\mathbf{F} = e\mathbf{E} + \frac{e}{\hbar c}\mathbf{v} \times \mathbf{B}$ and the other is due to a temperature

³In the case of bare particles we don't have a backflow current. This will become important in 5.2!

gradient, $\propto \nabla_{\mathbf{r}} T/T$. The linearized BE gets the form

$$\frac{\partial}{\partial t} g_{\mathbf{k}} + \overbrace{\left(-\frac{\partial f_{\mathbf{k}}^{0}}{\partial \epsilon_{\mathbf{k}}}\right)}^{\sim \nabla_{\mathbf{r}} T} \underbrace{\epsilon_{\mathbf{k}} \mathbf{v}_{\mathbf{k}} \cdot \frac{\nabla_{\mathbf{r}} T}{T}}_{\sim \mathbf{F}} + e \mathbf{E} \mathbf{v}_{\mathbf{k}} \left(\frac{\partial f_{\mathbf{k}}^{0}}{\partial \epsilon_{\mathbf{k}}}\right) + \frac{e}{\hbar c} \mathbf{v}_{\mathbf{k}} \times \mathbf{B} \frac{\partial g_{\mathbf{k}}}{\partial \mathbf{k}} = C_{\mathbf{k}} \tag{3.4}$$

as given e.g. in [11] (without the temperature gradient). Note that the leading order contribution to the term that contains the magnetic field comes from $\frac{\partial g_{\mathbf{k}}}{\partial \mathbf{k}}$.

The scattering operator $C_{\mathbf{k}}$ has the usual form

$$C_{\mathbf{k}} = \sum_{\mathbf{k'}} \left[C_{\mathbf{k}, \mathbf{k'}} g_{\mathbf{k'}} - C_{\mathbf{k}, \mathbf{k'}} g_{\mathbf{k}} \right]$$
(3.5)

with the first term describing scattering "in" to the state \mathbf{k} and the second term describing scattering "out" of the state \mathbf{k} . The relaxation time $\tau_{\mathbf{k}}$ for state \mathbf{k} is defined as $1/\tau_{\mathbf{k}} \equiv \sum_{\mathbf{k}'} C_{\mathbf{k},\mathbf{k}'}$.

Our goal is to solve (3.4) for $g_{\mathbf{k}}$ as this quantity can tell us what particles can contribute to transport. Starting with this transport equation we will derive different transport properties of cuprates (in the NS). It is the starting point of the computation of the transport properties of our interest.

3.2 Considering interactions between quasiparticles - Landau's Fermiliquid theory (FLT)

In the previous section we considered particles that contribute to transport as "free", that means noninteracting, particles. We are going to take interactions between them into consideration in this section. It will turn out that the deviation from equilibrium $g_{\mathbf{k}}$ in the noninteracting case has not the same meaning as the deviation in the interacting case $\tilde{g}_{\mathbf{k}}$. To be precise quantities referring to interaction among particles are denoted by a tilde in this section.

We are concentrating on the l.h.s. of the BE in the following two sections as this is the more interesting one. The collision operator $C_{\mathbf{k}}$ (3.5) changes only with the replacement $g_{\mathbf{k}} \to \tilde{g}_{\mathbf{k}}$ when we are dealing with quasiparticle interaction.

The key step for dealing with interaction among particles is to expand the energy of the system around the Fermi-level. We can write the energy of the system as a functional of the departure from equilibrium $g_{\mathbf{k}}$, $E[g_{\mathbf{k}}]$. A Taylor-expansion up to second order gives

$$E[g_{\mathbf{k}}] = E_0 + \sum_{\mathbf{k}\sigma} \epsilon_{\mathbf{k}\sigma} g_{\mathbf{k}\sigma} + \frac{1}{2} \sum_{\mathbf{k}\mathbf{k}'\sigma\sigma'} f_{\mathbf{k}\mathbf{k}'}^{\sigma\sigma'} g_{\mathbf{k}\sigma} g_{\mathbf{k}'\sigma'}$$
(3.6)

where a summation over all spins σ and momenta \mathbf{k} is done. The function $f_{\mathbf{k}\mathbf{k}'}^{\sigma\sigma'}$ takes the interaction between the particles into consideration. Interacting particles are called, due to Landau, quasiparticles.

An expression that connects the change in energy $\delta E_{\mathbf{k}\sigma}$ of the system with a change in the number of particles $g_{\mathbf{k}}$ can be achieved by the derivative $\frac{\delta E}{\delta g_{\mathbf{k}}}$. Thus the energy of one excited (interacting) particle, $\tilde{\epsilon}_{\mathbf{k}\sigma}$, can be obtained from equation (3.6) by a partial derivative of the energy.

$$\tilde{\epsilon}_{\mathbf{k}\sigma} = \frac{\delta E}{\delta g_{\mathbf{k}\sigma}} = \epsilon_{\mathbf{k}\sigma} + \sum_{\mathbf{k}'\sigma'} f_{\mathbf{k}\mathbf{k}'}^{\sigma\sigma'} g_{\mathbf{k}'\sigma'}$$
(3.7)

Contrary to the noninteracting case we have an extra term due to the interaction among particles in (3.7). The energy of the excited quasiparticles, $\tilde{\epsilon}_{\mathbf{k}\sigma}$, is proportional to $g_{\mathbf{k}}$. The idea to describe these interacting particles is due to Landau and is called Landau's theory of Fermi liquids (FLT). Due to the interaction between the particles different quantities like mass, susceptibility etc. are renormalized.

In general we should consider the free energy F instead of E and perform the functional derivative $\frac{\delta F}{\delta g_{\mathbf{k}}}$ on this magnitude. In this case we would get only a slightly different expression because we take the chemical potential μ into account: $\tilde{\epsilon}_{\mathbf{k}\sigma} = \frac{\delta F}{\delta g_{\mathbf{k}\sigma}} = (\epsilon_{\mathbf{k}} - \mu) + \sum_{\mathbf{k}'\sigma'} f_{\mathbf{k}\mathbf{k}'}^{\sigma\sigma'} g_{\mathbf{k}\sigma}$. But if we consider the chemical potential μ to be constant in the area around the FS we get exactly the same result as given in (3.7).

Let's look first at the consequences of the interaction on the current. In the absence of interactions between particles we can write the "bare" current \mathbf{j}_0 in the way: $\mathbf{j}_0 = e \sum_{\mathbf{k}\sigma} \mathbf{v}_{\mathbf{k}} g_{\mathbf{k}\sigma}$, as already done before. When we are dealing with quasiparticles the function $f_{\mathbf{k}\mathbf{k}'}^{\sigma\sigma'}$ becomes important, as can be seen in (3.6). Analogous to the bare

current \mathbf{j}_0 we define the dressed current \mathbf{j} by

$$\mathbf{j} = e \sum_{\mathbf{k}\sigma} \mathbf{v}_{qp} \tilde{g}_{\mathbf{k}\sigma} \tag{3.8}$$

with the quasiparticle velocity \mathbf{v}_{qp} , $\mathbf{v}_{qp} = \frac{\partial \tilde{\epsilon}_{\mathbf{k}\sigma}}{\partial \mathbf{k}}$.

A fundamental question is the relation between $g_{\mathbf{k}\sigma}$ and $\tilde{g}_{\mathbf{k}\sigma}$ as this explains the connection between the "noninteracting" \mathbf{j}_0 and the "interacting" current \mathbf{j} . The equilibrium-distribution depends in the case of $g_{\mathbf{k}\sigma}$ on $\epsilon_{\mathbf{k}} - \mu$ whereas in the case of $\tilde{g}_{\mathbf{k}\sigma}$ it depends on $\tilde{\epsilon}_{\mathbf{k}} - \mu$.

$$g_{\mathbf{k}\sigma} = n_{\mathbf{k}\sigma} - n_{\mathbf{k}}^{0} (\epsilon_{\mathbf{k}} - \mu) \tag{3.9}$$

$$\tilde{g}_{\mathbf{k}\sigma} = n_{\mathbf{k}\sigma} - n_{\mathbf{k}}^{0}(\tilde{\epsilon}_{\mathbf{k}} - \mu)$$
 (3.10)

We label the equilibrium and the actual distribution with n instead of f in order to avoid confusion with $f_{\mathbf{k}\mathbf{k}'}^{\sigma\sigma'}$.

A connection between $g_{\mathbf{k}\sigma}$ and $\tilde{g}_{\mathbf{k}\sigma}$ can be found when we expand the term $n_{\mathbf{k}}^{0}(\epsilon_{\mathbf{k}} - \mu + \tilde{\epsilon}_{\mathbf{k}} - \epsilon_{\mathbf{k}})$, given above, to first order in the following manner

$$\tilde{g}_{\mathbf{k}\sigma} = n_{\mathbf{k}\sigma} - n_{\mathbf{k}}^{0}(\tilde{\epsilon}_{\mathbf{k}} - \mu) = n_{\mathbf{k}\sigma} - n_{\mathbf{k}}^{0}(\epsilon_{\mathbf{k}} - \mu + \tilde{\epsilon}_{\mathbf{k}} - \epsilon_{\mathbf{k}})
= \underbrace{n_{\mathbf{k}\sigma} - n_{\mathbf{k}}^{0}(\epsilon_{\mathbf{k}} - \mu)}_{g_{\mathbf{k}\sigma}} - (\tilde{\epsilon}_{\mathbf{k}} - \epsilon_{\mathbf{k}}) \frac{dn_{\mathbf{k}}^{0}(\epsilon_{\mathbf{k}} - \mu)}{d\epsilon_{\mathbf{k}}}$$

which shows that the magnitudes $g_{\mathbf{k}\sigma}$ and $\tilde{g}_{\mathbf{k}\sigma}$ are not identical! This has important consequences on transport properties. Note that $-\frac{dn_{\mathbf{k}}^{0}(\epsilon_{\mathbf{k}}-\mu)}{d\epsilon_{\mathbf{k}}} \to \delta(\epsilon_{\mathbf{k}}-\mu)$ for $T \to 0.4$ From equation (3.7) can followed that $\tilde{\epsilon}_{\mathbf{k}} - \epsilon_{\mathbf{k}} = \sum_{\mathbf{k}'\sigma'} f_{\mathbf{k}\mathbf{k}'}^{\sigma\sigma'} g_{\mathbf{k}'\sigma'}$. So we finally obtain the connection between noninteracting and interacting deviation from equilibrium as

$$\tilde{g}_{\mathbf{k}\sigma} = g_{\mathbf{k}\sigma} + \left(-\frac{dn_{\mathbf{k}}^{0}(\epsilon_{\mathbf{k}} - \mu)}{d\epsilon_{\mathbf{k}}} \right) \sum_{\mathbf{k}'\sigma'} f_{\mathbf{k}\mathbf{k}'}^{\sigma\sigma'} g_{\mathbf{k}'\sigma'}$$
(3.11)

Dealing with interaction the total current is described by equation (3.8), where the quantity $\tilde{g}_{\mathbf{k}\sigma}$ can be expressed in terms of $g_{\mathbf{k}\sigma}$ like it is shown in (3.11). As particles are interacting there is a backflow of quasiparticles in a interacting system. This backflow has to be added to the current as it is done in equation (3.8).

 $^{^4}n_{f k}^0=rac{1}{e^{eta(\epsilon_{f k}-\mu)}+1}$ as usual.

It is important to know that in the FLT the current is not necessary parallel to the velocity of the quasiparticles due to $f_{\mathbf{k}\mathbf{k}'}^{\sigma\sigma'}$. This fact forces us to think which quantity, \mathbf{j} or v, has to be used in a transport equation in an electromagnetic field for an interacting system. Remember that the Lorenz force depends on the velocity of a particle which is proportional to the current in a noninteracting system.

3.3 The transport equation of interacting particles in an electromagnetic field

It is know from electrodynamics that the electric and the magnetic field, E and H, can be derived from a vector-potential **A** and a scalar potential Φ . We are choosing the Coulomb gauge, so the electric and magnetic field are given by:

$$\mathbf{E} = -\frac{1}{c} \frac{\partial \mathbf{A}}{\partial t}$$

$$\mathbf{H} = \nabla \times \mathbf{A}$$

In the absence of a electromagnetic field $(\mathbf{A}(\mathbf{r},t)=0)$ the momentum of the particle is k. Turning on a electromagnetic field changes the situation. The canonically conjugated to the position r is no longer the momentum k. Instead of this we get the momentum in an electromagnetic field \mathcal{K} , with

$$\mathcal{K} = \mathbf{k} + \frac{e\mathbf{A}}{c} \tag{3.12}$$

A particle moving in a vector potential $\mathbf{A}(\mathbf{r},t)$ can therefore be described by inserting an extra term due to the vector potential $\mathbf{A}(\mathbf{r},t)$ in the Hamiltonian.

$$H = \frac{1}{2m} \sum_{i} \left[\mathcal{K}_{i} - \frac{e\mathbf{A}(\mathbf{r}, t)}{c} \right]^{2} + V$$
 (3.13)

where we are considering a system of particles and an interaction V between the particles due to a Coulomb interaction. Note that \mathbf{k} , determined from (3.12) is inserted in (3.13).

The equations of motion of a particle in an electromagnetic field can be derived from the Hamiltonian given in (3.13).

$$\dot{r}_i = \frac{\partial H}{\partial \mathcal{K}_i} = \frac{1}{m} \left[\mathcal{K}_i - \frac{eA_i(\mathbf{r}, t)}{c} \right]$$
 (3.14)

$$\dot{\mathcal{K}}_{i} = -\frac{\partial H}{\partial r_{i}} = -\frac{e}{mc} \frac{\partial A_{j}}{\partial r_{i}} \left[\mathcal{K}_{j} - \frac{eA_{j}(\mathbf{r}, t)}{c} \right]$$
(3.15)

From the gauge we have chosen it can be immediately seen from (3.14) that the force on a particle in an electromagnetic field is given by⁵

$$m\ddot{\mathbf{r}} = \left[\frac{d\mathcal{K}}{dt} + e\mathbf{E}\right] = e\mathbf{E} + \frac{e}{c}\mathbf{v} \times \mathbf{H}$$
 (3.16)

So the well-known result was rederived, namely that the momentum \mathbf{k} has to be replaced by $\left[\mathcal{K} - \frac{e\mathbf{A}}{c}\right]$ in an electromagnetic field.

A vector potential **A** shifts the origin in momentum space by an amount $\frac{e\mathbf{A}(\mathbf{r},t)}{c}$ away from the origin without an electromagnetic field.

As we are interested in a derivation of the transport equation of an interacting system in presence of an electromagnetic field we have to study the Hamiltonian given in (3.13) and consider interaction between the particles.

The relation for momenta of particles in an electromagnetic field $d\mathcal{K}_i$ and momenta of particles without electromagnetic field dk_i is the following $dk_i = d\mathcal{K}_i - \sum_j \frac{e}{c} \frac{\partial A_i}{\partial r_j} dr_j$, with i, j = x, y, z, because of the condition $\mathbf{k} = \mathcal{K} - \frac{e\mathbf{A}}{c}$ already pointed out before. When we turn on an electromagnetic field in an interacting system we have to make this replacement in the local energy $\tilde{\epsilon}_k$. So we generalize the formula for the local energy shown in (3.7) to

$$d\tilde{\epsilon}_{k} = \sum_{i} \left[v_{i} dk_{i} + \sum_{\mathbf{k}'} f_{\mathbf{k}\mathbf{k}'} [\nabla_{r_{i}} n_{\mathbf{k}'}] dr_{i} \right] = \sum_{i,j} \left\{ v_{i} \left[d\mathcal{K}_{i} - \frac{e}{c} \frac{\partial A_{i}}{\partial r_{j}} dr_{j} \right] + \sum_{\mathbf{k}'} f_{\mathbf{k}\mathbf{k}'} [\nabla_{r_{i}} n_{\mathbf{k}'}] dr_{i} \right\}$$
(3.17)

where i, j = x, y, z as usual. Note that we replaced $g_{\mathbf{k}}$ by $\sum_{i} [\nabla_{r_i} n_{\mathbf{k}}] dr_i$ in this equation. The equations of motion for this Hamiltonian change with respect to the equations given in (3.14) by considering the interaction, denoted by the local energy $\tilde{\epsilon}$.

$$\dot{\tilde{r}}_i = \left(\frac{\partial \tilde{\epsilon}_k}{\partial \mathcal{K}_i}\right)_r = v_i \tag{3.18}$$

$$-\dot{\tilde{\mathcal{K}}}_{i} = \left(\frac{\partial \tilde{\epsilon}_{k}}{\partial r_{i}}\right)_{\mathcal{K}} = \sum_{\mathbf{k}'} f_{\mathbf{k}\mathbf{k}'} \left(\frac{\partial n_{\mathbf{k}'}}{\partial r_{i}}\right)_{\mathbf{k}'} - \sum_{i} \frac{e}{c} \frac{\partial A_{j}}{\partial r_{i}} v_{j}$$
(3.19)

⁵The velocity of a particle in an electro-magnetic field is given by $\mathbf{v} = \frac{1}{m} \left[\mathcal{K} - \frac{e\mathbf{A}}{c} \right]$ which can be seen from equation (3.14).

These equations describe the motion of interacting particles, considered by $f_{\mathbf{k}\mathbf{k}'}^{\sigma\sigma'}$ in an electromagnetic field.

Our goal, to derive a transport equation of quasiparticles, can be achieved when we study the flow of quasiparticles in phase space. Because of the connection between \mathbf{k} and \mathcal{K} the two distributions $n_{\mathbf{k}}$ and $n_{\mathcal{K}}$ are identical in real space, but shifted with $\frac{e}{c}\mathbf{A}$ in reciprocal space. The following transport equation can be followed from Liouville's equation $(\frac{dn}{dt} = 0!)$ neglecting collisions.

$$\left(\frac{\partial n_{\mathcal{K}}}{\partial t}\right)_{\mathcal{K},r} + \left(\frac{\partial n_{\mathcal{K}}}{\partial r_{i}}\right)_{\mathcal{K}} \underbrace{\left(\frac{\partial \tilde{\epsilon}_{k}}{\partial \mathcal{K}_{i}}\right)_{r}}_{\tilde{\kappa}} - \left(\frac{\partial n_{\mathcal{K}}}{\partial \mathcal{K}_{i}}\right)_{r} \underbrace{\left(\frac{\partial \tilde{\epsilon}_{k}}{\partial r_{i}}\right)_{\mathcal{K}}}_{r} = 0$$
(3.20)

where the third term takes interaction and the external field into account (compare to (3.18)).

As the momentum K depends on the vector potential \mathbf{A} equation (3.20) is not easy to handle. It is convenient to express the given transport equation (without collisions) in terms of the momentum \mathbf{k} . Therefore it is useful to figure out a connection between derivatives of the partition function $n_{\mathbf{k}}$ and n_{K} , given by equation 3.12.

$$\left(\frac{\partial n_{\mathcal{K}}}{\partial t}\right)_{\mathcal{K},\mathbf{r}} = \left(\frac{\partial n_{\mathbf{k}}}{\partial t}\right)_{\mathbf{k},\mathbf{r}} + \sum_{i} \frac{e}{c} \frac{\partial n_{\mathbf{k}}}{\partial k_{i}} \frac{\partial A_{i}}{\partial t} \tag{3.21}$$

$$\left(\frac{\partial n_{\mathcal{K}}}{\partial r_{i}}\right)_{\mathcal{K}} = \left(\frac{\partial n_{\mathbf{k}}}{\partial r_{i}}\right)_{\mathbf{k}} + \sum_{i} \frac{e}{c} \frac{\partial n_{\mathbf{k}}}{\partial k_{j}} \frac{\partial A_{j}}{\partial r_{i}}$$
(3.22)

$$\left(\frac{\partial n_{\mathcal{K}}}{\partial \mathcal{K}_{i}}\right)_{\mathbf{r}} = \left(\frac{\partial n_{\mathbf{k}}}{\partial k_{i}}\right)_{\mathbf{r}} \tag{3.23}$$

When we insert these three properties in the transport equation in \mathcal{K} -space, equation (3.20), we get a transport equation in \mathbf{k} -space, with the local energy $\tilde{\epsilon}$ given in (3.17).⁶ So we can write a transport equation with interaction between particles in the presence of an electromagnetic field in terms of momenta \mathbf{k} by using (3.20).⁷

$$\frac{\partial n_{\mathbf{k}}}{\partial t} + e\mathbf{E} \cdot \nabla_{\mathbf{k}} n_{\mathbf{k}} + \mathbf{v}_{\mathbf{k}} \cdot \nabla_{\mathbf{r}} n_{\mathbf{k}} + \frac{e}{c} [\mathbf{v}_{\mathbf{r}} \times \mathbf{H}] \cdot \nabla_{\mathbf{k}} n_{\mathbf{k}} - \sum_{\mathbf{k}'} \nabla_{\mathbf{k}} n_{\mathbf{k}} \cdot \nabla_{\mathbf{r}} n_{\mathbf{k}'} f_{\mathbf{k}\mathbf{k}'} = 0 \quad (3.24)$$

where the last term on the l.h.s. contains the particle-particle interaction. The third and the last term on the l.h.s. can be put together to $\mathbf{v_k} \cdot \nabla_{\mathbf{r}} \tilde{g}_{\mathbf{k}}$ which can be seen from

⁶Note $-\frac{e}{c}\frac{\partial n_{\mathbf{k}}}{\partial k_{j}}\frac{\partial A_{j}}{\partial r_{i}}v_{i} + \frac{\partial n_{\mathbf{k}}}{\partial k_{i}}\frac{e}{c}v_{j}\frac{\partial A_{i}}{\partial r_{j}} = \frac{e}{c}[\mathbf{v}_{p}\times\mathbf{H}]_{j}\cdot\nabla_{\mathbf{k}}n_{\mathbf{k}}$ which turns out to be important when we insert (3.21) and (3.18) in (3.20).

⁷Remember the gauge we have!

(3.11).

The quasiparticles are moving as they felt the presence of a Lorenz force, determined by their velocity, acting on them, which was not clear from the beginning as the current and the velocity of quasiparticles are not necessarily parallel.

The final result for the transport equation dealing with FLT is obtained when linearizing, $n_{\mathbf{k}} = n_{\mathbf{k}}^0 + g_{\mathbf{k}}$, the transport equation (3.24). The relation found in (3.11) is used to get short expressions.

1. In the case of a **DC magnetic field H**₀ we obtain the following transport equation for the system. We obtain the first contribution to the Lorenz-force by $[\mathbf{v_k} \times \mathbf{H}_0] \cdot \nabla_{\mathbf{k}} g_{\mathbf{k}}$, as $[\mathbf{v_k} \times \mathbf{H}_0] \cdot \nabla_{\mathbf{k}} n_{\mathbf{k}}^0 = 0$. But as we have interaction among the particles we have another first order term that comes from the partial derivative of the local energy $\tilde{\epsilon}$ with respect to \mathbf{k} . Thus we obtain two terms contributing to the Lorenz-force that are of first order.

$$\frac{e}{c} [\mathbf{v_k} \times \mathbf{H}_0] \cdot \nabla_{\mathbf{k}} g_{\mathbf{k}} + \frac{e}{c} \left[\nabla_{\mathbf{k}} \left(\sum_{\mathbf{k'}} f_{\mathbf{k}\mathbf{k'}} g_{\mathbf{k'}} \right) \times \mathbf{H}_0 \right] \cdot \nabla_{\mathbf{k}} n_{\mathbf{k}}^0$$

When we insert this contribution in equation (3.24) we get the transport equation in the presence of an DC-magnetic field.

$$\frac{\partial g_{\mathbf{k}}}{\partial t} + \mathbf{v}_{\mathbf{k}} \cdot \nabla_{\mathbf{r}} \tilde{g}_{\mathbf{k}} + \frac{e}{c} (\mathbf{v}_{\mathbf{k}} \times \mathbf{H}_0) \nabla_{\mathbf{k}} \tilde{g}_{\mathbf{k}} + e \mathbf{E} \cdot \nabla_{\mathbf{k}} n_{\mathbf{k}}^0 = 0$$
 (3.25)

Note that the time derivative of $g_{\mathbf{k}}$ vanishes in the DC-case.

The DC field \mathbf{H}_0 acts on the departure $\tilde{g}_{\mathbf{k}}$ from local equilibrium, instead of $g_{\mathbf{k}}$ when FL-corrections are considered. This equation is the start of the study of electrical quantities like the DC-conductivity, the Hall-conductivity, magnetoresistance etc..

2. Applying a **AC** magnetic field on a sample has different consequences. The application of a time-dependent magnetic field **H** is associated with the propagating electromagnetic wave in the sample. As **E** and **H** are first order perturbations of

⁸Remember $\nabla_{\mathbf{k}} n_{\mathbf{k}}^0 = \frac{\partial n_{\mathbf{k}}^0}{\partial \epsilon_{\mathbf{k}}} \mathbf{v}_{\mathbf{k}}$. And therefore we obtain zero in the 0-th order.

the system, the same order as $g_{\mathbf{k}}$, the transport equation can be written as

$$\frac{\partial g_{\mathbf{k}}}{\partial t} + \mathbf{v}_{\mathbf{k}} \cdot \nabla_{\mathbf{r}} \tilde{g}_{\mathbf{k}} + e \left[\mathbf{E} + \frac{\mathbf{v}_{\mathbf{k}}}{c} \times \mathbf{H} \right] \cdot \nabla_{\mathbf{k}} n_{\mathbf{k}}^{0} = 0$$
 (3.26)

because $\nabla_{\mathbf{k}} n_{\mathbf{k}}^0$ is no more parallel to $\mathbf{v}_{\mathbf{k}}$, thus it gives the leading order contribution to the Lorenz-force. When we are dealing with a fast varying electromagnetic field we can consider $n_{\mathbf{k}} \approx n_{\mathbf{k}}^0$ (which is true in most cases). The term given by the AC-magnetic field can be neglected and equation (3.26) simplifies to:

$$\frac{\partial g_{\mathbf{k}}}{\partial t} + \mathbf{v}_{\mathbf{k}} \cdot \nabla_{\mathbf{r}} \tilde{g}_{\mathbf{k}} + e \mathbf{E} \cdot \nabla_{\mathbf{k}} n_{\mathbf{k}}^{0} = 0$$
(3.27)

Introducing the scattering operator given in equation (3.5) (of course in terms of $\tilde{g}_{\mathbf{k}}$) allows us to obtain the full BE in the interacting case. Note that in the steady state case, $\frac{\partial g_{\mathbf{k}}}{\partial t} = 0$, everything in the BE is expressed in terms of $\tilde{g}_{\mathbf{k}}$. So we can solve the BE, taking interaction into account, without a knowledge of $f_{\mathbf{k}\mathbf{k}'}^{\sigma\sigma'}$! The steady state case will be considered in the following chapters. In this chapters we make the replacement $g_{\mathbf{k}} \to \tilde{g}_{\mathbf{k}}$. Note that this is not more valid in the case of AC-transport.

One last comment on the effect of charged quasiparticles will finish this chapter. When we consider screening between quasiparticles, due to a Coulomb-interaction between them, the external electric field has to be modified. So the electric field \mathbf{E} used in the transport equation (3.24) has to be replaced by a sum of the external field and a internal field due to screening, $\mathbf{E} = \mathbf{E}_{ext} + \mathbf{E}_{sc}$. This is done in the Landau-Silinequations.

Chapter 4

Experimental results for BSCCOVariation of τ over the FS

In this chapter we will provide the experimental results that will be compared with the model we are going to construct. Experimental data for the quantities we compare our model with are given. At least the shape, the magnitude and the temperature behavior of the computed transport properties are a first test of the model we are proposing. Several experimental results can be found in [39].

Furthermore we discuss the consequences of a single relation-time for cuprates. Drude's theory of metals [2], suggested in 1900, is able to describe electric and thermal conductivity using the kinetic theory of gases. The characteristic quantity in his approach is an average relaxation-time τ_D , $\tau_D \approx 10^{-14} s - 10^{-15} s$ at room temperature, which is an average relaxation time for every electron in the sample.

In the language of the BE we can write the linearized BE, given in (3.4), in the case of one single scattering time as

$$\frac{\partial}{\partial t}g_{\mathbf{k}} + e\mathbf{E}\mathbf{v}_{\mathbf{k}}\frac{\partial f^{0}}{\partial \epsilon_{\mathbf{k}}} + \frac{e}{\hbar c}(\mathbf{v}_{\mathbf{k}} \times \mathbf{B}) \cdot \left[\frac{\partial}{\partial \mathbf{k}}g_{\mathbf{k}}\right] = -\frac{g_{\mathbf{k}}}{\tau_{D}}$$
(4.1)

where the r.h.s. simplifies to just one term. Note that the relaxation time for every state \mathbf{k} in the reciprocal space $\tau_{\mathbf{k}}$ is the same, $\tau_{\mathbf{k}} = \tau_D \ \forall \mathbf{k}$ in the Drude approach.

Equation (4.1) allows us to write the current, which is produced by the "free" particles, as $e \sum_{\mathbf{k}} \mathbf{v}_{\mathbf{k}} g_{\mathbf{k}}$. Combing this result with Ohm's law we get the electrical conductivities $\sigma^{\mu\nu}$.

$$\mathbf{j} = \bar{\sigma} \mathbf{E} = e \sum_{\mathbf{k}} \mathbf{v}_{\mathbf{k}} g_{\mathbf{k}} \tag{4.2}$$

Equation (4.2) allows us to compute different conductivities as a function of the temperature T. When we compare this with experimental results we can find out whether we can describe cuprates with a simple Drude-model.

4.1 DC-conductivity σ^{xx}

We start our analysis with the easiest quantity, the DC-conductivity. Every term in (4.1) has no time-dependence in this case. Furthermore no magnetic field is turned on. Thus the first and the third term on the l.h.s. of (4.1) vanish. The transport-equation simplifies to the expression for the "free" particles:

$$g_{\mathbf{k}} = -e\mathbf{E}\mathbf{v}_{\mathbf{k}}\tau_{\mathbf{k}}\left(\frac{\partial f^{0}}{\partial \epsilon_{\mathbf{k}}}\right) \tag{4.3}$$

Equation (4.2) allows us, using this knowledge, to compute the DC-conductivity σ^{xx} . We just insert (4.3) into (4.2) and obtain:

$$\sigma^{xx} = e^2 \sum_{\mathbf{k}} (v_{\mathbf{k}}^x)^2 \tau_{\mathbf{k}} \left(-\frac{\partial f^0}{\partial \epsilon_{\mathbf{k}}} \right)$$
 (4.4)

Which means that $\sigma^{xx} \propto \tau_{\mathbf{k}}$. Thus we expect σ^{xx} to have the same temperature dependence as $\tau_{\mathbf{k}}$. At this stage it is not clear that the other factors in (4.4) are independent of T.

In the zero temperature case we can identify $\left(-\frac{\partial f^0}{\partial \epsilon_{\mathbf{k}}}\right)$ with a δ -function (remember that the equilibrium distribution f^0 is the Fermi-Dirac-distribution which is a step function in the zero temperature case). So $\left(-\frac{\partial f^0}{\partial \epsilon_{\mathbf{k}}}\right)$ gives only a contribution when $\epsilon = \mu$, thus $\left(-\frac{\partial f^0}{\partial \epsilon_{\mathbf{k}}}\right) = \delta(\epsilon - \mu)$.

Our next goal is to bring (4.4) in the form that is known from the Drude-model. First we have to write the sum in (4.4) as an integral.

$$d\mathbf{k} = dA_{\epsilon} \cdot dk_{\perp} = dA_{\epsilon} \frac{d\epsilon}{|\nabla_{\mathbf{k}} \epsilon|} = dA_{\epsilon} \frac{d\epsilon}{\hbar |\mathbf{v}_{\mathbf{k}}|}$$

¹The minus-sign in front of the derivative of f^0 with respect to ϵ takes care of the right sign in the δ -function.

Now we can use the well-known formula that transforms a sum into an $integral^2$ and obtain

$$\sigma^{xx} = \frac{2 \cdot e^2}{(2\pi)^3 \hbar} \int \frac{(v_{\mathbf{k}}^x)^2}{|\mathbf{v}_{\mathbf{k}}|} \tau_{\mathbf{k}} \delta(\epsilon - \mu) dA_{\epsilon} d\epsilon = \frac{e^2}{4\pi^3 \hbar} \int_{\epsilon = \mu} \frac{(v_{\mathbf{k}}^x)^2}{|\mathbf{v}_{\mathbf{k}}|} \cdot \tau_{\mathbf{k}} dA_{\epsilon}$$

The δ -function in (4.4) restricts us on the FS. Averaging the product $\frac{(v_{\mathbf{k}}^x)^2}{|\mathbf{v}_{\mathbf{k}}|} \cdot \tau_{\mathbf{k}}$ has the result $\langle \frac{(v_{\mathbf{k}}^x)^2}{|\mathbf{v}_{\mathbf{k}}|} \cdot \tau_{\mathbf{k}} \rangle = \langle \frac{v \cdot \tau_D}{3} \rangle_{FS}$. So we are left with an integral $\int dA_{\epsilon} = 4\pi k_f^2$, thus³

$$\sigma^{xx} = \frac{e^2}{4\pi^3\hbar} \frac{v(\epsilon_f) \cdot \tau_D}{3} 4\pi k_f^2 = \frac{e^2 k_f^3 \tau_D}{3m^* \pi^2}$$

From this equation we get the final result:

$$\sigma^{xx} = \frac{e^2 n}{m^*} \tau_D \tag{4.5}$$

The proportionality between σ^{xx} and τ_D , that was already pointed out above, is shown explicitly in equation (4.5).

It is worth to mention that the derivation above was done in the 3D-case. As we are interested in cuprates we are interested in the 2D case, as argued in chapter 2. However it is worth to consider the consequences of a treatment within the Drude approach (independent of the dimension).

4.1.1 Experimental results: Resistivity ρ^{xx} in BSCCO

The material of our interest, BSCCO, has a fairly easy geometry. As this material has no chains BSCCO-data should be understood by just looking at the CuO_2 -planes shown in figure 2.2. We are dealing with a 2D-system in these materials. As a consequence of the fourfold symmetry of the lattice the FS, that is connected to the lattice symmetry, has the same fourfold symmetry, which can be seen in figure 2.4.

Experiments measure the DC-resistivity, measured in $\mu\Omega cm$, vs. the temperature, which is measured in Kelvin.

Our model tries to fit the data given by [14] and [15] which show good agreement with

 $^{^{2}\}sum_{\mathbf{k}} \rightarrow \frac{1}{(2\pi)^{D}} \int d^{D}k.$

³Remember $v(\epsilon_f) = \frac{\hbar k_f}{m^*}$ and $k_f = (3\pi^2 n)^{\frac{1}{3}}$

each other.

Measurements by [14] showed that single crystals of Bi2212 have a transition temperature between 82K-84K. Down to 150K a linear temperature dependence of the resistivity ρ^{xx} is obtained in their experiment. They detected the rounding of ρ at temperatures < 110K.

Quijadas group presents experimental results [15] where a modest normal state anisotropy in the in-plane resistivity, that means in the resistivity in the CuO_2 -planes, is observed. The material his group measured was $Bi_2Sr_2CaCu_2O_8$, Bi2212, with a T_c of $\approx 80K$. Introducing Ca-atoms in the BSCCO-sample separates the planes strongly from each other. The experiments by Sunshine [21] measure the DC-resistivity of BSCCO (material: $Bi_{2.2}Sr_2Ca_{0.8}Cu_2O_{8+\delta}$) and show a big sensitivity of these samples dependent on doping. These experiments provide useful data to study the effect of doping on the resistivity.

The doping dependence of another interesting sample, $Bi_2Sr_{2-z}La_zCuO_{6-\delta}$, that has a very similar structure, was also studied by Ando et al. [23]. This group measured the doping dependence of the in plane-resistivity of Bi2201 samples in a temperature range between 10K to 300K. These samples have a $T_c \approx 35K$, thus a smaller one than Bi2212-materials have. The same temperature dependence of this sample as a function of the doping can also be seen in [1], [26]. The results of Andos group are in relatively good agreement with Wang [17] who measured the in-plane resistivity in the same range.

Rullier-Albenque [10] reports the effects of electron irradiation on Bi2212-samples $(Bi_2Sr_2CaCu_2O_8)$. The effect of the radiation raises the DC-resistivity but not in such a strong manner as doping does. Therefore the curve, measured after irradiation is still in the same resistivity range as before.

Further experimental data on the resistivity on Bi-based cuprates are given by Martin et al. [20] (experiments on $Bi_2(Sr, Ca)_3Cu_2O_x$ -samples) and Jin [19] (material: $Bi_{1.95}Sr_{1.65}La_{0.4}CuO_{6+\delta}$, $T_c \approx 15K$). Jins group reports a slope for Bi2201 samples that has approximately the same magnitude as the slope for the samples of the Bi2212 type.

All experiments have a linear T-dependence in ρ^{xx} for $T > T_c$ in common. The critical temperature for Bi2212 is measured to $T_c \approx 84K$. The slope of the linear part of the DC-resistivity $\Delta \rho / \Delta T$ is given by $\Delta \rho / \Delta T \approx 0.5(\mu \Omega cm)/K$. The doping dependences of the resistivity-curves can also be obtained from given experiments. Figure 4.1 shows the DC-resistivity σ^{xx} for Bi2201 for different doping rates. Experimental results for Bi2212 differ only slightly from them. Doping of the sample changes the offset and the slope of the curve as can be seen in this figure. The model we are going to propose is able to model the effect of doping by changing one parameter (θ - which describes the size of the cold region).

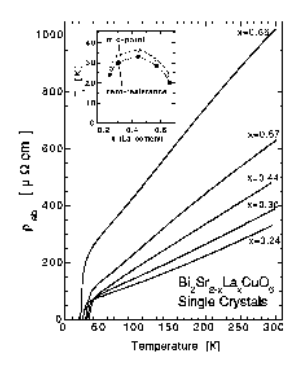


Figure 4.1: The DC-resistivity ρ^{xx} of a Bi2201-sample is measured vs. T reported in [1]. The doping dependence of ρ^{xx} can be studied.

4.2 Hall-conductivity σ^{xy}

The Hall-conductivity σ^{xy} can be derived from equation (4.5) in an easy way, when we remember the formula for the Hall-resistivity R_H , given by $R_H = \frac{1}{nec} = \frac{\sigma^{xy}}{H \cdot \sigma^{xx} \sigma^{yy}}$. In the case of an isotropic sample, which is the case for BSCCO, $\sigma^{xx} = \sigma^{yy}$ and we obtain $R_H = \frac{\sigma^{xy}}{H \cdot (\sigma^{xx})^2}$.

It was pointed out by Anderson that the physical quantity we should look at, dealing with the Hall-effect, is not the Hall-resistivity but the Hall-angle, that is given by:

$$\tan(\theta_H) = \frac{\sigma^{xy}}{\sigma^{xx}} \tag{4.6}$$

because it shows an easy temperature-dependence. The formula for R_H allows us to get an expression for σ^{xy} , $\sigma^{xy} = \frac{H \cdot (\sigma^{xx})^2}{nec}$. So the final formula for the Hall-angle has the form (in the Drude approach):

$$\tan(\theta_H) = \frac{H}{nec}\sigma^{xx} = \frac{eH}{m^*c}\tau_D \tag{4.7}$$

As $\tan(\theta_H) \propto \tau_D$ (compare to (4.7)) we expect the same temperature dependence for the Hall-angle $(\tan(\theta_H) \propto \tau_D)$ as for the DC-conductivity $(\sigma^{xx} \propto \tau_D)$. Experiments show a different temperature dependence of these quantities.

We are reporting some experimental results for $\cot \theta_H$, the inverse Hall-angle now.

4.2.1 Experimental results: Hall-angle $tan(\theta_H)$ in cuprates

We are referring to recent experiments, carried out by Konstantinovic [27] and Ando [1]. In both experiments $\cot \theta_H$ is measured vs. T^2 for Bi2212 or Bi2201-samples. Independently the groups figured out that the temperature dependence of $\cot \theta_H$ changes from $\cot \theta_H \propto T^2$ for underdoped to $\cot \theta_H \propto T^{1.65}$ for overdoped materials. Their conclusion is that doping decreases the slope of the inverse Hall-angle. Note that the experiments by Ando were done by a magnetic field of 10T, Konstantinovic experiments however with a magnetic field of 1T. This information is important as the magnetic field is a parameter in the numerical program that computes the Hall-angle using the model we propose.

Figure 4.2, taken from [1], shows the measured inverse Hall-angle $\cot \theta_H$ vs. T^{α} , $\alpha = 1.70$ (optimally doped) and $\alpha = 1.60$ (overdoped) for different doping of the Bi2201-sample. It shows that no T^2 -behavior for overdoped materials is observed. Note that x labels the percentage of La atoms in figure 4.2, thus increasing x decreases the number of holes (i.e. underdoping) and vice versa.

Note that the Hall-angle has no units as it is a ratio of two conductivities.

Experiments observe that ρ^{xx} and $\cot(\theta_H)$ show a different temperature dependence. This can not explained by a simple Drude-model, used in the derivation of (4.5) and (4.7). Cuprates don't behave like a metal and furthermore they have to have more than one relaxation time.

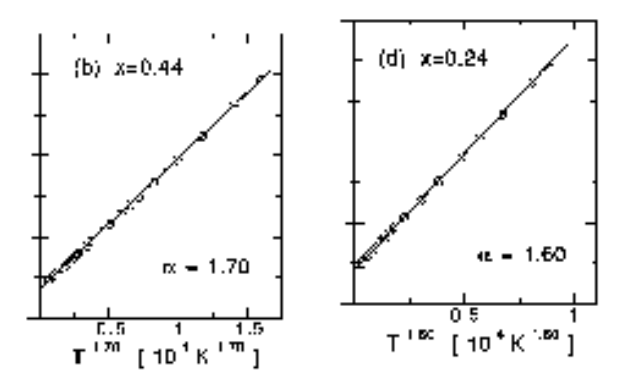


Figure 4.2: Experiments by Ando [1] show that the slope of $\cot \theta_H$ decreases with increasing doping (left: optimally doped; right: overdoped). Measurements are done with a magnetic field of 10T.

The conclusion that was derived from the ARPES data, see figure 2.3, is also confirmed by the experimental data, namely that a single relaxation time is not able to describe the physics happening in cuprates.

4.3 Thermoelectric power (TEP) of BSCCO

The TEP is defined as the ratio between the thermopower S^{xx} and the DC-conductivity σ^{xx} times the temperature. Note the difference between the thermopower $S^{\mu\nu}$ and the TEP.

$$TEP = \frac{S^{xx}}{T\sigma^{xx}} \tag{4.8}$$

Obertelli et al., [33], measured the TEP of $Bi_2Sr_2CaCu_2O_{8+\delta}$ (Bi2212) as a function of the temperature with varying doping. As our model is only valid in the NS of BSCCO the data from this group are only of interest in the optimally doped and in the overdoped regime. When we go to the underdoped region the pseudogap opens and a treatment with the BE is no more valid.

The doping dependence of Bi2201 can be studied in the experiment of McIntosh and Kaiser [31]. They report measurements of the TEP of La-doped $Bi_2Sr_{2-x}La_xCuO_{6+y}$ samples in a temperature range between 0 and 300K. Also Choi's group, [4], measured the TEP of $Bi_2Sr_{2-x}La_xCuO_{6+z}$. In their experiment the La-doping varied between

0.1 and 0.9. The experiments [31] and [4] can be compared as they measure the same materials.

A typical experimental result for the TEP is shown in figure 4.3. A strong variation of the TEP with varying doping can be seen in the figure. It turns out that the TEP depends mostly on the shape of the FS which determines the density of states. Experiments measure the TEP in $\mu V/K$.

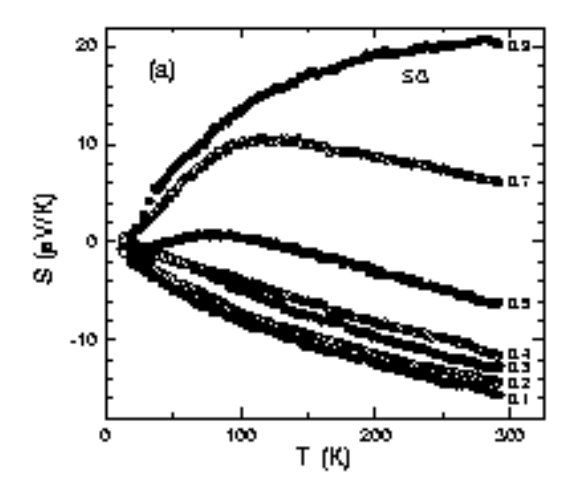


Figure 4.3: TEP experiment taken from [4]. The TEP of Bi2201 is measured for different doping as a function of T.

4.4 Magnetoresistance MR in BSCCO

The MR is defined as

$$MR = \frac{\Delta \sigma^{xx}(\mathbf{B})}{\sigma^{xx}} \tag{4.9}$$

so it measures the ratio between the change in the DC-conductivity due to an magnetic field and the DC-conductivity without an magnetic field.

The same group mentioned above, Ando [1], measured the transversal and the longitudinal MR of Bi2201-samples as a function of doping. The result is shown in figure 4.4. It shows the dimensionless MR vs. the temperature T in a temperature-range between 0K and 300K for different doping. Ando's results allow us to get an impression how doping changes the MR. They found out that increasing doping decreases the MR.

Note that we are only interested in the transversal MR, as our model computes only this MR. Figure 4.4 shows the transverse (solid circles) and the longitudinal MR (open circles) for overdoped (left figure) and optimally doped (right figure) *Bi*-based samples. Doping decreases the MR as can be seen in this figure. The two plots at the bottom represent the underdoped case!

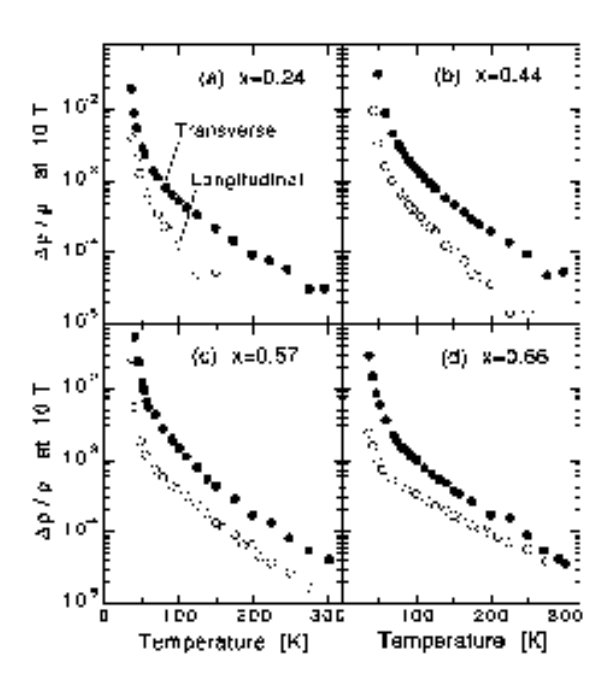


Figure 4.4: The experiment from Ando, [1], shows the MR dependent on temperature for optimally doping (right top) (b), overdoped (left) (a) and underdoped samples ((c) and (d)). Note that this group measured transversal (solid cicles) and longitudinal (open circles) MR.

A Kohler-plot, where the ratio $\Delta \rho^{xx}/[\rho^{xx}tan(\theta_H)^2]$ is plotted vs. T, is done in some papers, e.g. [6]. The cited group claims that this dimensionless ratio saturates to a value of about 6. When we test our model we are going to check this result as well.

4.5 Thermal Hall-conductivity κ^{xy}

 κ^{xy} measures the effect of a magnetic field on particles that transport heat. It is defined in the same manner as σ^{xy} , where the charge e is replaced by the energy of a particle $\epsilon_{\mathbf{k}}$, which means we have to sum over all energies $\epsilon_{\mathbf{k}}$ to get κ^{xy} . Chapter 5 will explain

this in much more detail.

Unfortunately we didn't find any data on the thermal Hall-conductivity of BSCCOmaterials. As YBCO has also the layered structure we can get an impression of the
magnitude and the shape of κ^{xy} from the YBCO data. These data are plotted in
figure 4.5. Zhang's group [24] found the temperature dependence of $\kappa^{xy} \propto T^{-1.19}$ (for YBCO). Experiments measure κ^{xy} in $W/m \cdot K$ for given magnetic field **B**. Of course
this quantity varies with the magnetic field.

Figure 4.5 contains also a plot of the Lorenz-number, which compares the thermal conductivity with the electrical conductivity. The group of Zhang used thermal and electrical Hall-conductivities to make sure that there is no contribution due to phonons in the ratio. The value they observe attains the value $\pi^2/3$ near 500K which is predicted by the Wiedemann-Franz law. For small T cuprates don't behave metal-like. This was already pointed out when we looked at the different temperature dependences of ρ^{xx} and $\cot(\theta_H)$ which can not be explained within the framework of Drude.

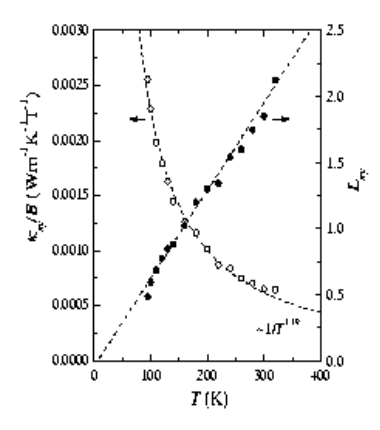


Figure 4.5: The Lorenz-number (solid circles) and κ^{xy} can be extracted from this figure taken from [24]. Their experiment uses a magnetic field to get rid of contributions from phonons to κ^{xy} and the Lorenz number.

Chapter 5

Two patch model for the collision operator

We are going to introduce a phenomenological model, whose goal it is to describe experimental data of transport properties of *BSCCO*, given in chapter 4, now. It was argued in chapter 2 that it is reasonable to describe *BSCCO* in terms of a BE. But as transport data can't be explained with a single relaxation time we suggest a model with two relaxation times. Our interest in DC-properties simplifies our analysis a lot, as we don't have to take FL-corrections explicitly into consideration.

It can be seen from the linearized BE, $\frac{\partial}{\partial t}g_{\mathbf{k}} + e\mathbf{E}\mathbf{v}_{\mathbf{k}}\frac{\partial f_{\mathbf{k}}^0}{\partial \epsilon_{\mathbf{k}}} + \frac{e}{\hbar c}\mathbf{v}_{\mathbf{k}} \times \mathbf{B}\frac{\partial g_{\mathbf{k}}}{\partial \mathbf{k}} = C_{\mathbf{k}}$, given in (3.25), that it is essential to model the collision-operator $C_{\mathbf{k}}$ in it. Note that we are dealing with the steady-state case. So the first term $\frac{\partial}{\partial t}g_{\mathbf{k}}$ vanishes. The material is assumed to be isotropic, which means that also the factor $\nabla_{\mathbf{r}}g_{\mathbf{k}}$ in (3.25) doesn't contribute. As we have only terms in the expression that are of the kind $\tilde{g}_{\mathbf{k}}$ we can make the replacement $\tilde{g}_{\mathbf{k}} \to g_{\mathbf{k}}$ and obtain the equation above.

Because of the term $\frac{\partial f_{\mathbf{k}}^0}{\partial \epsilon_{\mathbf{k}}}$ in the BE the transport process happens at and around the FS.¹

Following the ARPES data shown in figure 2.3 we want to construct a model with alternating big and small scattering around the FS, which is done by introducing two patches in every quadrant of the first BZ. The regions with a big lifetime have low scattering and are called cold regions (they are along the zone-diagonals in the first BZ). In the hot regions (at the nodes) we have big scattering and therefore a small lifetime.

 $^{^{1}}$ In the 0K case we get only a contribution to transport from the FS. In this case we get singular integrals at the FS because of the step in the distribution-function. A more sophisticated method has to be used in the low-temperature limit to compute transport properties. A powerful method is the tetrahedron method, described in the Appendix.

The idea of cold and hot-patches in mind we model the scattering operator $C_{\mathbf{k}}$ with two different scattering rates in different regions of the FS (shown in figure (5.1)).

Our phenomenological two-patch-model (TPM) tries to improve the coldspot-model by Millis and Ioffe [29], who argued to obtain the correct temperature dependence of magnetotransport quantities using only special regions of the FS, namely the "cold spots" that are on the diagonals of the first BZ. They gave four general reasons why the FS should be governed by two different lifetimes, dependent on the position on the FS. Hlubina and Rice [28] suggested a hot spot model to describe the resistivity. The cold spot and the hot spot model were compared with their different scattering matrices in [36].

We are considering both regions in our model to give a better fit of experimental data. The mentioned models show that both can describe single data well, but not a set of different transport properties. Furthermore we consider heat transport that seems to be influenced by the hot regions. That's why we consider both region in our approach. Zheleznyak et al. [5] claimed to get good agreement with experimental results by considering two regions (a cold and a hot one) with different lifetimes τ_1 and τ_2 . This group suggested a ratio between the relaxation rates in the cold and the hot regions of $\frac{\tau_1}{\tau_2} \approx 3.9$. With this ratio of the lifetimes they were able to fit experimental data for the AC Hall-effect well. Our goal is slightly different as we want to introduce a model that fits experimental DC-data of different transport quantities, which are given in chapter 4, for the NS of BSCCO. Anyway the ratio they claim for $\frac{\tau_1}{\tau_2}$ is important as it gives us a hint whether our model is reasonable or not.

As scattering in the cold regions is smaller than in the hot regions, (quasi)particles in the two regions have different average velocities. The knowledge of the energy-dispersion $(\rightarrow FS)$ allows us to compute the velocities \mathbf{v}_c and \mathbf{v}_h in the regions of our interest. We are using a dispersion relation that was proposed in [16].

In this chapter we will follow the ideas given above. Our first task is to find a possibility to describe the two different regions (cold and hot regions) of the FS in a

mathematical way. This is done in section 5.1.

As we are interested in the temperature dependence of transport quantities we have to consider every possible scattering around the FS and apply a temperature dependence to it. We split the first BZ symmetrically into cold and hot regions in order to get a symmetrical scattering matrix.

As a first approximation we use step-functions (θ -functions) to describe the cold and the hot regions of the FS. Later we will switch to functions that change in a smooth way between the cold region and the hot region. Of course the smooth change between the two regions is more sensible from a physical point of view. However it complicates the calculations.

In section 5.2 the FS of *BSCCO* is reproduced by a tight binding fit. Velocities and densities of states are derived for the different regions. We conclude the chapter with analytical calculations of transport quantities whose experimental values are given in chapter 4.

5.1 How to describe the idea of hot and cold regions?

As a first try to describe the two regions we introduce a very easy but discontinuous model. We are starting with the case T=0K, which means we are completely restricted on the FS.

In this (discontinuous) model two step-functions, defined on the FS, are used to describe the cold and the hot region in every quadrant of the first BZ. The model is generalized to temperatures T > 0K afterwards. After this we will improve this model and will introduce a model that describes a smooth change between the cold and the hot region.

5.1.1 Description with step-function

Starting with the zero-temperature case we define two step-functions Φ and Ψ on the FS in the following way:

$$\Phi_{\mathbf{k}} = \begin{cases}
1 & \text{in cold region} \\
0 & \text{otherwise}
\end{cases}$$
(5.1)

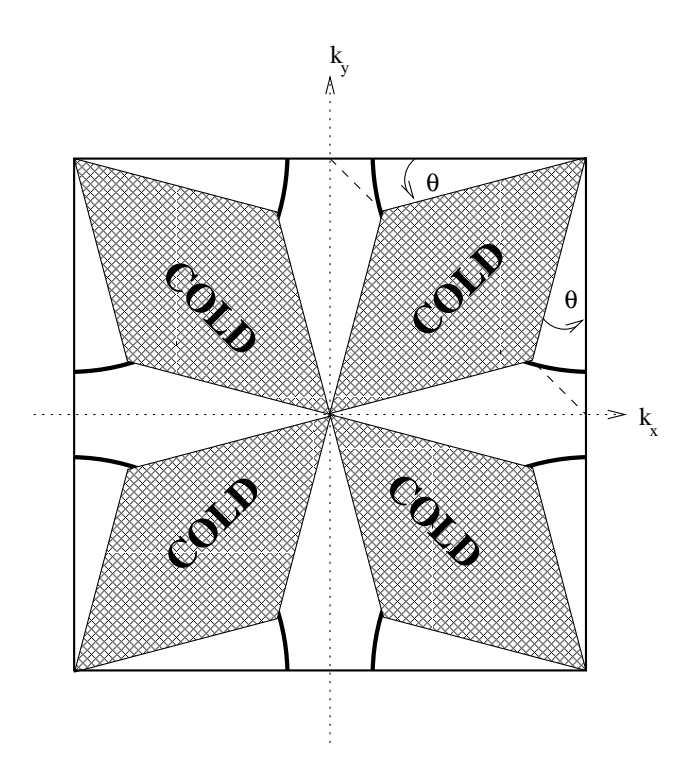


Figure 5.1: The cold region of the first BZ is symmetrically divided into cold and hot regions. We can model the cold region by a product of four θ -functions. Note that the angle θ parameterizes the size of the cold region.

$$\Psi_{\mathbf{k}} = \begin{cases}
1 & \text{in hot region} \\
0 & \text{otherwise}
\end{cases}$$
(5.2)

Note that these functions are only defined on the FS!

We normalize the length of the arc to 1, i.e. we normalize the length of the FS in the first quadrant to 1. Now we can write that the length of the cold region of the Fermi surface has the length α .² Figure 5.2 shows the geometry which we introduced above.

The two step functions Φ and Ψ allow us to write down the scattering matrix $C_{\mathbf{k},\mathbf{k}'}$ used in the collision operator $C_{\mathbf{k}} = \sum_{\mathbf{k}'} C_{\mathbf{k},\mathbf{k}'} [g_{\mathbf{k}'} - g_{\mathbf{k}}]$ in the following way

$$C_{\mathbf{k},\mathbf{k}'} = a\Phi_{\mathbf{k}}\Phi_{\mathbf{k}'} + b\Psi_{\mathbf{k}}\Psi_{\mathbf{k}'} + c[\Phi_{\mathbf{k}}\Psi_{\mathbf{k}'} + \Psi_{\mathbf{k}'}\Phi_{\mathbf{k}'}]$$
(5.3)

²The arc is normalized to one using $\frac{1}{N_{\mathbf{k}}} \sum_{\mathbf{k}} [\Phi_{\mathbf{k}} + \Psi_{\mathbf{k}}] = 1$. So the length of the cold region, α , can be easily obtained from $\alpha = \frac{1}{N_{\mathbf{k}}} \sum_{\mathbf{k}} \Phi_{\mathbf{k}}$.

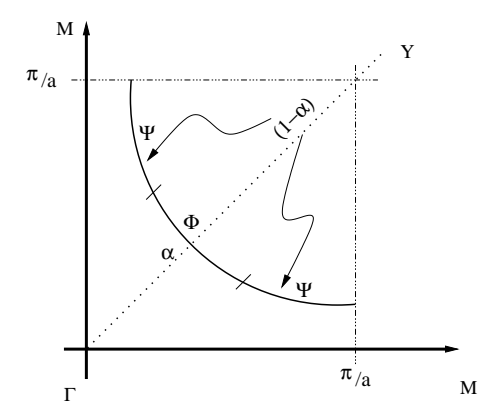


Figure 5.2: The figure shows the FS with the cold and the hot regions for the T=0K-case. The functions Ψ and Φ are defined in the way described in the text. Normalizing the length of the arc of the FS to 1 allows us to write the length of the cold region as α .

where the constant a represents the scattering inside the cold region, constant b represents the scattering in the hot region and the constant c represents the inter-patch scattering.³

Note that the scattering matrix is constructed in a symmetrical way (especially the last term in (5.3) was symmetrized!). That means it is symmetric around the Γ -Y-direction like shown in figure 5.2. The symmetric construction of this operator will become of great help later.

We give the constants a,b and c inside the collision-operator (5.3) of our model the following phenomenological temperature-dependences:

$$a = \bar{a} \cdot T^2 \tag{5.4}$$

$$b = \bar{b} \tag{5.5}$$

$$c = \bar{c} \cdot T \tag{5.6}$$

where \bar{a} , \bar{b} and \bar{c} are temperature independent. In other words scattering inside the cold region is $\propto T^2$, scattering inside the hot region is independent of temperature and scattering between the two regions is $\propto T$. This choice is reasonable as the lifetime inside the cold region is FL-like, thus $\propto T^2$, as (quasi)particles in this region have a

 $^{^3}$ In the cold-spot model of Millis and Ioffe [29] the scattering matrix is constructed with terms $\propto \sin^2$ and \cos^2 obeying the lattice symmetry. So they can generate a model that has big scattering in the hot region and small scattering in the cold region.

quite big lifetime. We know from experiments that the resistivity perpendicular to the CuO_2 -planes, ρ^c , which is governed by the hot regions as the inter-plane hopping is maximal for momenta parallel to $(\pi,0)$, is almost independent of temperature [18]. Thus the temperature dependence of a and b is reasonable. For c we choose a temperature dependence that is between T^2 and T^0 . So we apply a temperature dependence $\propto T$. We know from chapter 3 that summing over the scattering matrix $\sum_{\mathbf{k}'} C_{\mathbf{k},\mathbf{k}'}$ gives us the inverse relaxation time $\tau_{\mathbf{k}}^{-1}$. Thus this calculation will tell us the (different) relaxation times in the cold and in the hot regions.

$$\frac{1}{\tau_{\mathbf{k}}} = \sum_{\mathbf{k}'} C_{\mathbf{k},\mathbf{k}'} = a\Phi_{\mathbf{k}} \sum_{\mathbf{k}'} \Phi_{\mathbf{k}'} + b\Psi_{\mathbf{k}} \sum_{\mathbf{k}'} \Psi_{\mathbf{k}'} + c\Phi_{\mathbf{k}} \sum_{\mathbf{k}'} \Psi_{\mathbf{k}'} + c\Psi_{\mathbf{k}} \sum_{\mathbf{k}'} \Phi_{\mathbf{k}'}$$

$$= \sum_{\mathbf{k}'} \Phi_{\mathbf{k}'} [a\Phi_{\mathbf{k}} + c\Psi_{\mathbf{k}}] + \sum_{\mathbf{k}'} \Psi_{\mathbf{k}'} [c\Phi_{\mathbf{k}} + b\Psi_{\mathbf{k}}]$$

$$= \alpha [a\Phi_{\mathbf{k}} + c\Psi_{\mathbf{k}}] + (1 - \alpha)[c\Phi_{\mathbf{k}} + b\Psi_{\mathbf{k}}]$$

with the area of the cold region $\alpha = \sum_{\mathbf{k}} \Phi_{\mathbf{k}}$ and the area of the hot region $1-\alpha = \sum_{\mathbf{k}} \Psi_{\mathbf{k}}$. A general expression for the relaxation time has the form:

$$\tau_{\mathbf{k}} = \frac{1}{\Phi_{\mathbf{k}} C_{\Phi} + \Psi_{\mathbf{k}} C_{\Psi}} \tag{5.7}$$

with the constants $C_{\Phi} = \alpha a + (1 - \alpha)c$ and $C_{\Psi} = \alpha c + (1 - \alpha)b$. When we generalize to the case of functions that change smoothly between the patches we have to remember this.

Using this result we find an expression for the relaxation times in our model (in the case of step functions): 4

$$\tau_{\mathbf{k}} = \begin{cases} \frac{1}{\alpha a + (1 - \alpha)c} & \text{in cold region, } \tau_c \\ \frac{1}{\alpha c + (1 - \alpha)b} & \text{in hot region, } \tau_h \end{cases}$$
 (5.8)

with the relaxation time in the cold region τ_c and in the hot region τ_h respectively. Zheleznyak et al. [5] pointed out that the ratio between the two scattering times τ_c

⁴When we insert the temperature dependence for a,b and c given in equations (5.4) (to get a dimensionless result) we obtain: $\tau_c = \frac{\hbar}{\alpha \frac{\hbar \bar{a}}{k_B^2} (k_B T)^2 + (1-\alpha) \frac{\hbar \bar{c}}{k_B} (k_B T)}$ and $\tau_h = \frac{\hbar}{(1-\alpha)\hbar \bar{b} + \alpha \frac{\hbar \bar{c}}{k_B} (k_B T)}$, where we have multiplied by \hbar to define everything in terms of energies. The dimension of the relaxation time is $|\tau| = 1s$.

We obtain the following dimensions: $\left[\frac{\hbar\bar{a}}{k_B^2}\right] = \frac{1}{eV}$, $\left[\hbar\bar{b}\right] = eV$ and $\left[\frac{\hbar\bar{c}}{k_B}\right] = 1$. These should be the quantities we are searching for. As we are searching for these quantities (given in terms of energies) we have to give the temperature in eV and multiply by a factor (because of \hbar !) in our program.

and τ_h is of interest to fit experimental results for the Hall-conductivity. If we look at the low and at the high-temperature limit of this ratio we get a linear temperature dependence for this ratio, which means the ratio between the two lifetimes τ_c and τ_h is not independent of temperature:

$$\begin{split} \frac{\tau_h(T)}{\tau_c(T)} &= \frac{\alpha a + (1-\alpha)c}{\alpha c + (1-\alpha)b} &= \frac{\alpha \bar{a} T^2 + (1-\alpha)\bar{c} T}{\alpha \bar{c} T + (1-\alpha)\bar{b}} = T \frac{\alpha \bar{a} T + (1-\alpha)\bar{c}}{\alpha \bar{c} T + (1-\alpha)\bar{b}} \\ &\lim_{T \to 0} \frac{\tau_h(T)}{\tau_c(T)} &= \frac{\bar{c}}{\bar{b}} \cdot T = \frac{\tau_h}{\tau_c} [T, \alpha = 0] \\ &\lim_{T \to \infty} \frac{\tau_h(T)}{\tau_c(T)} &= \frac{\bar{a}}{\bar{c}} \cdot T = \frac{\tau_h}{\tau_c} [T, \alpha = 1] \end{split}$$

In the low-temperature-limit we get a result that represents the case where we don't have a cold region. The whole first BZ is hot for $T \to 0K$. The opposite limit represents the case of no hot region, thus the whole BZ is cold for $T \to \infty$.

The step-functions we are using in this subsection allow us to write arbitrary velocities \mathbf{v} in terms of a "cold" and a "hot" velocity:

$$\mathbf{v} = \mathbf{v}_c \Phi_{\mathbf{k}} + \mathbf{v}_h \Psi_{\mathbf{k}} \tag{5.9}$$

The underlying assumption is that there is only one velocity in every patch. Later we are generalizing the idea of two different velocities in each patch and will compute the velocity at every point and decide what the character of the point is (cold or hot?). It is of peculiar interest how the scattering matrix $C_{\mathbf{k},\mathbf{k}'}$ acts on an arbitrary velocity $\mathbf{v}_{\mathbf{k}}$. This problem is also pointed out in the article of Abrahams and Varma [38] that constructed a different model to describe transport for cuprates.⁵ The symmetrical construction of the scattering matrix $C_{\mathbf{k},\mathbf{k}'}$ and the fact that every velocity (at the FS) has its negative velocity on the opposite side of the FS tells us that the sum $\sum_{\mathbf{k}'} C_{\mathbf{k},\mathbf{k}'} \mathbf{v}_{\mathbf{k}'}$ over the FS (later over the whole BZ) vanishes in our model,

$$\sum_{\mathbf{k}'} C_{\mathbf{k},\mathbf{k}'} \mathbf{v}_{\mathbf{k}'} = 0 \tag{5.10}$$

⁵In their small angle forward scattering model they model the scattering operator $C_{\mathbf{k},\mathbf{k}'}$ such that it contains a large angle scattering part and a small angle forward scattering part.

Due to the factor $\frac{\partial f_{\mathbf{k}}^0}{\partial \epsilon_{\mathbf{k}}}$ in the BE the equation allows only wave-vectors on the FS to be a solution of it in the case of zero temperature. However our interest in the temperature dependence of transport quantities forces us to raise the temperature.

When we raise the temperature from 0K to some finite temperature the term $\frac{\partial f_{\mathbf{k}}^0}{\partial \epsilon_{\mathbf{k}}}$ given in the BE, is no more a δ -function. It's like a Gaussian with some width which is $\approx k_B T$. This fact makes it necessary to split the complete first BZ into a cold and a hot part, as shown in figure 5.1. In order to conserve the symmetry of $C_{\mathbf{k},\mathbf{k}'}$, the symmetry around the diagonals should be conserved. This fact forces us to parameterize the cold and hot regions in a way similar to the suggestion of Hlubina and Rice [28].

At finite temperature we describe the cold area of our model in the first quadrant of the BZ as a product of four step functions (compare to figure 5.3). An angle dependent parameterization of this region seems obvious, as this allows us to vary the size of the cold (thus also of the hot) region. Constants that only depend on an angle θ (which parameterizes the size of the cold region) are introduced. The θ -dependence of the constants is given by:

$$a = \cot(\theta) > 0 \tag{5.11}$$

$$b = \tan(\theta) > 0, a > b \tag{5.12}$$

$$c = \pi(1 - \tan(\theta)) > 0$$
 (5.13)

$$d = \pi(1 - \cot(\theta)) < 0 \tag{5.14}$$

These constants allow us to write down four lines that separate the cold and the hot regions. Figure 5.3 shows how we split the first BZ into these two regions. It also tells us how to write down the cold regions using step-functions.

As there are four separated cold regions we obtain four cold areas in the first BZ. Only one of them is described in figure 5.3.

As we started to write the cold region with the function $\Phi_{\mathbf{k}}$ in the T=0K-case, will continue with this notation. The whole cold region is given by:

$$\Phi(\mathbf{k}) = \sum_{i=1}^{4} \Phi_i(\mathbf{k}) \tag{5.15}$$

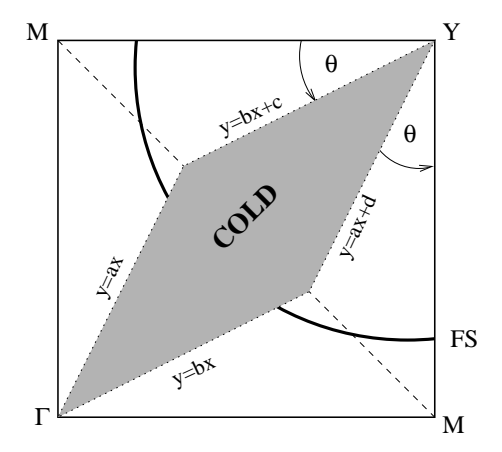


Figure 5.3: The cold region of the first quadrant of the BZ is described as a product of four θ -functions, which are determined by the angle-dependent constants a, b, c and d.

where the $\Phi_i(\mathbf{k})$ are given by

$$\begin{split} &\Phi_1(\mathbf{k}) &= \Theta(ak_x-k_y)\Theta(k_y-bk_x)\Theta(bk_x+c-k_y)\Theta(k_y-ak_x-d) \\ &\Phi_2(\mathbf{k}) &= \Theta\left(-\frac{1}{b}k_x-k_y\right)\Theta\left(k_y+\frac{1}{a}k_x\right)\Theta\left(-\frac{1}{a}k_x+c-k_y\right)\Theta\left(k_y+\frac{1}{b}k_x-d\right) \\ &\Phi_3(\mathbf{k}) &= \Theta(bk_x-k_y)\Theta(k_y-ak_x)\Theta(ak_x-d-k_y)\Theta(k_y-bk_x+c) \\ &\Phi_4(\mathbf{k}) &= \Theta\left(-\frac{1}{a}k_x-k_y\right)\Theta\left(k_y+\frac{1}{b}k_x\right)\Theta\left(-\frac{1}{b}k_x-d-k_y\right)\Theta\left(k_y+\frac{1}{a}k_x+c\right) \end{split}$$

with the indices *i* referring to the cold region in the four quadrants. As everything that is not cold is hot (in the case of the step-function) the cold regions describe the hot region indirectly, using $\Psi_{\bf k} = 1 - \Phi_{\bf k}$.

The case of the description of the cold/hot region with step-functions is very useful, as it teaches us how to describe the regions when dealing with a smooth change between them.

5.1.2 Description with a smooth function

In the previous subsection we described the cold and hot regions with a discontinuous function, a θ -function. Due to this discontinuous change between this regions the lifetime around the FS also changes discontinuously (compare to (5.8)) which is very unlikely in nature. We try to get rid of this discontinuity by introducing a function that changes rapidly but smoothly between the cold and the hot region. Another

reason for an introduction of a smooth change between the cold and the hot region is the divergence of the magnetoresistance in the case of the step function (described below).

Zheleznyak et al. suggested a smooth transition function [6] that has the properties we

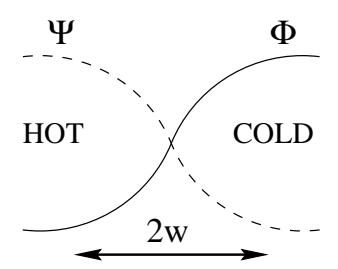


Figure 5.4: The figure shows the case where cold and hot regions have an overlap in common. The transition width w is a parameter what allows to study the effects of this region on transport properties. Note that the functions Φ and Ψ don't vanish completely outside the transition region.

are interested in. In this section we will replace the θ -function by a smooth functions, making the substitution⁶

$$\theta(x) \to \lim_{w \to 0} \frac{1 + \tanh \frac{x}{w}}{2} \tag{5.16}$$

with the transition width w explained in figure 5.4. Note that the functions Φ and Ψ don't vanish completely outside the transition region! So we have some finite (very small) contribution of one function in the other patch next to the transition region (compare to figure 5.4). In the case of the smooth change between the cold and the hot region we have to use equation (5.7) for the calculation of $\tau_{\mathbf{k}}$.

As we choose a function with a variable width w the θ -function used before can be obtained from the limit $\theta(x) = \lim_{w \to 0} \frac{1 + \tanh \frac{x}{w}}{2}$.

The variable width w allows us to study the effect of a change in w on the transport properties of cuprates. We'll see what transport quantity is sensitive to the width w and which is not.

Similar to the case of the step function we can write the cold region, this time only

⁶One can easily show that the relation $\frac{1+\tanh\frac{x}{w}}{2} = 1-f\left(\frac{x}{w/2}\right)$ is valid, where f is the Fermi-function, $f(x) = \frac{1}{e^{\beta x}+1}$.

⁷Note that this smooth function decays exponentially for |x| > 2w!

in the first quadrant, as a product of four tanh-functions. The cold region of the first quadrant is now given by:

$$\Phi_{\mathbf{k}} = \prod_{i=1}^{4} \Phi_i(\mathbf{k}) \tag{5.17}$$

with

$$\Phi_{1}(\mathbf{k}) = \frac{1}{2} \left[1 - \tanh\left(\frac{k_{y} - ak_{x}}{w}\right) \right]
\Phi_{2}(\mathbf{k}) = \frac{1}{2} \left[\tanh\left(\frac{k_{y} - bk_{x}}{w}\right) + 1 \right]
\Phi_{3}(\mathbf{k}) = \frac{1}{2} \left[1 - \tanh\left(\frac{k_{y} - bk_{x} - c}{w}\right) \right]
\Phi_{4}(\mathbf{k}) = \frac{1}{2} \left[\tanh\left(\frac{k_{y} - ak_{x} - d}{w}\right) + 1 \right]$$

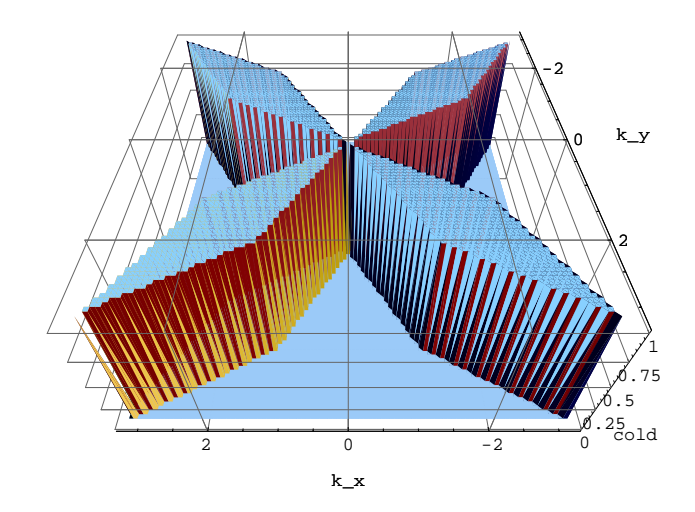
where the coefficients a, b, c, d (given in equation (5.11) etc.) are determined by the angle θ that determines the size of the cold region. Note that we insert the factor $\frac{1}{16}$, because every function $\Phi_1(k)$ - $\Phi_4(k)$ makes a jump of the height 2. Thus each function $\Phi_1(k)$ - $\Phi_4(k)$ has to be divided by 2.

Note that equation (5.7) simplifies to (5.8) in the limit $w \to 0$.

Finally we plot the difference between the discontinuous and the continuous change between the regions in figure (5.5). The "3D-plot" illustrates the TPM.

We conclude this section with a final remark on the functions that describe the cold and the hot regions.

By construction the functions Ψ and Φ have the same symmetry as the FS which will be introduced in the next section. Thus the introduced functions $\Phi_{\mathbf{k}}, \Psi_{\mathbf{k}}$ are even functions. They are symmetric to the k_x and k_y -axis (they have fourfold-symmetry!). It is shown in the Appendix that the derivatives of these functions, $\frac{\partial \Phi_{\mathbf{k}}}{\partial k_{x/y}}$, $\frac{\partial \Psi_{\mathbf{k}}}{\partial k_{x/y}}$, are odd functions. Also the useful relation $\frac{\partial \Phi_{\mathbf{k}}}{\partial k_x} = -\frac{\partial \Psi_{\mathbf{k}}}{\partial k_x}$ (the same is of course valid for derivatives with respect to k_y) is shown there.



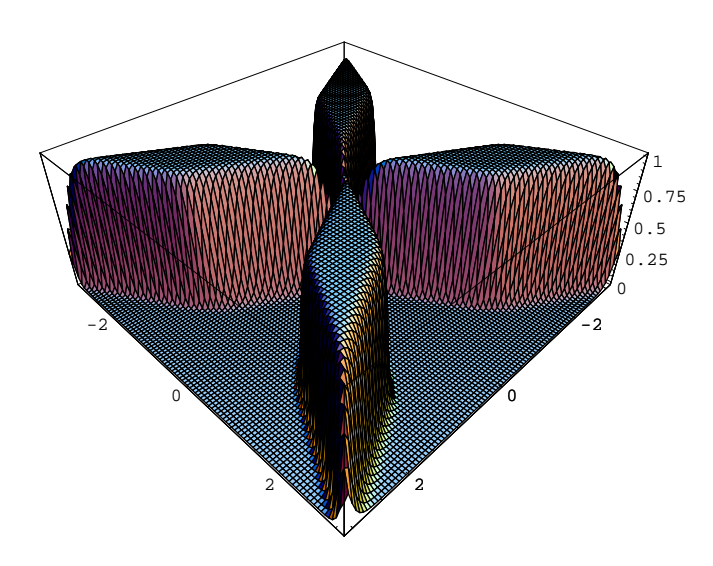


Figure 5.5: The upper picture shows the case of the step functions. So the cold and the hot regions are strictly separated. The lower picture shows the case of a smooth change between the two regions with w = 0.1. The angle of both cases is $\theta = \pi/6$.

i	c_i/eV	η_i
1	0.1305	1
2	-0.5951	$\frac{1}{2}[\cos(k_x) + \cos(k_y)]$
3	0.1636	$\cos(k_x)\cdot\cos(k_y)$
4	-0.0519	$\frac{1}{2}[\cos(2k_x) + \cos(2k_y)]$
5	-0.1117	$\frac{1}{2}[\cos(2k_x)\cos(k_y) + \cos(2k_y)\cos(k_x)]$
6	0.0510	$\cos(2k_x)\cdot\cos(2k_y)$

Table 5.1: The table shows the parameter suggested by [16] to fit the FS of BSCCO.

5.2 Constructing the Fermi-surface

Our main goal is to calculate the temperature dependence of transport properties of cuprates within the TPM-framework. A good knowledge of the FS is of peculiar interest for the computation of magnitudes like velocities, densities of states etc.. The detailed shape of the FS is very important to derive transport-quantities like DC-conductivity, Hall-conductivity etc., from the model in a numerical way.

To model the FS of *BSCCO* we follow the tight-binding fit given by Norman [16]. The tight binding fit contains hopping up to the fifth nearest neighbor! Note that we used this fit to generate the FS showed in figure 2.4.

From the FS we can derive the velocity at every point inside the first BZ and the density of states $N(\epsilon)$. Quantities we will need for further calculations.

The FS of Bi2212 is reproduced by $\xi(k_x, k_y) = 0$, where $\xi(k_x, k_y)$ is given by:

$$\xi(k_x, k_y) = \sum_{i=1}^{6} c_i \cdot \eta_i(k_x, k_y)$$
 (5.18)

with the values c_i , η_i given in the table below: Obviously we didn't write down explicitly the lattice-spacing a in every function given in the table above. The lattice constant a for BSCCO is given by

$$a = 3.76 \cdot 10^{-10} m = 3.76 A^{\circ} \tag{5.19}$$

The FS of BSCCO has, as the lattice, fourfold symmetry like it is shown in figure 2.4.

5.2.1 Velocities in the cold and in the hot regions

It was pointed out by Zheleznyak [5] that the velocity and the relaxation time varies in the two regions. His group considered only two values, a cold and a hot one, for these quantities to describe the transport process, whereas we are going to compute the velocity (from the energy-dispersion-relation given in (5.18)) and the relaxation time (compare to (5.8)) for each (discretized) point inside the first BZ.

In order to get a feeling for the magnitude of the velocity in the cold and hot region of optimally doped Bi2212 we need to figure out the energy gap in the dispersion-relation in the directions (π, π) and $(0, \pi)$. Experimental data for optimally doped Bi2212, given in [13], show that the energy difference $\Delta \epsilon$ in M-Y-direction is $\Delta \epsilon^{MY} = 0.087 eV$. In the diagonal direction, $\Gamma - Y$ -direction, the difference is given by $\Delta \epsilon^{\Gamma Y} = 0.6 eV$.

The absolute values of the two different velocities v_c and v_h^8 can be computed from the values of $\Delta \epsilon$ given above. Figure (5.6) describes which **k**-points we have to determine to estimate the absolute value of the velocities v_c and v_h .

We obtain the velocities v_f^{MY} and $v_f^{\Gamma Y}$ (the cold and the hot velocities) from the equation, $v=\frac{1}{\hbar}\frac{\Delta\epsilon}{\Delta k_f}$ with the energy-differences $\Delta\epsilon$ given in [13]. When we solve the equations $f(x,k_f^{MY})=0$ ($f(x,k_f^{MY})=0$) ($f(x,k_f^{MY})=0$) ($f(x,k_f^{MY})=0$) we obtain the wave-vectors of interest, described in figure 5.6. A numerical solution gives us the velocities $f(x,k_f^{MY})=0$ ($f(x,k_f^{MY})=0$) we obtain the wave-vectors of interest, described in figure 5.6.

$$v_f^{MY} = 0.154 \frac{eV \cdot a}{\hbar} \tag{5.20}$$

$$v_f^{\Gamma Y} = 0.487 \frac{eV \cdot a}{\hbar} \tag{5.21}$$

and therefore their ratio as:¹⁰

$$\frac{v_f^{\Gamma Y}}{v_f^{MY}} = \frac{v_c}{v_h} = 3.16 \tag{5.22}$$

⁸In the program we are computing the velocity at every point of the lattice. A simplification of this deals with only two different velocities - a cold and a hot velocity.

⁹Compare to figure 5.6.

 $^{^{10}}$ It is interesting that $v_f^{\Gamma Y}$ is almost independent on doping. On the other hand v_f^{MY} depends on it.

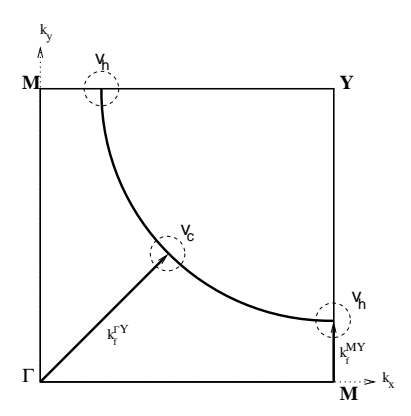


Figure 5.6: We introduce the two wave-vectors k_f^{MY} and $k_f^{\Gamma Y}$ in this figure. These wave-vectors allow us (together with the values of $\Delta \epsilon$) to compute the absolute value of the velocities v_c and v_h .

Which means particles moving in the cold region move much faster than particles in the hot region.

Obviously transport properties are connected to the number of available (quasi)particles as well. Thus our next important step is to compute the density of states in the cold and in the hot region or better the angle dependent density of energy states $N(\epsilon, \theta)$.

5.2.2 Density of energy states in cold and hot region

We want to compute the density of states in the cold and in the hot region of Bi2212 numerically in this subsection. Thus we have to divide the first BZ such that it differs between cold and hot regions, as shown before. The possibility of changing the size of the cold region by changing θ has to be included into the density of energy states $N(\epsilon)$. Inside one patch the densities $N_c(\epsilon)$ or $N_h(\epsilon)$ are only dependent on the energy ϵ . The energy-dependent density of states $N(\epsilon)$ is defined in the following way:

$$N(\epsilon) = \frac{1}{N_k} \sum_{\mathbf{k}} \delta(\epsilon_{\mathbf{k}} - \epsilon)$$
 (5.23)

where N_k is the number of considered energy-values.

Figure (5.1) shows the two regions on the FS, which are determined by θ . The tight binding fit given in equation (5.18) allows us to compute the density of states in the

cold and in the hot regions (for variable θ), $N_c(\epsilon) = \frac{1}{N_k} \sum_{\mathbf{k}} \delta(\epsilon_{\mathbf{k}} - \epsilon) \Phi_{\mathbf{k}}$ and $N_h(\epsilon)$ analogously.

Figure (5.7) shows the energy densities N_c and N_h for different sizes (different θ) of the cold region. The figure was obtained by a mash of $n_k = 1024$. The energy was splitted in 500 equal values. Note that the figure represents the case w = 0, thus the case of step functions.

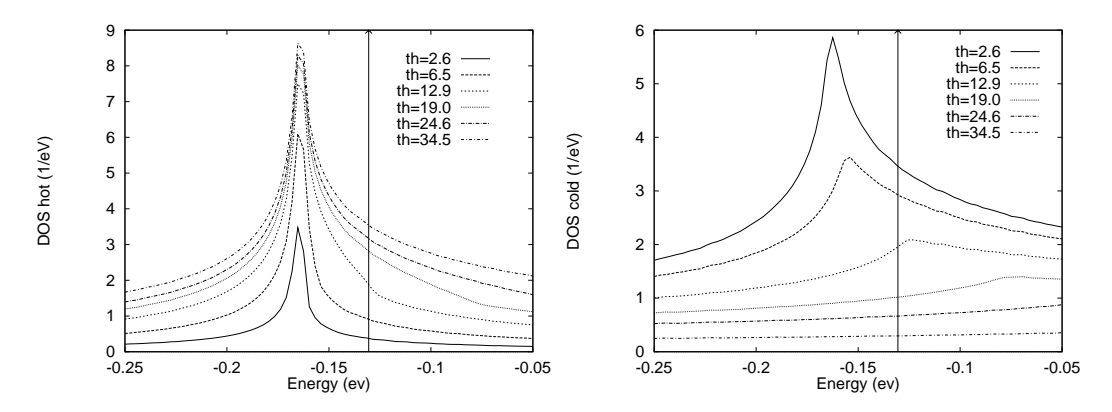


Figure 5.7: The two plots show the density of states around the Fermi level, $\epsilon_F = -0.1305 eV$. The left picture shows the density of states in the neighborhood of the Fermi surface in the hot region for different angles θ . The maximum in N_h (van-Hove singularity) is about 35meV away from the Fermi-level. The density of states in the cold region, shown in the right picture, changes much more with varying θ than N_h . The derivative of the density of states changes its sign at the FS at $\theta \approx 10^{\circ}$. For $\theta \approx 10^{\circ}$ the maximum in N_c is on the Fermi surface.

It is remarkable that the distribution in the hot region is quite symmetric around the van Hove singularity (VHS), which is about 35meV away from the Fermi-energy. The shape of the density remains the same for different angles θ . Only the absolute value increases with increasing angle. The first derivative of this density of states at the Fermi level, which is at $\epsilon_f \approx -0.13eV$, is always negative.

The cold density of states is not as symmetric around the van Hove singularity as it is the hot one. As can be seen from the graphs N_c decreases with increasing angle θ . Also $N'_c(\epsilon_f)$ changes its sign, dependent on θ , $N'_c(\epsilon_f) = 0$ for $\theta \approx 10^\circ$. These properties of N will become important for the calculation of the thermopower.

The change in the sign of $N'_c(\epsilon_f)$ can be understood, as we have two different types of FS's dependent on the angle θ . When $\theta > \theta_{critic}$ we have a closed FS (left figure in

$\theta/^{\circ}$	2.6	6.5	12.9	19.0	24.6	34.6
α (cold)	0.942	0.856	0.713	0.578	0.453	0.231
$1 - \alpha \text{ (hot)}$	0.058	0.144	0.287	0.422	0.547	0.769
$N_c(\theta) _{\epsilon_F}/a^3eV$	1.72	1.46	0.98	0.51	0.33	0.15
$N_c'(\theta) _{\epsilon_F}/a^3(eV)^2$	-15	-9.45	13.7	1.87	0.74	0.29
$\frac{N_c'}{N_c} _{\epsilon_F}/eV$	-8.72	-6.47	13.98	3.67	2.24	1.93

Table 5.2: Dependent on the angle θ the density of states and its derivative is computed.

figure 5.8). Therefore the particles are electron-like. For angles $\theta < \theta_{critic}$ we have an open FS (right figure). These particles behave like holes.¹¹

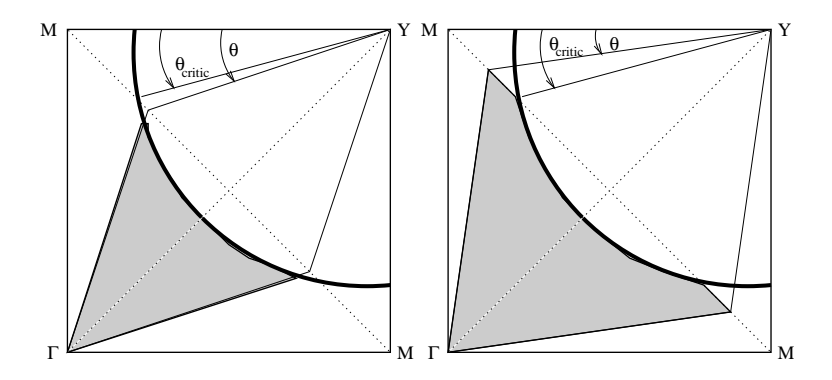


Figure 5.8: It can be seen that the FS changes from an open one to a closed FS (depending on the angle θ). Thus the character of the particles changes from electron-like to hole-like with increasing θ . The left figure shows a closed FS (electrons), whereas the right figure shows a open FS (holes).

In the table below shows the size of the cold/hot region, the density of states of both regions at the FS and its first derivatives can be found dependent on θ . The derivatives of N_c were obtained graphically.

¹¹The critical angle θ_{critic} is given by $\theta_{critic} \approx 9.5^{\circ}$.

5.2.3 Van-Hove singularities (VHS)

In general we can obtain a singularity or a singular point when the condition $\nabla \cdot \epsilon_{\mathbf{k}} = 0$ is satisfied.¹² In the case of the nearest neighbor hopping we obtain the condition for singular points

$$\nabla \cdot \epsilon_{\mathbf{k}} = 2t \left\{ \begin{array}{c} \sin(k_x) \\ \sin(k_y) \end{array} \right\} = 0$$

that has to satisfied to obtain an extremum in the energy. The condition mentioned above doesn't tell us about the character of the extremum.

We obtain nine possible critical points in the first BZ $\begin{pmatrix} k_x = 0, \pm \pi \\ k_y = 0, \pm \pi \end{pmatrix}$. The possible singular points and their character in the case of nearest-neighbor-hopping is shown in figure (5.9).

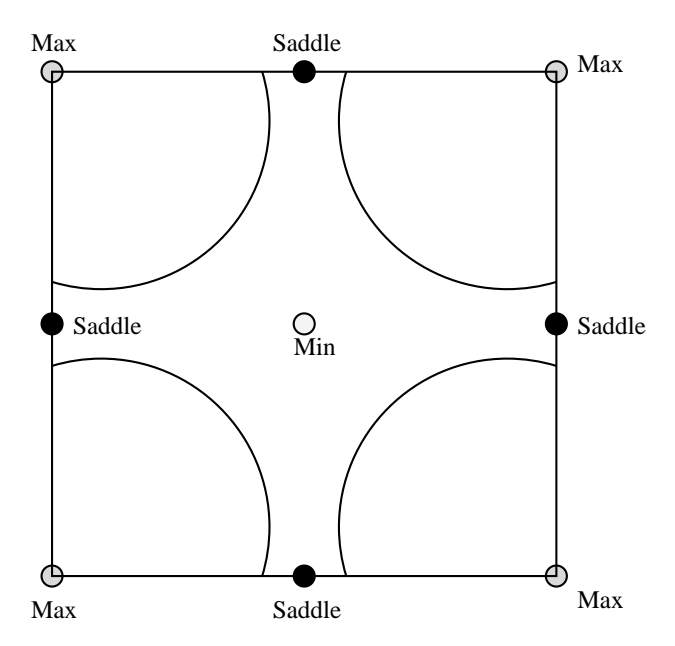


Figure 5.9: The picture shows the minima/maxima and the saddle points in the energy obtained from a nearest neighbor hopping model.

As shown in figure (5.9) we obtain VHS, singularities in the density of states, in the

¹²In the nearest neighbor-hopping case the energy-dispersion has the form known from the Hubbard model: $\epsilon_{\mathbf{k}} = -2t[\cos(k_x) + \cos(k_y)]$.

four points: $(0, \pi)$, $(\pi, 0)$, $(-\pi, 0)$, $(-\pi, -\pi)$.

To compute the energy difference between the Fermi energy and the VHS we have to use (5.18) which models the FS of Bi2212. In $(0, \pi)$ we obtain the difference between the Fermi-energy and the VHS from (5.18) as:

 $(0.1305eV) - (0.1636eV) + (-0.0519eV) + (0.0510eV) \approx -35meV$. The (logarithmic) divergence in the density of states is $\approx 35meV$ away from the Fermi-energy, which is in agreement with figure 5.7.

5.3 The different types of transport

It was already pointed out in chapter 3 that the BE includes only two forcing terms, namely an external electric field \mathbf{E} or an external temperature-gradient ∇T .

We are introducing all possible currents \mathbf{j} that occur due to one (or both) of the external fields described above. A electrical current is named \mathbf{j}_e , whereas a heat current \mathbf{j}_Q has the label Q. In matrix notation all possible currents are given by:

$$\begin{pmatrix} \mathbf{j}_e \\ \mathbf{j}_Q \end{pmatrix} = \begin{pmatrix} \bar{\sigma} & \bar{S} \\ \bar{S} & \bar{\kappa} \end{pmatrix} \begin{pmatrix} \mathbf{E} \\ -\frac{\nabla T}{T} \end{pmatrix}$$
 (5.24)

with the electrical conductivity tensor $\bar{\sigma}$, the thermal conductivity tensor $\bar{\kappa}$ and the thermopower \bar{S} that connects a temperature gradient with e electric current or vice versa. The definition given in (5.24) is symmetric as we use the term $\nabla T/T$ to describe the temperature gradient.

Castellani et al. [8] used a slightly different notation as used in (5.24) as they define the transport equation without dividing by T. Our formulas agree with their results besides this difference.

Typical sums we have to compute when we are estimating the tensors given in (5.24) are of the form $e^{2-\alpha} \sum_{\mathbf{k}\mathbf{k}'} \epsilon_{\mathbf{k}}^{\alpha} v_{\mathbf{k}}^{\mu} \hat{A}_{\mathbf{k}\mathbf{k}'}^{-1}(\mathbf{k}) v_{\mathbf{k}'}^{\nu} \left(-\frac{\partial f_{\mathbf{k}}^{0}}{\partial \epsilon_{\mathbf{k}'}}\right)$ (compare to [2]), where \hat{A}^{-1} is a matrix that follows directly from the BE given in chapter 3 and will be introduced in the next section. Electrical conductivities, σ^{xx} , σ^{xy} and $\Delta \sigma^{xx}(\mathbf{B})$, are obtained for $\alpha = 0$. In the case $\alpha = 2$ we obtain thermal conductivities, like κ^{xy} . For $\alpha = 1$ we obtain e.g. S^{xx} . The three different cases will be the object of the following three sections.

5.4 Electrical Conductivity $\sigma^{\mu\nu}$

This section deals with electrical, thus charge transport. 13 Every moving "free" particle carries the charge e.

We are going to compute the DC-conductivity σ^{xx} , the Hall-conductivity σ^{xy} and the change in the longitudinal DC-conductivity due to a magnetic field $\Delta \sigma^{xx}(\mathbf{B})$ in this section using the TPM. The results can be compared with the experimental values given in chapter 4.

Our proceding is exactly the same as in [11] and [38]. We start with a linearized BE, introduce an operator \hat{A} , solve the BE in terms of free particles and finally obtain a general formula for the conductivity tensor $\sigma^{\mu\nu}$. The choice of the scattering matrix $C_{\mathbf{k},\mathbf{k}'}$ is of course different from [38].

In a general approach the current is given by $\mathbf{j} = e \sum_{\mathbf{k}} \mathbf{v}_{\mathbf{k}} \cdot g_{\mathbf{k}}$, with the number of free particles $g_{\mathbf{k}}$.¹⁴ that has to be determined from the BE (3.25) for a DC magnetic field.

Considering the steady-state, isotropic case we can rewrite the BE given in (3.25) in the following linearized way:

$$e\mathbf{E}\mathbf{v}_{\mathbf{k}}\left(\frac{\partial f_{\mathbf{k}}^{0}}{\partial \epsilon_{\mathbf{k}}}\right) + \frac{e}{\hbar c}(\mathbf{v}_{\mathbf{k}} \times \mathbf{B})\frac{\partial g_{\mathbf{k}}}{\partial \mathbf{k}} = C_{\mathbf{k}}$$
 (5.25)

with the external electric field and magnetic field **E** and **B**.

The scattering operator $C_{\mathbf{k}}$ has the usual form $C_{\mathbf{k}} = \sum_{\mathbf{k}'} \left[C_{\mathbf{k},\mathbf{k}'} g_{\mathbf{k}'} - C_{\mathbf{k},\mathbf{k}'} g_{\mathbf{k}} \right]$ given in equation (3.5) and the relaxation time of state \mathbf{k} is defined as $1/\tau_{\mathbf{k}} \equiv \sum_{\mathbf{k}'} C_{\mathbf{k},\mathbf{k}'}$ as already mentioned in chapter 3. We can solve equation (5.25) by rewriting it as:

$$\left[\frac{e}{\hbar c}(\mathbf{v}_{\mathbf{k}} \times \mathbf{B}) \cdot \nabla_{\mathbf{k}} + \frac{1}{\tau_{\mathbf{k}}}\right] g_{\mathbf{k}} - \sum_{\mathbf{k}'} C_{\mathbf{k}, \mathbf{k}'} g_{\mathbf{k}'} =$$

$$= \left[e\mathbf{v}_{\mathbf{k}} \mathbf{E}\right] \cdot \left(-\frac{\partial f_{\mathbf{k}}^{0}}{\partial \epsilon_{\mathbf{k}}}\right)$$
(5.26)

¹³Which is equivalent with the case $\alpha = 0$.

¹⁴Actually we have to use $\tilde{g}_{\mathbf{k}}$ in this formula. As we are interested in the steady state case everything is expressed in $\tilde{g}_{\mathbf{k}}$. So we make the replacement $\tilde{g}_{\mathbf{k}} \to g_{\mathbf{k}}$ for the rest of this work. Note that this is not valid for $\frac{\partial}{\partial t} g_{\mathbf{k}} \neq 0$!

Defining an operator $\hat{A}_{\mathbf{k},\mathbf{k}'}$, with

$$\hat{A}_{\mathbf{k},\mathbf{k}'} \equiv \left[\frac{1}{\tau_{\mathbf{k}}} + \frac{e}{\hbar c} (\mathbf{v}_{\mathbf{k}} \times \mathbf{B}) \cdot \nabla_{\mathbf{k}} \right] \delta_{\mathbf{k},\mathbf{k}'} - C_{\mathbf{k},\mathbf{k}'}$$
 (5.27)

allows us to write the l.h.s. of (5.26) in the form $\sum_{\mathbf{k'}} \hat{A}_{\mathbf{k},\mathbf{k'}} g_{\mathbf{k'}}$. Therefore we have to invert $\hat{A}_{\mathbf{k},\mathbf{k'}}$ in order to solve equation (5.26). As the magnetic field is treated as a small perturbation of the transport process we split $\hat{A}_{\mathbf{k},\mathbf{k'}}$ into two parts, $\hat{A}_{\mathbf{k},\mathbf{k'}} = \hat{K}_{\mathbf{k},\mathbf{k'}} + \hat{M}_{\mathbf{k},\mathbf{k'}}^B$ with a magnetic field independent part $K_{\mathbf{k},\mathbf{k'}}$, $\hat{K}_{\mathbf{k},\mathbf{k'}} = \frac{1}{\tau_{\mathbf{k}}} \delta_{\mathbf{k},\mathbf{k'}} - C_{\mathbf{k},\mathbf{k'}}$, and a part that contains the magnetic field $\hat{M}_{\mathbf{k},\mathbf{k'}}^B$, $\hat{M}_{\mathbf{k},\mathbf{k'}}^B = \left[\frac{e}{\hbar c}(\mathbf{v}_{\mathbf{k}} \times \mathbf{B}) \cdot \nabla_{\mathbf{k}}\right] \delta_{\mathbf{k},\mathbf{k'}}$. A perturbation-expansion of $\hat{A}_{\mathbf{k},\mathbf{k'}}$ allows us to get the inverse of this operator as

$$\hat{A}_{\mathbf{k},\mathbf{k}'}^{-1} = \hat{K}_{\mathbf{k},\mathbf{k}'}^{-1} - \hat{K}_{\mathbf{k},\mathbf{k}'}^{-1} \hat{M}_{\mathbf{k}^{i},\mathbf{k}^{j}}^{B} \hat{K}_{\mathbf{k}^{j},\mathbf{k}'}^{-1}
+ \hat{K}_{\mathbf{k},\mathbf{k}^{i}}^{-1} \hat{M}_{\mathbf{k}^{i},\mathbf{k}^{j}}^{B} \hat{K}_{\mathbf{k}^{j},\mathbf{k}^{k}}^{-1} \hat{M}_{\mathbf{k}^{k},\mathbf{k}^{l}}^{B} \hat{K}_{\mathbf{k}^{l},\mathbf{k}'}^{-1} + \mathcal{O}(B^{3})$$
(5.28)

with a summation over repeated indexes. Dependent on the quantity of interest we get a contribution from the different terms in this expansion. The first term contributes to the DC-conductivity, the second term to the Hall-conductivity and the third term to the magnetoresistance.

It follows from the BE (5.26) that the number of "free" particles contributing to transport is given by

$$g_{\mathbf{k}} = 2\sum_{\mathbf{k'}} \hat{A}_{\mathbf{k},\mathbf{k'}}^{-1} \left[e\mathbf{v}_{\mathbf{k'}} \mathbf{E} \right] \cdot \left(-\frac{\partial f_{\mathbf{k}}^{0}}{\partial \epsilon_{\mathbf{k'}}} \right)$$
 (5.29)

with \hat{A}^{-1} given in (5.28). The factor of 2 is due the spin degeneracy.

Using Ohm's law, $j^{\mu} = \sigma^{\mu\nu} E^{\nu}$ we can derive a formula for the electrical conductivity-tensor $\sigma^{\mu\nu}$ by inserting (5.29) in the equation for the current given above, similar like it was done in (4.2). We obtain the formula for the electrical conductivity in the most general form:

$$\sigma^{\mu\nu} = 2e^2 \sum_{\mathbf{k},\mathbf{k}'} v_{\mathbf{k}}^{\mu} \hat{A}_{\mathbf{k},\mathbf{k}'}^{-1} v_{\mathbf{k}'}^{\nu} \left(-\frac{\partial f_{\mathbf{k}}^0}{\partial \epsilon_{\mathbf{k}'}} \right)$$
 (5.30)

with the inverse of the operator $\hat{A}_{\mathbf{k},\mathbf{k}'}$ defined in (5.27) and the factor of 2 due to the spin.¹⁵

¹⁵We see at this equation that we are mostly interested how the operator \hat{A}^{-1} acts on an arbitrary velocity v^{ν} .

It can be seen in (5.28) that our basic task is to figure out how the operator \hat{K}^{-1} acts on an arbitrary velocity. It follows immediately from (5.10):

$$\sum_{\mathbf{k}'} \hat{K}_{\mathbf{k},\mathbf{k}'} v_{\mathbf{k}'}^{\nu} = \frac{1}{\tau_{\mathbf{k}}} \sum_{\mathbf{k}'} v_{\mathbf{k}'}^{\nu} \delta_{\mathbf{k},\mathbf{k}'} - \sum_{\mathbf{k}'} C_{\mathbf{k},\mathbf{k}'} v_{\mathbf{k}'}^{\nu} \stackrel{(5.10)}{=} \frac{v_{\mathbf{k}}^{\nu}}{\tau_{\mathbf{k}}} \Rightarrow$$

$$\sum_{\mathbf{k}'} \hat{K}_{\mathbf{k},\mathbf{k}'}^{-1} v_{\mathbf{k}'}^{\nu} = \tau_{\mathbf{k}} v_{\mathbf{k}}^{\nu} \tag{5.31}$$

Note that the second equation follows directly from the first, when we multiply it with \hat{K}^{-1} .

We are going to use the result, given in (5.31), to get the different conductivities of our interest.¹⁶

5.4.1 DC-conductivity σ^{xx}

We obtain the leading term to σ^{xx} from the first term in (5.28). When we plug this term into (5.30) we only get one extra $\tau_{\mathbf{k}}$ in the final answer due to (5.31):¹⁷

$$\sigma^{xx} = 2e^2 \sum_{\mathbf{k}} \left(-\frac{\partial f}{\partial \epsilon_{\mathbf{k}}} \right) (v_{\mathbf{k}}^x)^2 \tau_{\mathbf{k}}$$
 (5.32)

with the functions $\Phi_{\mathbf{k}}$ and $\Psi_{\mathbf{k}}$ introduced in section 5.1. Equation (5.7) allows us to compute the T-dependence of σ^{xx} . Note that it is impossible to get an offset to the resistivity at a temperature T = 0K (residual resistivity) when we are dealing with a finite width w, because the term $\Phi_{\mathbf{k}}C_{\Phi} + \Psi_{\mathbf{k}}C_{\Psi} \neq 0$ for every point that contributes to transport. If the transition width w is big enough $\Psi_{\mathbf{k}}$ vanishes nowhere around the FS. So we get a temperature independent contribution to the resistivity that is $\propto \bar{b}(1-\alpha)$.

The fact that we have to choose proper values for the scattering-parameters a, b and c forces us to try to find out which parameters rule the DC-conductivity. Thus we go on with an analytical calculation of the DC-conductivity in the case of the step-functions (w=0). In the limit $w\to 0$ we can write the scattering time $\tau_{\mathbf{k}}$ as $\tau_{\mathbf{k}} = \tau_c \Phi_{\mathbf{k}} + \tau_h \Psi_{\mathbf{k}}$. Our task is to find the contribution from each region to the conductivity, σ_c^{xx} and σ_h^{xx} .

¹⁶Note that \hat{K}^{-1} conserves the energy. Thus the term $\left(-\frac{\partial f_{\mathbf{k}}^{0}}{\partial \epsilon_{\mathbf{k}'}}\right)$ can be put in front of this operator.

¹⁷This equation is the starting point for the numerical computation of the DC-conductivity in our program.

We are going to use the following formula

$$\lim_{w \to 0} \sigma^{xx} = 2e^2 \sum_{\mathbf{k}} \left(-\frac{\partial f}{\partial \epsilon_{\mathbf{k}}} \right) (v_{\mathbf{k}}^x)^2 \cdot (\tau_c \Phi_{\mathbf{k}} + \tau_h \Psi_{\mathbf{k}})$$
 (5.33)

to obtain the DC-conductivity. Because of the fourfold symmetry of the FS it is enough to compute σ^{xx} in the first quadrant (with a proper normalization).¹⁸

The dimension of of the conductivity $[\sigma^{xx}] = \frac{1}{\Omega m}$ thus the resistivity for that experimental results are given in chapter 4 has the dimension $[\rho^{xx}] = \Omega m$.¹⁹ (5.33) shows that the total resistivity is given by a parallel wiring between the cold and the hot region.²⁰ As the total DC-conductivity is just a sum of a "cold" and "hot" part, we concentrate on the contribution σ_c^{xx} from the cold region for the moment.²¹

$$\lim_{w \to 0} \sigma_c^{xx} = 2 \cdot \frac{e^2}{2} v_c^2 \cdot \tau_c \frac{1}{N_k} \sum_{\mathbf{k}} \delta(\epsilon_{\mathbf{k}} - \epsilon_f) \Phi_{\mathbf{k}} = e^2 v_c^2 N_c(\epsilon_f)$$

with the density of states inside the cold region $N_c(\epsilon_f) = \frac{1}{N_k} \sum_{\mathbf{k}} \delta(\epsilon_{\mathbf{k}} - \epsilon_f) \Phi_{\mathbf{k}}$.

Indeed this equation is a simplification, as the velocity is taken to be constant²² inside the cold region. Anyway it will give us an idea which parameter is of special importance for σ^{xx} .

The total DC-conductivity is $\sigma^{xx} = \sigma_c^{xx} + \sigma_h^{xx}$,

$$\lim_{v \to 0} \sigma^{xx} = e^2 \left[v_c^2 \tau_c N_c(\epsilon_f) + v_h^2 \tau_h N_h(\epsilon_f) \right]$$
(5.34)

The table, given in the section 5.2 allows us to figure out which term of the two in the brackets in equation (5.34) is the bigger one. By looking at this table it turns out that the conductivity is dominated by the cold regions, because the velocity v_c (compare (5.22)!) and the relaxation-time τ_c is much bigger there.

¹⁸The whole function in (5.33) is symmetric around the k_x and k_y -axis!

¹⁹Experimental data are given in $[\rho^{xx}] = \mu\Omega \cdot cm$.

 $^{^{20}\}mathrm{A}$ dimensional analysis gives us: $[\sigma^{xx}] = \frac{e^2(eV)^2a^2}{\hbar^2a^3} \cdot s \cdot \frac{1}{eV} = \frac{1}{\Omega m}.$ Because of the converting of \hbar and e into SI-units we have to insert a factor of $3.698 \cdot 10^6$, which we call cfactor, in our program. The numerical value of the conductivity becomes $\sigma^{xx} = 3.698 \cdot 10^6 \times RES \times \frac{\bar{\tau}}{\bar{a}_l} \frac{1}{\Omega m}$, where RES is a numerical value obtained by the program. The quantities $\bar{\tau}$ and \bar{a}_l are given in the following units: $[\bar{a}_l] = 1A^{\circ}, \ [\bar{\tau}] = 10^{-15}s.$

 $^{^{21}(}v_{\mathbf{k}}^{x})^{2} = \frac{v_{c}^{2}}{2}$

²²In the program we compute the velocity at every point of the lattice. Thus the assumption of a constant velocity inside the cold spot is not used!

Our interest in the temperature dependence of the resistivity forces us to insert the temperature-dependence of the coupling constants, a, b and c, given in (5.4) into (5.34):

$$\lim_{w \to 0} \rho^{xx} = \frac{1}{e^2} \frac{1}{v_c^2 \tau_c N_c(\epsilon_f) + v_h^2 \tau_h N_h(\epsilon_f)}$$

$$= \frac{1}{e^2} \frac{bc(1-\alpha)^2 + \alpha(ab+c^2) + \alpha^2(ac-ab-c^2)}{v_c^2 N_c(\epsilon_f)[c\alpha + (1-\alpha)b] + v_h^2 N_h(\epsilon_f)[a\alpha + (1-\alpha)c]}$$

$$= \frac{1}{e^2} \frac{\bar{b}\bar{c}(1-\alpha)^2 + (\alpha\bar{a}\bar{b} + \bar{c}^2\alpha - \alpha^2\bar{a}\bar{b} - \alpha^2\bar{c}^2)T + \alpha^2\bar{a}\bar{c}T^2}{v_c^2 N_c(\epsilon_f)[\bar{c}T\alpha + (1-\alpha)\bar{b}] + v_h^2 N_h(\epsilon_f)[\bar{a}T^2\alpha + (1-\alpha)\bar{c}T]}T$$

$$T_{\approx 0} = \frac{1}{e^2} \cdot \frac{(1-\alpha)\bar{c}}{v_c^2 N_c(\epsilon_f)} \cdot \left[\frac{\bar{b}(1-\alpha) + \alpha\left(\frac{\bar{a}\bar{b} + \bar{c}^2}{\bar{c}}\right) \cdot T}{(1-\alpha)\bar{b} + \bar{c}\left[\alpha + \left(\frac{v_h}{v_c}\right)^2 \frac{N_h(\epsilon_f)}{N_c(\epsilon_f)}(1-\alpha)\right] \cdot T} \right] \cdot T$$

$$= \frac{1}{e^2} \frac{(1-\alpha)\bar{c}}{v_c^2 N_c(\epsilon_f)} \cdot \left[\frac{1 + \frac{\alpha}{1-\alpha}\left[\frac{\bar{a}}{\bar{c}} + \frac{\bar{c}}{\bar{b}}\right] \cdot T}{1 + \frac{\bar{c}}{\bar{b}}\left[\frac{\alpha}{1-\alpha} + \left(\frac{v_h}{v_c}\right)^2 \frac{N_h(\epsilon_f)}{N_c(\epsilon_f)}\right] T} \right] \cdot T$$

$$Taylor-expansion$$

A Taylor expansion of the marked term to first order gives us an easy result for the DC-resistivity in the low temperature limit:

$$\lim_{w \to 0} \rho^{xx} = \frac{1}{e^2} \cdot \frac{(1-\alpha)\bar{c}}{v_c^2 N_c(\epsilon_f)} \cdot \left[T + \left(\frac{\alpha}{1-\alpha} \frac{\bar{a}}{\bar{c}} - \frac{\bar{c}}{\bar{b}} \left(\frac{v_h}{v_c} \right)^2 \frac{N_h(\epsilon_f)}{N_c(\epsilon_f)} \right) \cdot T^2 \right]$$
 (5.35)

Experimental data (compare to chapter 4) show that the DC-resistivity is proportional to T in a large temperature range (up to temperatures $\approx 1000K!$). In the limit of low temperatures and w = 0 we can write the resistivity ρ^{xx} in a linear form,

$$\rho^{xx} = \rho_0 + \frac{\Delta \rho^{xx}}{\Delta T} \cdot T \tag{5.36}$$

with the zero-temperature offset ρ_0 and the slope $\frac{\Delta \rho^{xx}}{\Delta T}$. Note that we are able to obtain an offset in the resistivity (from the hot-scattering b) within the framework of our model by inserting a finite transition width w into the model.

We obtain the linear temperature dependence of the resistivity, because the correction in (5.35) is quite small as it contains a factor $\propto T^2$, also in our TPM.

$$\lim_{T,w\to 0} \rho^{xx}(T) = \frac{1}{e^2} \cdot \frac{(1-\alpha)\bar{c}}{v_c^2 N_c(\epsilon_f)} \cdot T \tag{5.37}$$

As we know the velocity in the cold region from equation (5.20) and $N_c(\epsilon_f)$ from the table given in section 5.2, we can use equation (5.37) to estimate the value of the parameter \bar{c} . In a first guess we set $\alpha = 0.5$, which is the case when the first BZ is equally divided into a cold and a hot area.

It can be seen in equation (5.37) that the slope is governed by \bar{c} .

As we are interested in the description of Bi2212, we have to choose \bar{c} in such a way that it matches the slope that is experimentally measured. Just to get an impression of the magnitude of \bar{c} we insert the experimental value for the slope of Bi2212 which is roughly given (compare to chapter 4) by

$$\frac{\Delta \rho^{xx}}{\Delta T}|_{Bi2212} \approx 0.5 \frac{\mu \Omega cm}{K} \tag{5.38}$$

A comparison of this quantity with (5.37) allows us to obtain a first guess for \bar{c} . We find out that $\bar{c} \approx 0.5 \cdot 10^{12} \frac{1}{sK}$ for Bi2212.

Our interest in dimensionless quantities forces us to multiply this value with $\frac{\hbar}{k_B}$. We obtain as a first guess for $\frac{\hbar \bar{c}}{k_B}$: $\frac{\hbar \bar{c}}{k_B} \approx 5$. This result will be the starting value for the fitting procedure. For sure we will have to change it slightly especially when we insert a finite w but this gives us a quite good starting point for $\frac{\hbar \bar{c}}{k_B}$.

Another important quantity, the Hall-angle, shows a proportionality $\propto T^2$ (compare to section 4.2).

It is necessary to compute the Hall-conductivity σ^{xy} to obtain the Hall-angle $\cot \theta_H(T)$. Once we figured out σ^{xy} we will concentrate on the temperature dependence of the Hall-angle in the framework of the TPM and compare it to experimental results.

5.4.2 Hall-conductivity σ^{xy}

Figure 5.10 sketches the geometry of the applied external fields in the Hall-experiment. The electric field yields to the x-direction and the magnetic field in z-direction.

We obtain σ^{xy} also from (5.30), but the leading contribution to it is obtained from the second term (5.28), thus we replace $\hat{A}_{\mathbf{k},\mathbf{k}'}^{-1} \to -\hat{K}_{\mathbf{k},\mathbf{k}'}^{-1}\hat{M}_{\mathbf{k}',\mathbf{k}''}\hat{K}_{\mathbf{k}'',\mathbf{k}'''}^{-1}$ in (5.30). ²³ Again we make use of the relation given in (5.31): $\hat{K}^{-1}\mathbf{v} = \tau_{\mathbf{k}}\mathbf{v}$. Inserting this formulas

²³It is clear that we can't get a Hall-conductivity without an magnetic field! Thus the second term in (5.28) gives the first contribution.

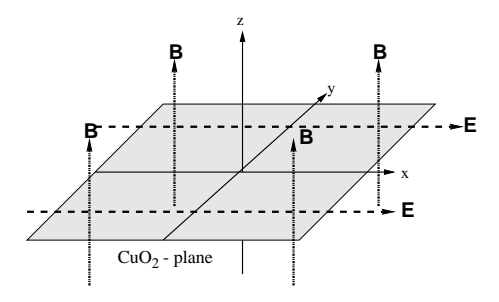


Figure 5.10: The geometry of the Hall-experiment.

into (5.30) gives us σ^{xy} . The important term inside the the operator \hat{A}^{-1} is $(\mathbf{v_k} \times \mathbf{B}) \cdot \nabla_{\mathbf{k}}$, given by the magnetic field. It can be written as

$$(\mathbf{v_k} \times \mathbf{B}) \cdot \nabla_{\mathbf{k}} = B(v_{\mathbf{k}}^y \cdot \partial_{k_x} - v_{\mathbf{k}}^x \cdot \partial_{k_y})$$
 (5.39)

We obtain σ^{xy} with a minus sign in front of the expression due to (5.28).²⁴

$$\sigma^{xy} = -2 \cdot e^{2} \sum_{\mathbf{k},\mathbf{k}',\mathbf{k}'',\mathbf{k}'''} v_{\mathbf{k}}^{x} \hat{K}_{\mathbf{k},\mathbf{k}'}^{-1} \hat{M}_{\mathbf{k}',\mathbf{k}''} \hat{K}_{\mathbf{k}'',\mathbf{k}'''}^{-1} v_{\mathbf{k}'''}^{y} \left(-\frac{\partial f_{\mathbf{k}}}{\partial \epsilon_{\mathbf{k}'''}} \right)$$

$$\stackrel{(5.39)}{=} -2 \cdot \frac{e^{3}B}{\hbar c} \sum_{\mathbf{k}',\mathbf{k}''} \tau_{\mathbf{k}'} v_{\mathbf{k}'}^{x} \left[v_{\mathbf{k}'}^{y} \cdot \partial_{k'_{x}} - v_{\mathbf{k}'}^{x} \cdot \partial_{k'_{y}} \right] \delta_{\mathbf{k}',\mathbf{k}''} \tau_{\mathbf{k}''} v_{\mathbf{k}''}^{y} \left(-\frac{\partial f_{\mathbf{k}}}{\partial \epsilon_{\mathbf{k}''}} \right)$$

$$= -2 \cdot \frac{e^{3}B}{\hbar c} \sum_{\mathbf{k}'} \tau_{\mathbf{k}'} v_{\mathbf{k}'}^{x} \left[v_{\mathbf{k}'}^{y} \cdot \partial_{k'_{x}} - v_{\mathbf{k}'}^{x} \cdot \partial_{k'_{y}} \right] \tau_{\mathbf{k}'} v_{\mathbf{k}'}^{y} \left(-\frac{\partial f_{\mathbf{k}}}{\partial \epsilon_{\mathbf{k}'}} \right)$$

which can be simplified to the final formula for the Hall-conductivity σ^{xy} : ²⁵

$$\sigma^{xy} = -2\frac{e^3 B}{\hbar c} \sum_{\mathbf{k}} \tau_{\mathbf{k}} v_{\mathbf{k}}^x \left[v_{\mathbf{k}}^y \cdot \partial_{k_x} - v_{\mathbf{k}}^x \cdot \partial_{k_y} \right] \tau_{\mathbf{k}} v_{\mathbf{k}}^y \left(-\frac{\partial f_{\mathbf{k}}}{\partial \epsilon_{\mathbf{k}}} \right)$$
 (5.40)

that contains derivatives of the velocity and of the scattering time $\tau_{\mathbf{k}}$ with respect to k_x and k_y . Exactly the same formula is given in [34]. This equation is the starting point of the computation of σ^{xy} used in our program.

²⁴The factor of 2 is inserted because of the spin.

²⁵Note that the magnetic field **B**, used in this equation, has not the dimension T. Here $[B] = \frac{V}{m}$, thus $\left[\frac{B}{c}\right] = \frac{V \cdot s}{m \cdot m} = T$. A dimensional analysis of this formula gives us (in SI-units): $\left[\sigma^{xy}\right] = \frac{e^3 B \cdot c}{\hbar c \cdot c} \frac{1}{m^3} \frac{1}{eV} \cdot s \frac{m}{s} \frac{m}{s} \cdot m \cdot s \cdot \frac{m}{s} = \frac{e^2 \cdot V \cdot s}{m^2 \cdot eV \cdot s} \frac{m}{s} \frac{1}{V} = \frac{1}{\Omega \cdot m}$. Remember that $\hbar = 6.5822 \cdot 10^{-16} eV \cdot s$. It is convenient to write all the constants in terms of atomic quantities.

In our program we have the numerical equation: $\sigma^{xy} = 85.356 \cdot \tilde{a} \cdot \bar{B} \cdot \bar{\tau}^2 \times RES \frac{1}{\Omega m}$, where the quantities are given in same terms as introduced before and RES is the numerical result given by our program.

We can write the scattering time $\tau_{\mathbf{k}}$, (given in equation (5.7)) in the way $\tau_{\mathbf{k}} = \frac{1}{\Phi_{\mathbf{k}}[\alpha a + (1-\alpha)c] + \Psi_{\mathbf{k}}[c\alpha + (1-\alpha)b]}$, what allows us to compute the derivative of $\tau_{\mathbf{k}}$ with respect to k_x or k_y using the quotient-rule.²⁶

$$\frac{\partial \tau_{\mathbf{k}}}{\partial k_x} = -\tau_{\mathbf{k}}^2 \left[C_{\Phi} \frac{\partial \Phi_{\mathbf{k}}}{\partial k_x} + C_{\Psi} \frac{\partial \Psi_{\mathbf{k}}}{\partial k_x} \right] = -\tau_{\mathbf{k}}^2 \frac{\partial \Phi_{\mathbf{k}}}{\partial k_x} \left[C_{\Phi} - C_{\Psi} \right]$$
 (5.41)

$$\frac{\partial \tau_{\mathbf{k}}}{\partial k_{y}} = -\tau_{\mathbf{k}}^{2} \left[C_{\Phi} \frac{\partial \Phi_{\mathbf{k}}}{\partial k_{y}} + C_{\Psi} \frac{\partial \Psi_{\mathbf{k}}}{\partial k_{y}} \right] = -\tau_{\mathbf{k}}^{2} \frac{\partial \Phi_{\mathbf{k}}}{\partial k_{y}} \left[C_{\Phi} - C_{\Psi} \right]$$
 (5.42)

with the temperature dependent constants $C_{\Phi} = \alpha a + (1 - \alpha)c$ and $C_{\Psi} = \alpha c + (1 - \alpha)b$. Finally we write down the total Hall-conductivity combining the result given in (5.41) with (5.40).

$$\sigma^{xy} = \underbrace{-2\frac{e^{3}B}{\hbar c}\sum_{\mathbf{k}}\left(-\frac{\partial f_{\mathbf{k}}}{\partial \epsilon_{\mathbf{k}}}\right)\tau_{\mathbf{k}}^{2}v_{\mathbf{k}}^{x}\left[v_{\mathbf{k}}^{y}\cdot\frac{\partial v_{\mathbf{k}}^{y}}{\partial k_{x}}-v_{\mathbf{k}}^{x}\cdot\frac{\partial v_{\mathbf{k}}^{y}}{\partial k_{y}}\right]}_{+2\frac{e^{3}B}{\hbar c}\sum_{\mathbf{k}}\left(-\frac{\partial f_{\mathbf{k}}}{\partial \epsilon_{\mathbf{k}}}\right)\tau_{\mathbf{k}}^{3}v_{\mathbf{k}}^{x}(v_{\mathbf{k}}^{y})^{2}\left[C_{\Phi}-C_{\Psi}\right]\frac{\partial \Phi_{\mathbf{k}}}{\partial k_{x}}}_{\sigma_{2}^{xy}\propto\tau^{3}}$$

$$-2\underbrace{\frac{e^{3}B}{\hbar c}\sum_{\mathbf{k}}\left(-\frac{\partial f_{\mathbf{k}}}{\partial \epsilon_{\mathbf{k}}}\right)\tau_{\mathbf{k}}^{3}(v_{\mathbf{k}}^{x})^{2}v_{\mathbf{k}}^{y}\left[C_{\Phi}-C_{\Psi}\right]\frac{\partial \Phi_{\mathbf{k}}}{\partial k_{y}}}_{\sigma_{2}^{xy}\propto\tau^{3}}}_{\sigma_{2}^{xy}\propto\tau^{3}}$$
(5.43)

This means we get three terms that give a contributions to the Hall-conductivity. The same reasoning as in the case of the resistivity states that we obtain also an offset to the Hall-conductivity when inserting a finite width w into our model.

The first term, σ_1^{xy} , which contains the derivatives of the velocity, and the terms σ_2^{xy} and σ_3^{xy} that contain derivatives of the relaxation time $\tau_{\mathbf{k}}$ with respect to k_x and to k_y . It turns out in the numerical analysis of (5.43) that we get the main contribution to σ^{xy} from the first term σ_1^{xy} in the low temperature limit (up to 400K) for sufficient big w. However for small w it becomes more and more important. So we can recover the T^3 -dependence of σ^{xy} from (5.43).

²⁶Remember the property $\frac{\partial \Phi_{\mathbf{k}}}{\partial k_x} = -\frac{\partial \Psi_{\mathbf{k}}}{\partial k_x}$ and $\frac{\partial \Phi_{\mathbf{k}}}{\partial k_y} = -\frac{\partial \Psi_{\mathbf{k}}}{\partial k_y}$ shown in the Appendix.

Hall-angle $\tan \theta_H(T)$

The ratio between the two conductivities σ^{xy} and σ^{xx} is called Hall-angle and is defined in the manner:

$$\tan \theta_H(T) = \frac{\sigma^{xy}}{\sigma^{xx}} \tag{5.44}$$

It was shown in chapter 4 that we would expect the same temperature dependence of $\cot \theta_H$ as σ^{xx} has in a simple Drude model. But the experiments described in chapter 4 showed that $\cot \theta_H \propto T^2$. Thus σ^{xy} should be proportional to T^{-3} .

When we insert the equations given in (5.32) and (5.43) we arrive at this formula for the inverse Hall-angle:

$$\cot \theta_H(T) = \frac{2e^2 \sum_{\mathbf{k}} \left(-\frac{\partial f}{\partial \epsilon_{\mathbf{k}}} \right) (v_{\mathbf{k}}^x)^2 \tau_{\mathbf{k}}}{\sigma^{xy}}$$
 (5.45)

with the denominator given in (5.43). So we can compute the Hall-angle numerically. This allows us to check the temperature-dependence of the Hall-angle that is experimentally measured.

The next quantity of interest that can be achieved from the electrical conductivity is the magnetoresistance.

5.4.3 Magnetoresistance MR

The divergence in the MR in the case w = 0 was pointed out by Zheleznyak et al. [6]. This divergence forced us to introduce a smooth change between the cold and hot regions in section 5.1.

When we apply a electric field and a magnetic field in the manner shown in figure (5.10) we obtain a higher resistivity, as there are electrons bended from their straight movement ($\|\mathbf{E}\|$) due to an additional force (Lorenz-force!). Thus we expect the resistivity to grow. The MR tells us how the resistivity changes when we turn on a magnetic field. It is defined by:

$$MR = \frac{\Delta \rho^{xx}(\mathbf{B})}{\rho^{xx}(0)} \tag{5.46}$$

with the longitudinal resistivity $\rho^{xx}(\mathbf{B})$ with and $\rho^{xx}(0)$ without an external magnetic field \mathbf{B} .

As we know the solution for the conductivity $\sigma^{\mu\nu}$, equation (5.30), we would like to write equation (5.46) in a more convenient form.

$$\frac{\Delta \rho^{xx}(\mathbf{B})}{\rho^{xx}(0)} = \frac{\rho^{xx}(\mathbf{B}) - \rho^{xx}(0)}{\rho^{xx}(0)} = \frac{\rho^{xx}(\mathbf{B})}{\rho^{xx}(0)} - 1$$

$$= \frac{\sigma^{xx}(0)}{\sigma^{xx}(\mathbf{B})} - 1 = \frac{\sigma^{xx}(0)}{\Delta \sigma^{xx}(\mathbf{B}) + \sigma^{xx}(0)} - 1 = -\frac{\Delta \sigma^{xx}(\mathbf{B})}{\Delta \sigma^{xx}(\mathbf{B}) + \sigma^{xx}(0)}$$

$$\approx -\frac{\Delta \sigma^{xx}(\mathbf{B})}{\sigma^{xx}(0)}$$

A more sophisticated approximation gives us $\frac{\Delta \rho^{xx}(\mathbf{B})}{\rho^{xx}(0)} = -\frac{\Delta \sigma^{xx}(\mathbf{B})}{\sigma^{xx}(0)} - \tan^2 \theta_H$ [6], which we are going to use for the MR.

$$MR = -\frac{\Delta \sigma^{xx}(\mathbf{B})}{\sigma^{xx}(0)} - \tan^2 \theta_H$$
 (5.47)

with the Hall-angle $\tan \theta_H$ defined in (5.44) and $\sigma^{xx}(0)$ known from (5.32). $\Delta \sigma^{xx}(\mathbf{B})$ is the only unknown quantity in (5.47).

Again we only take the leading order contribution to the MR, to be accurate to $\Delta \sigma^{xx}(\mathbf{B})$, given by the third term in (5.28). Note that the first order term in (5.28) doesn't give a contribution to $\sigma^{xx}(\mathbf{B})$, because $\sigma^{xx}(\mathbf{B}) \sim \sum_{\mathbf{k}} v^x \cdot (\hat{M}_B \times v^x) = 0$, which means that we get the first contribution to $\sigma^{xx}(\mathbf{B})$ from the third term in (5.28), which is $\hat{K}^{-1}\hat{M}_B\hat{K}^{-1}\hat{M}_B\hat{K}^{-1}$.

Therefore $\Delta \sigma^{xx}(\mathbf{B})$ is obtained from ²⁷

$$\Delta \sigma^{xx}(\mathbf{B}) = 2e^2 \sum_{\mathbf{k}, \mathbf{k}', \mathbf{k}''', \mathbf{k}'''', \mathbf{k}'''', \mathbf{k}'''''} v_{\mathbf{k}}^x \hat{K}_{\mathbf{k}, \mathbf{k}'}^{-1} \hat{M}_{\mathbf{k}', \mathbf{k}''} \hat{K}_{\mathbf{k}''', \mathbf{k}'''}^{-1} \hat{M}_{\mathbf{k}''', \mathbf{k}''''} \hat{K}_{\mathbf{k}''', \mathbf{k}''''}^{-1} \hat{K}_{\mathbf{k}'''', \mathbf{k}''''}^{-1} v_{\mathbf{k}'''''}^{-1} \left(-\frac{\partial f^0}{\partial \epsilon_{\mathbf{k}''''''}} \right)$$

We know that as well the scattering operator \hat{K}^{-1} as the operator due to the magnetic field \hat{M}_B conserve the energy.²⁸ Therefore we can put the partial derivative of the Fermi-function in front.

Again we use (5.31) and simplify the equation above to:

$$\Delta \sigma^{xx}(\mathbf{B}) = 2e^2 \sum_{\mathbf{k}',\mathbf{k}'',\mathbf{k}'''} \left(-\frac{\partial f}{\partial \epsilon_{\mathbf{k}'}} \right) \tau_{\mathbf{k}'} v_{\mathbf{k}'}^x \hat{M}_{\mathbf{k}',\mathbf{k}''} \hat{K}_{\mathbf{k}'',\mathbf{k}'''}^{-1} \cdot \sum_{\mathbf{k}''''} \hat{M}_{\mathbf{k}''',\mathbf{k}''''} \tau_{\mathbf{k}''''} v_{\mathbf{k}''''}^x \right)$$

²⁷Again we insert the factor of 2 due to the spin.

²⁸Remember that \hat{M}_B just rotates the direction of the velocity. It doesn't change its magnitude!

Our next task is to simplify the last sum on the r.h.s, $\sum_{\mathbf{k}''''} \hat{M}_{\mathbf{k}''',\mathbf{k}''''} \tau_{\mathbf{k}''''} \tau_{\mathbf{k}''''} \tau_{\mathbf{k}''''}$

$$\begin{split} \sum_{\mathbf{k}''''} \hat{M}_{\mathbf{k}''',\mathbf{k}''''} \tau_{\mathbf{k}''''} v_{\mathbf{k}''''}^x &= \frac{eB}{\hbar c} \sum_{\mathbf{k}''''} \left[v_{\mathbf{k}'''}^y \partial_{k_x'''} - v_{\mathbf{k}'''}^x \partial_{k_y'''} \right] \delta_{\mathbf{k}''',\mathbf{k}''''} \tau_{\mathbf{k}''''} v_{\mathbf{k}''''}^x \\ &= \frac{eB}{\hbar c} \left[v_{\mathbf{k}'''}^y \partial_{k_x'''} - v_{\mathbf{k}'''}^x \partial_{k_y'''} \right] \tau_{\mathbf{k}'''} v_{\mathbf{k}'''}^x \\ &= \frac{eB}{\hbar c} \tau_{\mathbf{k}'''} \left[v_{\mathbf{k}'''}^y \partial_{k_x'''} v_{\mathbf{k}'''}^x - v_{\mathbf{k}'''}^x \partial_{k_y'''} \tau_{\mathbf{k}'''} \right] + \\ &+ \frac{eB}{\hbar c} v_{\mathbf{k}'''}^x \left[v_{\mathbf{k}'''}^y \partial_{k_x'''} \tau_{\mathbf{k}'''} - v_{\mathbf{k}'''}^x \partial_{k_y'''} \tau_{\mathbf{k}'''} \right] \end{split}$$

We already calculated the derivative $\partial_{k_x} \tau_{\mathbf{k}}$ in (5.41). So we simplify this equation by using this result:

$$\begin{split} \sum_{\mathbf{k}''''} \hat{M}_{\mathbf{k}''',\mathbf{k}''''} \tau_{\mathbf{k}''''} v_{\mathbf{k}''''}^x &= \frac{eB}{\hbar c} \left\{ \tau_{\mathbf{k}'''} \left[v_{\mathbf{k}'''}^y \partial_{k_x'''} v_{\mathbf{k}'''}^x - v_{\mathbf{k}'''}^x \partial_{k_y'''} v_{\mathbf{k}'''}^x \right] \right. \\ &+ \tau_{\mathbf{k}'''}^2 \left(C_{\Phi} - C_{\Psi} \right) \left[v_{\mathbf{k}'''}^x v_{\mathbf{k}'''}^x \frac{\partial \Phi_{\mathbf{k}}}{\partial k_y} - v_{\mathbf{k}'''}^x v_{\mathbf{k}'''}^y \frac{\partial \Phi_{\mathbf{k}}}{\partial k_x} \right] \right\} \end{split}$$

with the temperature dependent constants C_{Φ} and C_{Ψ} defined before. So we get a contribution that is $\propto \tau$ and another part $\propto \tau^2$ from this part.

When we insert this result in the equation above, the initial equation becomes:

$$\Delta \sigma^{xx}(\mathbf{B}) = 2e^{2} \sum_{\mathbf{k}',\mathbf{k}'',\mathbf{k}'''} \left(-\frac{\partial f}{\partial \epsilon_{\mathbf{k}'}} \right) \tau_{\mathbf{k}'} v_{\mathbf{k}'}^{x} \hat{M}_{\mathbf{k}',\mathbf{k}''} \hat{K}_{\mathbf{k}'',\mathbf{k}'''}^{-1}$$

$$\cdot \left[\frac{eB}{\hbar c} \left\{ \tau_{\mathbf{k}'''} \left[v_{\mathbf{k}'''}^{y} \partial_{k_{x}'''} v_{\mathbf{k}'''}^{x} - v_{\mathbf{k}'''}^{x} \partial_{k_{y}'''} v_{\mathbf{k}'''}^{x} \right] + \right.$$

$$\left. + \tau_{\mathbf{k}''''}^{2} \left(C_{\Phi} - C_{\Psi} \right) \cdot \left[v_{\mathbf{k}'''}^{x} v_{\mathbf{k}'''}^{x} \frac{\partial \Phi_{\mathbf{k}}}{\partial k_{y}} - v_{\mathbf{k}'''}^{x} v_{\mathbf{k}'''}^{y} \frac{\partial \Phi_{\mathbf{k}}}{\partial k_{x}} \right] \right\} \right]$$

Now we have to analyze how the operator \hat{K}^{-1} acts on the term on its right. As usual the operator \hat{K}^{-1} just puts another scattering time $\tau_{\mathbf{k}}$ in front of the term.²⁹ So we get rid of another sum and obtain:

$$\begin{split} \Delta\sigma^{xx}(\mathbf{B}) &= 2\frac{e^3B}{\hbar c}\sum_{\mathbf{k}',\mathbf{k}''}\left(-\frac{\partial f}{\partial\epsilon_{\mathbf{k}'}}\right)\tau_{\mathbf{k}'}v_{\mathbf{k}'}^x\hat{M}_{\mathbf{k}',\mathbf{k}''}\\ &\cdot\left\{\tau_{\mathbf{k}''}^2\left[v_{\mathbf{k}''}^y\partial_{k_x''}v_{\mathbf{k}''}^x-v_{\mathbf{k}''}^x\partial_{k_y''}v_{\mathbf{k}''}^x\right]+\right.\\ &\left.\left.+\tau_{\mathbf{k}''}^3\left(C_{\Phi}-C_{\Psi}\right)\left[(v_{\mathbf{k}''}^x)^2\frac{\partial\Phi_{\mathbf{k}''}}{\partial k_y''}-v_{\mathbf{k}''}^xv_{\mathbf{k}''}^y\frac{\partial\Phi_{\mathbf{k}''}}{\partial k_x''}\right]\right\} \end{split}$$

²⁹The term in the big bracket on the left side is antisymmetric as $\tau_{\mathbf{k}}$ and $\partial_{k_x} v_{\mathbf{k}}^x$ etc is symmetric and \mathbf{v} and $\partial \Phi_{\mathbf{k}}/\partial k_x$ etc. is antisymmetric. Thus summing the symmetric scattering-matrix $C_{\mathbf{k}\mathbf{k}'}$ over the first BZ gives us a zero-contribution!

Now we apply the second magnetic term \hat{M}_B on its right side. Summing over \mathbf{k}'' gives us:

$$\Delta \sigma^{xx}(\mathbf{B}) = 2 \frac{e^4 B^2}{(\hbar c)^2} \sum_{\mathbf{k}'} \left(-\frac{\partial f}{\partial \epsilon_{\mathbf{k}'}} \right) \tau_{\mathbf{k}'} v_{\mathbf{k}'}^x \left[v_{\mathbf{k}'}^y \partial_{k_x'} - v_{\mathbf{k}'}^x \partial_{k_y'} \right] \cdot \left\{ \underbrace{\tau_{\mathbf{k}'}^2 \left[v_{\mathbf{k}'}^y \partial_{k_x'} v_{\mathbf{k}'}^x - v_{\mathbf{k}'}^x \partial_{k_y'} v_{\mathbf{k}'}^x \right]}_{\tau^2 - term} + \underbrace{\tau_{\mathbf{k}'}^3 \left(C_{\Phi} - C_{\Psi} \right) \left[(v_{\mathbf{k}'}^x)^2 \frac{\partial \Phi_{\mathbf{k}'}}{\partial k_y'} - v_{\mathbf{k}'}^x v_{\mathbf{k}'}^y \frac{\partial \Phi_{\mathbf{k}'}}{\partial k_x'} \right]}_{\tau^3 - term} \right\}$$

$$(5.48)$$

The τ^2 -term gives two contributions, which are obtained by doing a derivative of the square bracket and of $\tau_{\mathbf{k}}^2$. The derivative of the square bracket is easy to be done. As regard the derivative of $\frac{\partial \tau_{\mathbf{k}}^2}{\partial k_x}$ and $\frac{\partial \tau_{\mathbf{k}}^2}{\partial k_y}$ using the relation between Φ and Ψ we obtain:

$$\frac{\partial \tau_{\mathbf{k}}^2}{\partial k_x} = -2\tau_{\mathbf{k}}^3 \frac{\partial \Phi_{\mathbf{k}}}{\partial k_x} \left[C_{\Phi} - C_{\Psi} \right] \tag{5.49}$$

$$\frac{\partial \tau_{\mathbf{k}}^2}{\partial k_y} = -2\tau_{\mathbf{k}}^3 \frac{\partial \Phi_{\mathbf{k}}}{\partial k_y} \left[C_{\Phi} - C_{\Psi} \right] \tag{5.50}$$

Inserting (5.49) and (5.50) into the expression of the τ^2 -term we obtain:

$$\begin{split} \tau_{\mathbf{k}'}v_{\mathbf{k}'}^{x}\left[v_{\mathbf{k}'}^{y}\partial_{k_{x}'}\right. &- v_{\mathbf{k}'}^{x}\partial_{k_{y}'}\right] \cdot \tau_{\mathbf{k}'}^{2}\left[v_{\mathbf{k}'}^{y}\partial_{k_{x}'}v_{\mathbf{k}'}^{x} - v_{\mathbf{k}'}^{x}\partial_{k_{y}'}v_{\mathbf{k}'}^{x}\right] \\ &= \tau_{\mathbf{k}'}^{3}v_{\mathbf{k}'}^{x}\left[v_{\mathbf{k}'}^{y}\frac{\partial v_{\mathbf{k}'}^{y}}{\partial k_{x}'}\frac{\partial v_{\mathbf{k}'}^{x}}{\partial k_{x}'} + (v_{\mathbf{k}'}^{y})^{2}\frac{\partial^{2}v_{\mathbf{k}'}^{x}}{\partial (k_{x}')^{2}} - v_{\mathbf{k}'}^{y}\frac{\partial v_{\mathbf{k}'}^{x}}{\partial k_{y}'}\frac{\partial v_{\mathbf{k}'}^{x}}{\partial k_{x}'} - v_{\mathbf{k}'}^{y}v_{\mathbf{k}'}^{x}\frac{\partial^{2}v_{\mathbf{k}'}^{x}}{\partial (k_{x}')^{2}} - v_{\mathbf{k}'}^{y}\frac{\partial v_{\mathbf{k}'}^{x}}{\partial k_{y}'} - v_{\mathbf{k}'}^{y}v_{\mathbf{k}'}^{y}\frac{\partial^{2}v_{\mathbf{k}'}^{x}}{\partial k_{y}'\partial k_{x}'} + v_{\mathbf{k}'}^{x}\left(\frac{\partial v_{\mathbf{k}'}^{x}}{\partial k_{y}'}\right)^{2} + (v_{\mathbf{k}'}^{x})^{2}\frac{\partial^{2}v_{\mathbf{k}'}^{x}}{\partial (k_{y}')^{2}}\right] \\ &+ 2\tau_{\mathbf{k}'}^{4}(C_{\Phi} - C_{\Psi})v_{\mathbf{k}'}^{x}\left\{\frac{\partial \Phi_{\mathbf{k}}}{\partial k_{y}}\left[v_{\mathbf{k}'}^{x}v_{\mathbf{k}'}^{y}\frac{\partial v_{\mathbf{k}'}^{x}}{\partial k_{x}'} - (v_{\mathbf{k}'}^{x})^{2}\frac{\partial v_{\mathbf{k}'}^{x}}{\partial k_{y}'}\right] \\ &- \frac{\partial \Phi_{\mathbf{k}}}{\partial k_{x}}\left[(v_{\mathbf{k}'}^{y})^{2}\frac{\partial^{2}v_{\mathbf{k}'}^{x}}{\partial k_{x}'} - v_{\mathbf{k}'}^{x}v_{\mathbf{k}'}^{y}\frac{\partial v_{\mathbf{k}'}^{x}}{\partial k_{y}'}\right] \\ &= \tau_{\mathbf{k}'}^{3}v_{\mathbf{k}'}\left[(v_{\mathbf{k}'}^{y})^{2}\frac{\partial^{2}v_{\mathbf{k}'}^{x}}{\partial (k_{x}')^{2}} + (v_{\mathbf{k}'}^{x})^{2}\frac{\partial^{2}v_{\mathbf{k}'}^{x}}{\partial (k_{y}')^{2}} - v_{\mathbf{k}'}^{x}\frac{\partial v_{\mathbf{k}'}^{y}}{\partial k_{y}'}\frac{\partial v_{\mathbf{k}'}^{x}}{\partial k_{x}'} \\ &- 2v_{\mathbf{k}'}^{y}v_{\mathbf{k}'}^{x}\frac{\partial^{2}v_{\mathbf{k}'}^{x}}{\partial (k_{x}')^{2}} + v_{\mathbf{k}'}^{x}\left(\frac{\partial v_{\mathbf{k}'}^{x}}}{\partial k_{y}'}\right)^{2}\right] \\ &+ 2\tau_{\mathbf{k}'}^{4}(C_{\Phi} - C_{\Psi})v_{\mathbf{k}'}^{x}\left\{\frac{\partial \Phi_{\mathbf{k}}}{\partial k_{y}}\left[v_{\mathbf{k}'}^{x}v_{\mathbf{k}'}^{y}\frac{\partial v_{\mathbf{k}'}^{x}}{\partial k_{x}'} - (v_{\mathbf{k}'}^{x})^{2}\frac{\partial v_{\mathbf{k}'}^{x}}{\partial k_{y}'}\right] \\ &- \frac{\partial \Phi_{\mathbf{k}}}{\partial k_{x}}\left[(v_{\mathbf{k}'}^{y})^{2}\frac{\partial v_{\mathbf{k}'}^{x}}{\partial k_{x}'} - v_{\mathbf{k}'}^{x}v_{\mathbf{k}'}^{y}\frac{\partial v_{\mathbf{k}'}^{x}}{\partial k_{y}'}\right]\right\} \end{aligned}$$

This equation gives us the terms obtained from the τ^2 -term. Still the τ^3 term is missing! The partial derivatives of τ^3 are:

$$\frac{\partial \tau_{\mathbf{k}}^3}{\partial k_x} = -3\tau_{\mathbf{k}}^4 \frac{\partial \Phi_{\mathbf{k}}}{\partial k_x} \left[C_{\Phi} - C_{\Psi} \right] \tag{5.51}$$

$$\frac{\partial \tau_{\mathbf{k}}^{3}}{\partial k_{y}} = -3\tau_{\mathbf{k}}^{4} \frac{\partial \Phi_{\mathbf{k}}}{\partial k_{y}} \left[C_{\Phi} - C_{\Psi} \right]$$
 (5.52)

Thus the τ^3 -term gives the contribution:

$$\begin{split} \tau_{\mathbf{k}'}v_{\mathbf{k}'}^{x} & \cdot & \left[v_{\mathbf{k}'}^{y}\partial_{k_{x}'} - v_{\mathbf{k}'}^{x}\partial_{k_{y}'}\right] \cdot \tau_{\mathbf{k}'}^{3}\left(C_{\Phi} - C_{\Psi}\right) \left[v_{\mathbf{k}'}^{x}v_{\mathbf{k}'}^{x}\frac{\partial\Phi_{\mathbf{k}'}}{\partial k_{y}'} - v_{\mathbf{k}'}^{x}v_{\mathbf{k}'}^{y}\frac{\partial\Phi_{\mathbf{k}'}}{\partial k_{x}'}\right] = \\ & = & \left(C_{\Phi} - C_{\Psi}\right)\tau_{\mathbf{k}'}^{4}v_{\mathbf{k}}^{x}\left\{v_{\mathbf{k}'}^{y}\left[2\frac{\partial v_{\mathbf{k}'}^{x}}{\partial k_{x}'}v_{\mathbf{k}'}^{x}\frac{\partial\Phi_{\mathbf{k}'}}{\partial k_{y}'} + \left(v_{\mathbf{k}'}^{x}\right)^{2}\frac{\partial^{2}\Phi_{\mathbf{k}'}}{\partial k_{x}'\partial k_{y}'} - \frac{\partial v_{\mathbf{k}'}^{x}}{\partial k_{x}'}v_{\mathbf{k}'}^{y}\frac{\partial\Phi_{\mathbf{k}'}}{\partial k_{x}'}\right. \\ & - v_{\mathbf{k}'}^{x}\frac{\partial v_{\mathbf{k}'}^{y}}{\partial k_{x}'}\frac{\partial\Phi_{\mathbf{k}'}}{\partial k_{x}'} - v_{\mathbf{k}'}^{x}v_{\mathbf{k}'}^{y}\frac{\partial^{2}\Phi_{\mathbf{k}'}}{\partial (k_{x}')^{2}}\right] \\ & - v_{\mathbf{k}'}^{x}\left[2\frac{\partial v_{\mathbf{k}'}^{x}}{\partial k_{x}'}v_{\mathbf{k}'}^{x}\frac{\partial\Phi_{\mathbf{k}'}}{\partial (k_{x}')^{2}}\right] \\ & - v_{\mathbf{k}'}^{x}\frac{\partial v_{\mathbf{k}'}^{y}}{\partial k_{y}'}\frac{\partial\Phi_{\mathbf{k}'}}{\partial k_{y}'} - v_{\mathbf{k}'}^{x}v_{\mathbf{k}'}^{y}\frac{\partial^{2}\Phi_{\mathbf{k}'}}{\partial (k_{y}')^{2}}\right] \\ & - v_{\mathbf{k}'}^{x}\frac{\partial v_{\mathbf{k}'}^{y}}{\partial k_{x}'}\frac{\partial\Phi_{\mathbf{k}'}}{\partial k_{x}'} - v_{\mathbf{k}'}^{x}v_{\mathbf{k}'}^{y}\frac{\partial^{2}\Phi_{\mathbf{k}'}}{\partial k_{y}'}\right] \\ & + 3\left(C_{\Phi} - C_{\Psi}\right)^{2}\tau_{\mathbf{k}'}^{5}v_{\mathbf{k}'}^{x}\left\{\frac{\partial\Phi_{\mathbf{k}'}}{\partial k_{y}'}v_{\mathbf{k}'}^{x}\left[\left(v_{\mathbf{k}'}^{x}\right)^{2}\frac{\partial\Phi_{\mathbf{k}'}}{\partial k_{x}'}\right]\right\} \\ & - & \left(C_{\Phi} - C_{\Psi}\right)^{2}\tau_{\mathbf{k}'}^{4}v_{\mathbf{k}'}^{x}\left\{2v_{\mathbf{k}'}^{x}v_{\mathbf{k}'}^{y}\frac{\partial\Phi_{\mathbf{k}'}}{\partial k_{x}'}\right\} - 2\left(v_{\mathbf{k}'}^{x}\right)^{2}v_{\mathbf{k}'}^{y}\frac{\partial\Phi_{\mathbf{k}'}}{\partial k_{x}'}\right\} \\ & - & \left(v_{\mathbf{k}'}^{y}\right)^{2}\frac{\partial v_{\mathbf{k}'}^{x}}{\partial k_{x}'}\left\{2v_{\mathbf{k}'}^{x}v_{\mathbf{k}'}^{y}\frac{\partial\Phi_{\mathbf{k}'}}{\partial k_{x}'}\right\} + 2\left(v_{\mathbf{k}'}^{x}\right)^{2}v_{\mathbf{k}'}^{y}\frac{\partial\Phi_{\mathbf{k}'}}{\partial k_{x}'}\right\} \\ & - & \left(v_{\mathbf{k}'}^{y}\right)^{2}\frac{\partial v_{\mathbf{k}'}^{x}}{\partial k_{x}'}\left\{2v_{\mathbf{k}'}^{x}v_{\mathbf{k}'}^{y}\frac{\partial\Phi_{\mathbf{k}'}}{\partial k_{x}'}\right\} - 2\left(v_{\mathbf{k}'}^{x}\right)^{2}v_{\mathbf{k}'}^{y}\frac{\partial\Phi_{\mathbf{k}'}}{\partial k_{x}'}\right\} \\ & - & \left(v_{\mathbf{k}'}^{y}\right)^{2}\frac{\partial v_{\mathbf{k}'}^{x}}{\partial k_{x}'}\frac{\partial\Phi_{\mathbf{k}'}}{\partial k_{x}'}\right\} \\ & - & \left(v_{\mathbf{k}'}^{y}\right)^{2}\frac{\partial v_{\mathbf{k}'}^{x}}{\partial k_{x}'}\left(\frac{\partial\Phi_{\mathbf{k}'}}{\partial k_{x}'}\right) - v_{\mathbf{k}'}^{x}\left(v_{\mathbf{k}'}^{y}\right)^{2}\frac{\partial\Phi_{\mathbf{k}'}}{\partial k_{x}'}\right\} \\ & - & \left(v_{\mathbf{k}'}^{y}\right)^{2}\frac{\partial v_{\mathbf{k}'}^{x}}{\partial k_{x}'}\frac{\partial\Phi_{\mathbf{k}'}}{\partial k_{x}'}\right\} \\ & - & \left(v_{\mathbf{k}'}^{y}\right)^{2}\frac{\partial v_{\mathbf{k}'}^{x}}{\partial k_{x}'}\left(\frac{\partial\Phi_{\mathbf{k}'}}{\partial k_{x}'}\right)$$

Now we put all the terms together and the expression for $\Delta \sigma^{xx}(\mathbf{B})$ becomes:

$$\Delta \sigma^{xx}(\mathbf{B}) = 2 \frac{e^4 B^2}{(\hbar c)^2} \sum_{\mathbf{k}} \left(-\frac{\partial f}{\partial \epsilon_{\mathbf{k}}} \right) \cdot \left\{ \tau_{\mathbf{k}}^3 v_{\mathbf{k}}^x \left[(v_{\mathbf{k}}^y)^2 \frac{\partial^2 v_{\mathbf{k}}^x}{\partial (k_x)^2} + (v_{\mathbf{k}}^x)^2 \frac{\partial^2 v_{\mathbf{k}}^x}{\partial (k_y)^2} - v_{\mathbf{k}}^x \frac{\partial v_{\mathbf{k}}^y}{\partial k_y} \frac{\partial v_{\mathbf{k}}^x}{\partial k_x} - 2 v_{\mathbf{k}}^y v_{\mathbf{k}}^x \frac{\partial^2 v_{\mathbf{k}}^x}{\partial k_x \partial k_y} + v_{\mathbf{k}}^x \left(\frac{\partial v_{\mathbf{k}}^x}{\partial k_y} \right)^2 \right]$$

$$(5.53)$$

$$+ \left(C_{\Phi} - C_{\Psi}\right) \tau_{\mathbf{k}}^{4} v_{\mathbf{k}}^{x} \left(2 \cdot \left[\frac{\partial \Phi_{\mathbf{k}}}{\partial k_{y}} v_{\mathbf{k}}^{x} - \frac{\partial \Phi_{\mathbf{k}}}{\partial k_{x}} v_{\mathbf{k}}^{y}\right] \cdot \left[v_{\mathbf{k}}^{y} \frac{\partial v_{\mathbf{k}}^{x}}{\partial k_{x}} - v_{\mathbf{k}}^{x} \frac{\partial v_{\mathbf{k}}^{x}}{\partial k_{y}}\right] \right.$$

$$+ 2v_{\mathbf{k}}^{x} v_{\mathbf{k}}^{y} \frac{\partial v_{\mathbf{k}}^{x}}{\partial k_{x}} \frac{\partial \Phi_{\mathbf{k}}}{\partial k_{y}} + 2(v_{\mathbf{k}}^{x})^{2} v_{\mathbf{k}}^{y} \frac{\partial^{2} \Phi_{\mathbf{k}}}{\partial k_{x} \partial k_{y}} + (v_{\mathbf{k}}^{x})^{2} \frac{\partial v_{\mathbf{k}}^{y}}{\partial k_{y}} \frac{\partial \Phi_{\mathbf{k}}}{\partial k_{x}} - (v_{\mathbf{k}}^{y})^{2} \frac{\partial^{2} \Phi_{\mathbf{k}}}{\partial (k_{x})^{2}} - 2(v_{\mathbf{k}}^{x})^{2} \frac{\partial v_{\mathbf{k}}^{x}}{\partial k_{y}} \frac{\partial \Phi_{\mathbf{k}}}{\partial k_{y}} - (v_{\mathbf{k}}^{x})^{3} \frac{\partial^{2} \Phi_{\mathbf{k}}}{\partial (k_{y})^{2}} \right)$$

$$+ 3 \left(C_{\Phi} - C_{\Psi}\right)^{2} \tau_{\mathbf{k}}^{5} (v_{\mathbf{k}}^{x})^{2} \cdot \left[v_{\mathbf{k}}^{x} \frac{\partial \Phi_{\mathbf{k}}}{\partial k_{y}} - v_{\mathbf{k}}^{y} \frac{\partial \Phi_{\mathbf{k}}}{\partial k_{x}}\right]^{2} \right\}$$

which is our final expression for $\Delta \sigma^{xx}(\mathbf{B})$. This result has to be inserted into (5.47) in order to figure out the temperature dependence of the MR.

Kohler-Plot

Zheleznyak et al. [6] argued in their theoretical paper that a plot of the ratio $\Delta \rho^{xx}/(\rho^{xx} \tan^2 \theta_H)$ saturates to a value that is about 5.5 for T > 350K. So the ratio of MR and inverse Hall-angle squared is expected to be independent of temperature for sufficient big temperatures.

We are plotting the Kohler-plot to test our TPM and to derive some properties or dependencies from the result. As this plot is a ratio of two quantities the interpretation is difficult.

Anyway we obtain a saturation for temperatures of this range for very similar numbers. This plot will be shown in chapter 7.

5.5 Thermal transport - conductivity tensor $\kappa^{\mu\nu}$

Equation (5.24) in section 5.3 describes every type of transport in a sample due to an applied electric field $\bf E$ or a temperature gradient $\nabla_{\bf r}T$. Section 5.4 dealt with the case of an applied electric field without a temperature gradient. Different conductivities $\sigma^{\mu\nu}$ were derived in this section. Now we are going to apply a temperature gradient $\nabla_{\bf r}T$ to the sample, but no electric field. The goal of this section is to compute the thermal conductivity tensor $\kappa^{\mu\nu}$ obtained from the TPM.

In contrast to the previous chapter the driving force of the kinetic equation is now

no more due to an electric field. The cause of the (quasi)particle movement is now a temperature gradient.

To obtain the thermal conductivity we have to solve the integrals introduced in section 5.3 for $\alpha = 2$.

As the distribution function is now **r**-dependent we have to linearize the BE using $f(\mathbf{k}, \mathbf{r}, T, t) = f_{\mathbf{k}}^0(\epsilon_{\mathbf{k}}, T(\mathbf{r})) + g_{\mathbf{k}}(\mathbf{r}, t)$ now. The departure from equilibrium $g_{\mathbf{k}}(\mathbf{r}, t)$ now has a spatial and a temperature dependence! Again we are interested in the steady-state case, thus the term $\frac{\partial}{\partial t}$ doesn't appear in our kinetic equation, equation (3.25). Considering the case of no external magnetic field first we can derive a formula when there is only a thermal gradient in the sample. From the total differential of $f(\mathbf{k}, \mathbf{r}, T, t)$ we obtain in leading order ³⁰

$$\begin{split} \frac{df(\mathbf{k}, \mathbf{r}, T, t)}{dt} &= \nabla_{\mathbf{r}} f(\mathbf{k}, \mathbf{r}, T) \cdot \nabla_{\mathbf{k}} \epsilon_{\mathbf{k}} - \nabla_{\mathbf{k}} f(\mathbf{k}, \mathbf{r}, T) \cdot \nabla_{\mathbf{r}} \epsilon_{\mathbf{k}} \\ &= \frac{\partial f_{\mathbf{k}}^{0}}{\partial \epsilon_{\mathbf{k}}} \frac{d \epsilon_{\mathbf{k}}}{d \mathbf{r}} \cdot \nabla_{\mathbf{k}} \epsilon_{\mathbf{k}} + \frac{\partial f_{\mathbf{k}}^{0}}{\partial T} \frac{d T}{d \mathbf{r}} \cdot \nabla_{\mathbf{k}} \epsilon_{\mathbf{k}} - \frac{\partial f_{\mathbf{k}}^{0}}{\partial \epsilon_{\mathbf{k}}} \nabla_{\mathbf{k}} \epsilon_{\mathbf{k}} \cdot \nabla_{\mathbf{r}} \epsilon_{\mathbf{k}} = \frac{\partial f_{\mathbf{k}}^{0}}{\partial T} \nabla_{\mathbf{r}} T \cdot \mathbf{v}_{\mathbf{k}} \end{split}$$

which represents the driving term in our kinetic equation.³¹ As $f_{\mathbf{k}}^0$ is the usual Fermi-distribution we are able to reexpress $\frac{\partial f_{\mathbf{k}}^0}{\partial T}$ in terms of $\frac{\partial f_{\mathbf{k}}^0}{\partial \epsilon_{\mathbf{k}}}$, ³²

$$\frac{\partial f_{\mathbf{k}}^{0}}{\partial T} = \left(-\frac{\partial f_{\mathbf{k}}^{0}}{\partial \epsilon_{\mathbf{k}}}\right) \frac{\epsilon_{\mathbf{k}}}{T} \tag{5.54}$$

The r.h.s. of the kinetic equation doesn't change at all. So we still have the collision-operator $C_{\mathbf{k}}$ defined in (5.3) there. Without an electric and magnetic field the transport gets the form:

$$\left(-\frac{\partial f_{\mathbf{k}}^{0}}{\partial \epsilon_{\mathbf{k}}}\right) \frac{\epsilon_{\mathbf{k}}}{T} \mathbf{v}_{\mathbf{k}} \cdot \nabla_{\mathbf{r}} T = C_{\mathbf{k}}$$
(5.55)

The comparison with (3.25) tells us that we replace $e\mathbf{E} \frac{\partial f_{\mathbf{k}}^0}{\partial \epsilon_{\mathbf{k}}} \to \left(-\frac{\partial f_{\mathbf{k}}^0}{\partial \epsilon_{\mathbf{k}}}\right) \frac{\epsilon_{\mathbf{k}} \nabla_{\mathbf{r}} T}{T}$ to obtain the tensor $\bar{\kappa}$. This replacement was also pointed out in [36]. So we have an extra factor

 $^{^{30}\}mathrm{As}$ we are dealing with the steady state case we drop the term $\frac{\partial f}{\partial t}.$

³¹Note that there is no magnetic field in the equation so far!

 $^{^{32}\}text{In the case }T=0 \text{ the formula }\left(-\frac{\partial f}{\partial \epsilon_{\mathbf{k}}}\right)=\delta(\epsilon_{\mathbf{k}}-\epsilon_{\mathbf{k}'}) \text{ is valid. When we do the derivative of the Fermi function we get: }\left(-\frac{\partial f_{\mathbf{k}}^0}{\partial \epsilon_{\mathbf{k}}}\right)=\frac{1}{k_BT}\frac{e^{\epsilon_{\mathbf{k}}/k_BT}}{(e^{\epsilon_{\mathbf{k}}/k_BT}+1)^2}. \text{ Thus we can write }\frac{\partial f_{\mathbf{k}}^0}{\partial T}=\left(\frac{\epsilon_{\mathbf{k}}}{k_BT^2}\frac{e^{\epsilon_{\mathbf{k}}/k_BT}}{(e^{\epsilon_{\mathbf{k}}/k_BT}+1)^2}\right)=\frac{\epsilon_{\mathbf{k}}}{T}\left(-\frac{\partial f_{\mathbf{k}}^0}{\partial \epsilon_{\mathbf{k}}}\right)$

of $\epsilon_{\mathbf{k}}$, the driving term due to the temperature gradient $\frac{\nabla_{\mathbf{r}}T}{T}$ and an extra "minus" in the equation! Finally we derive from (5.55):

$$-\sum_{\mathbf{k'}} \left[\frac{1}{\tau_{\mathbf{k}}} \delta_{\mathbf{k}, \mathbf{k'}} - C_{\mathbf{k}, \mathbf{k'}} \right] g_{\mathbf{k'}} = \left(-\frac{\partial f_{\mathbf{k}}^{0}}{\partial \epsilon_{\mathbf{k}}} \right) \frac{\epsilon_{\mathbf{k}}}{T} \mathbf{v}_{\mathbf{k}} \cdot \nabla_{\mathbf{r}} T$$

where the additional term due to the magnetic field is still missing.

In analogy to the previous section we define an operator \hat{A} , $\hat{A}_{\mathbf{k},\mathbf{k}'} \equiv \hat{K} + \hat{M}_B$. This operator is exactly the operator given in (5.27). We can compute the number of "free" (quasi)particles from equation (5.55) when we invert \hat{A} , which is done in (5.28). Note that $g_{\mathbf{k}}$ represents here the (quasi)particles that can carry heat (respectively energy).

$$g_{\mathbf{k}} = 2\sum_{\mathbf{k'}} \hat{A}_{\mathbf{k},\mathbf{k'}}^{-1} \left[\left(\frac{\partial f_{\mathbf{k}}^{0}}{\partial \epsilon_{\mathbf{k}}} \right) \frac{\epsilon_{\mathbf{k'}}}{T} \mathbf{v}_{\mathbf{k'}} \cdot \nabla_{\mathbf{r}} T \right]$$
(5.56)

with $\hat{A}_{\mathbf{k},\mathbf{k}'}^{-1}$ given in (5.28) and the spin degeneracy.

Equation (5.56) is the starting point of the computation of thermal conductivities.

In analogy to Ohm's law we define the thermal current as

$$\mathbf{j}_Q = -\bar{\kappa} \frac{\nabla_{\mathbf{r}} T}{T} \tag{5.57}$$

with the heat current \mathbf{j}_Q and the thermal conductivity tensor $\bar{\kappa}$.

A comparison with Ohms law, equation (4.2), shows that $\mathbf{E} \to \frac{\nabla_{\mathbf{r}}T}{T}$ and there is an extra "-" in equation (5.57). The minus-sign appears because (quasi)particles move from lower to higher temperatures. Whereas particles move with the electric field.

A dimensional analysis of the thermal conductivity κ gives us: $[\kappa] = \frac{W}{m}$, and the heat current \mathbf{j}_Q has the dimension $[\mathbf{j}_Q] = \frac{W}{m^2}$.

Considering the noninteracting regime (non Fermi-liquid-regime)³³, we can obtain the heat current in terms of "free" (quasi)particles $g_{\mathbf{k}}$,

$$\mathbf{j}_Q = \sum_{\mathbf{k}} \mathbf{v}_{\mathbf{k}} \epsilon_{\mathbf{k}} g_{\mathbf{k}} \tag{5.58}$$

³³which is not important in the DC-case!

that is very similar to the formula for the electric current, equation (4.2). The difference to the equations before is that the derivative of the Fermi-distribution $\left(-\frac{\partial f_{\mathbf{k}}^{0}}{\partial \epsilon_{\mathbf{k}'}}\right)$ doesn't simplify to a δ -function which is clear as we can only have a temperature gradient when the temperature T is not zero, $T \neq 0$.

In the case of the charge transfer each particle transported the same charge e, whereas in the case of heat current each contributing (quasi)particle carries some energy $\epsilon_{\mathbf{k}}$ whose magnitude is very similar to the Fermi-energy ϵ_f , $\epsilon_{\mathbf{k}} \approx \epsilon_f$, because only (quasi)particles around the FS can become free (quasi)particles. The chemical potential is set to be constant in this case.

From the equations (5.57), and (5.58) we can derive the formula for the thermal conductivity-tensor.

$$\kappa^{\mu\nu} = 2\sum_{\mathbf{k},\mathbf{k}'} v_{\mathbf{k}}^{\mu} \epsilon_{\mathbf{k}} \hat{A}_{\mathbf{k},\mathbf{k}'}^{-1} \epsilon_{\mathbf{k}'} v_{\mathbf{k}'}^{\nu} \left(-\frac{\partial f_{\mathbf{k}}^{0}}{\partial \epsilon_{\mathbf{k}'}} \right)$$
(5.59)

Now our main interest is how the operator \hat{A}^{-1} acts on the term $\mathbf{v_k} \epsilon_{\mathbf{k}}$. As \hat{A}^{-1} is a product of \hat{K}^{-1} and of \hat{M}_B which are energy conserving operators 34 , we derive immediately that the operator \hat{A}^{-1} conserves the energy. Thus the action of this operator on its right side in (5.59) is given by $\hat{A}_{\mathbf{k},\mathbf{k}'}^{-1}\epsilon_{\mathbf{k}'}\mathbf{v_{k'}} = \epsilon_{\mathbf{k}}\hat{A}_{\mathbf{k},\mathbf{k}'}^{-1}\mathbf{v_{k'}}$.

So the problem from the previous section remains. We have to know how the operator \hat{A}^{-1} acts on arbitrary velocities, which is known from equation (5.31).

5.5.1 Longitudinal thermal conductivity κ^{xx}

It follows from (5.59) that the longitudinal thermal (DC)-conductivity κ^{xx} is given by

$$\kappa^{xx} = 2\sum_{\mathbf{k}} v_{\mathbf{k}}^{x} \epsilon_{\mathbf{k}}^{2} \tau_{\mathbf{k}} v_{\mathbf{k}}^{x} \left(-\frac{\partial f_{\mathbf{k}}^{0}}{\partial \epsilon_{\mathbf{k}}} \right)$$
 (5.60)

The Sommerfeld expansion expansion allows us to compute the value of this sum or this integral respectively in an approximative way. This expansion works for integrals of the form above. The idea is to Taylor expand the integral in terms of the temperature

³⁴The scattering operator conserves energy like it was constructed and the operator \hat{M}_B conserves energy as it is a magnetic term that rotates the velocity but doesn't change it.

as
$$\left(-\frac{\partial f_{\mathbf{k}}^{0}}{\partial \epsilon_{\mathbf{k}}}\right)$$
 has a width of $k_{B}T.^{35}$

From this expansion we get the first term that gives contribution in the following form

$$\kappa^{xx} = a_1 \tau_{\mathbf{k}} v^2 T^2 N(\epsilon_f) \propto T^2 \tag{5.61}$$

with a_1 that is defined in terms of the Riemann Zeta-function, as usual in the Sommerfeld expansion. The factor of 1/2 that cancels the spin degeneracy, results from the fact that $v_x^2 = v_y^2 = \frac{1}{2}v^2$ in the isotropic case.

In a numerical analysis it is more useful to write down κ^{xx} in the way it is done in (5.60). It is interesting that we have only to replace e^2 by $\epsilon_{\mathbf{k}}^2$ when we want to switch from the computation of σ^{xx} to the computation of κ^{xx} . We can use the same loop to estimate κ^{xx} as we used for the computation of σ^{xx} .

5.5.2 Thermal Hall-conductivity κ^{xy}

We studied the effect of an applied temperature gradient on a sample that forces the (quasi)particles to transport heat. As also phonons can carry heat we have to think of a way how to figure out the contribution to the heat current from (quasi)particles.

The magnitude we want to analyze now, κ^{xy} , is of particular interest, as only charged particles are bended in a magnetic field. Thus the κ^{xy} allows us to study the heat transport of the (quasi)particles in the NS screening out phononic contributions. The geometry of this experiment is very similar to the Hall experiment, $\mathbf{B} = (0, 0, B)^T$, and the temperature gradient in x-direction, shown in figure (5.11).

In the case of an applied magnetic field we have to take the Lorenz force, included in (3.25), and a force due to a temperature gradient, given in (5.55), into account. So there is a force that acts on the moving charged particles and distorts them perpendicular to the temperature gradient.

³⁵In this case we have to expand the function $N(\epsilon)\epsilon^2$ in a Taylor series. This helps us get an expression for the integral $\int N(\epsilon_{\mathbf{k}})\epsilon_{\mathbf{k}}^2 \left(-\frac{\partial f_{\mathbf{k}}^0}{\partial \epsilon_{\mathbf{k}}}\right) d\epsilon_{\mathbf{k}} = \sum_{n=1}^{\infty} a_n T^{2n} \frac{d^{2n}}{d\epsilon^{2n}} (N(\epsilon_{\mathbf{k}})\epsilon_{\mathbf{k}}^2)|_{\epsilon=0}$. Compare to Ashcroft [2], Appendix C.

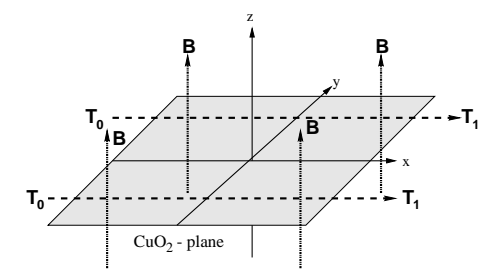


Figure 5.11: The geometry of the measurement for the thermal Hall-conductivity. The temperature gradient is realized by different temperatures at both sides of the sample, $T_0 \neq T_1$.

In this case we obtain the transport equation

$$\epsilon_{\mathbf{k}} \left(-\frac{\partial f_{\mathbf{k}}^{0}}{\partial \epsilon_{\mathbf{k}}} \right) \mathbf{v}_{\mathbf{k}} \cdot \frac{\nabla_{\mathbf{r}} T}{T} + \frac{e}{\hbar c} \mathbf{v}_{\mathbf{k}} \times \mathbf{B} \frac{\partial g_{\mathbf{k}}}{\partial \mathbf{k}} = C_{\mathbf{k}}$$
 (5.62)

Again we compute $g_{\mathbf{k}}$ by solving (5.62) which is done by inverting \hat{A} defined before. The number of "free" (quasi)particles can be obtained from (5.59) considering the second term in (5.28) for \hat{A}^{-1} .

Inserting $\hat{A}_{\mathbf{k},\mathbf{k}'}^{-1} = -\hat{K}^{-1}\hat{M}_B\hat{K}^{-1}$ in (5.59) gives us the thermal Hall-conductivity κ^{xy} :

$$\kappa^{xy} \stackrel{(5.59),(5.28)}{=} -2 \sum_{\mathbf{k},\mathbf{k}',\mathbf{k}'',\mathbf{k}'''} v_{\mathbf{k}}^{x} \epsilon_{\mathbf{k}} \hat{K}_{\mathbf{k},\mathbf{k}'}^{-1} \hat{M}_{B}(\mathbf{k}',\mathbf{k}'') \hat{K}_{\mathbf{k}'',\mathbf{k}'''}^{-1} v_{\mathbf{k}'''}^{y} \epsilon_{\mathbf{k}'''} \left(-\frac{\partial f_{\mathbf{k}}^{0}}{\partial \epsilon_{\mathbf{k}'''}} \right) \\
= -2 \frac{eB}{\hbar c} \sum_{\mathbf{k}} \epsilon_{\mathbf{k}}^{2} \left(-\frac{\partial f_{\mathbf{k}}^{0}}{\partial \epsilon_{\mathbf{k}}} \right) \tau_{\mathbf{k}}^{2} v_{\mathbf{k}}^{x} \left[v_{\mathbf{k}}^{y} \cdot \frac{\partial v_{\mathbf{k}}^{y}}{\partial k_{x}} - v_{\mathbf{k}}^{x} \cdot \frac{\partial v_{\mathbf{k}}^{y}}{\partial k_{y}} \right] \\
+ 2 \frac{eB}{\hbar c} \sum_{\mathbf{k}} \epsilon_{\mathbf{k}}^{2} \left(-\frac{\partial f_{\mathbf{k}}^{0}}{\partial \epsilon_{\mathbf{k}}} \right) \tau_{\mathbf{k}}^{3} v_{\mathbf{k}}^{x} (v_{\mathbf{k}}^{y})^{2} \left[C_{\Phi} \frac{\partial \Phi_{\mathbf{k}}}{\partial k_{x}} + C_{\Psi} \frac{\partial \Psi_{\mathbf{k}}}{\partial k_{x}} \right] \\
- 2 \frac{eB}{\hbar c} \sum_{\mathbf{k}} \epsilon_{\mathbf{k}}^{2} \left(-\frac{\partial f_{\mathbf{k}}^{0}}{\partial \epsilon_{\mathbf{k}}} \right) \tau_{\mathbf{k}}^{3} (v_{\mathbf{k}}^{x})^{2} v_{\mathbf{k}}^{y} \left[C_{\Phi} \frac{\partial \Phi_{\mathbf{k}}}{\partial k_{y}} + C_{\Psi} \frac{\partial \Psi_{\mathbf{k}}}{\partial k_{y}} \right] \tag{5.63}$$

Note that κ^{xy} is identical with the electrical hall-conductivity when we replace $e^2 \to \epsilon_{\mathbf{k}}^2$. So only an extra factor $\epsilon_{\mathbf{k}}^2$ as to be included in our program.

As we compute the energies in eV we can use the same number for the thermal Hall-conductivity as for the electrical Hall-conductivity. The only thing that changes are the units we obtain, $[\sigma^{xy}] = \frac{1}{\Omega m}$, whereas $[\kappa^{xy}] = \frac{W}{m}$.

The thermoelectric power, TEP, is the last transport quantity that we are going to compute. It is the only quantity that connects electrical and thermal transport.

5.6 Thermoelectric power TEP

The last missing tensors in (5.24) are going to be computed in this chapter.

We start defining the thermopower $S^{\mu\nu}$ which combines somehow the electrical and the thermal transport.

$$S^{\mu\nu} = -2e \sum_{\mathbf{k}\mathbf{k}'} \epsilon_{\mathbf{k}} v_{\mathbf{k}}^{\mu} \hat{A}_{\mathbf{k},\mathbf{k}'}^{-1} v_{\mathbf{k}'}^{\nu} \left(-\frac{\partial f_{\mathbf{k}}^{0}}{\partial \epsilon_{\mathbf{k}'}} \right)$$
 (5.64)

So this case is equivalent to the case $\alpha = 1$, discussed before.

Note that the function $\left(-\frac{\partial f_{\mathbf{k}}^{0}}{\partial \epsilon_{\mathbf{k}}}\right)$ is an even function around the chemical potential μ^{36} which means that the integral $\int d\epsilon \epsilon \left(-\frac{\partial f_{\mathbf{k}}^{0}}{\partial \epsilon_{\mathbf{k}}}\right) = 0$ for every temperature.

Therefore it is necessary to expand the energy density $N(\epsilon)$ also in a series to obtain the leading contribution to $S^{\mu\nu}$ defined in (5.64). We get a contribution to the thermopower $S^{\mu\nu}$ from the antisymmetric distribution of $N(\epsilon)$ around μ . A Taylor-expansion of $N(\epsilon)$ leads to

$$N(\epsilon) = N_{\mu} + N'(\mu) \cdot \epsilon + \mathcal{O}(\epsilon^2)$$

The sign of the thermopower tells us what particles generate transport (particles or holes). If $N'(\mu)$ is negative we have a positive thermopower (compare to (5.64)) which means we have holes moving. It turns out that the cold region dominates $S^{\mu\nu}$, so the sign of the thermopower can change like it is shown in figure 5.7.

When we solve (5.64) for S^{xx} we have to consider the first term in (5.28). This allows us to figure out the T-dependence of S^{xx} . It turned out in our analysis that the thermopower isn't sensitive to the transition width w. So we look at the limit $w \to 0$. We get two contributions to the thermopower, $\lim_{w\to 0} S^{xx} = S_c^{xx} + S_h^{xx}$, as we divided the first BZ into hot and cold regions.

Equation (5.31) allows us to obtain S^{xx} as:

$$S^{xx} = -e\frac{2}{N_k} \sum_{\mathbf{k}\mathbf{k}'} (\epsilon_{\mathbf{k}} - \mu) v_{\mathbf{k}}^x \hat{A}_{\mathbf{k}\mathbf{k}'}^{-1} v_{\mathbf{k}'}^x \left(-\frac{\partial f}{\partial \epsilon_{\mathbf{k}'}} \right) = e\frac{2}{N_k} \sum_{\mathbf{k}} (\epsilon_{\mathbf{k}} - \mu) \left(\frac{\partial f}{\partial \epsilon_{\mathbf{k}}} \right) (v_{\mathbf{k}}^x)^2 \tau_{\mathbf{k}}$$
(5.65)

$$^{36}f(\epsilon) = \frac{1}{e^{\beta\epsilon}+1} = 1/2\left(1-\tanh\frac{\beta\epsilon}{2}\right)$$
. Thus $\left(\frac{\partial f_{\mathbf{k}}^0}{\partial \epsilon_{\mathbf{k}}}\right) = -\beta/4\left[\frac{1}{\cosh\frac{\beta\epsilon}{2}}\right]$, which is an even function.

When we have only two lifetimes τ_c and τ_h and two velocities v_c and v_h in the two patches (in the $w \to 0$ -limit) we can simplify this easily (we only consider the cold contribution here; the hot contribution is obtained in the same way).

$$\begin{split} S_c^{xx} &= -ev_c^2\tau_c\frac{1}{N_k}\sum_{\mathbf{k}}(\epsilon_{\mathbf{k}}-\mu)\left(-\frac{\partial f}{\partial \epsilon_{\mathbf{k}}}\right)\Phi_{\mathbf{k}} \\ &= -ev_c^2\tau_c\frac{1}{N_k}\sum_{\mathbf{k}}\Phi_{\mathbf{k}}\int d\epsilon\delta(\epsilon-(\epsilon_{\mathbf{k}}-\mu))\cdot\epsilon\left(-\frac{\partial f}{\partial \epsilon_{\mathbf{k}}}\right) \\ &= -ev_c^2\tau_c\int d\epsilon\frac{1}{N_k}\sum_{\mathbf{k}}\Phi_{\mathbf{k}}\delta(\epsilon-(\epsilon_{\mathbf{k}}-\mu))\cdot\epsilon\left(-\frac{\partial f}{\partial \epsilon_{\mathbf{k}}}\right) \\ &= -ev_c^2\tau_c\int d\epsilon N_c(\epsilon-\mu)\cdot\epsilon\left(-\frac{\partial f}{\partial \epsilon_{\mathbf{k}}}\right) \\ &= -ev_c^2\tau_c\int d\epsilon N_c(\epsilon)\cdot(\epsilon-\mu)\left(-\frac{\partial f}{\partial \epsilon_{\mathbf{k}}}\right) \\ &= -ev_c^2\tau_c\int [(\epsilon-\mu)^2]N_c'(\epsilon_f)\left(-\frac{\partial f}{\partial \epsilon_{\mathbf{k}}}\right)d\epsilon \\ &= -ev_c^2\tau_c\cdot2N_c'(\epsilon_f)\cdot\int\frac{(\epsilon-\mu)^2}{2}\left(-\frac{\partial f}{\partial \epsilon_{\mathbf{k}}}\right)d\epsilon \\ &= -ev_c^2\tau_c\cdot2N_c'(\epsilon_f)\cdot(k_B\cdot T)^2\int\frac{x^2}{2}\left(-\frac{d}{dx}\frac{1}{e^x+1}\right)dx \\ &= -ev_c^2\tau_c\cdot2N_c'(\epsilon_f)\cdot(k_B\cdot T)^2\frac{\pi^2}{6} \end{split}$$

Thus we can write the thermopower S^{xx} as a sum of the cold and the hot contribution:

$$\lim_{w \to 0} S^{xx} = -e^{\frac{\pi^2}{3}} (k_B \cdot T)^2 \left[v_c^2 \cdot \tau_c N_c'(\epsilon_f) + v_h^2 \cdot \tau_h N_h'(\epsilon_f) \right]$$
 (5.66)

So we get in a thermopower S_c^{xx} that is proportional T^2 .

A dimensional analysis of S^{xx} gives us $[S^{xx}] = \frac{A}{m}$.

Now we are able to move on and to compute the thermoelectric power TEP which is defined by:

$$TEP = \frac{S^{xx}}{T\sigma^{xx}} \tag{5.67}$$

McIntosh et al. [31] pointed out that it is necessary to have a VHS in the electronic density to observe the behavior of the TEP measured experimentally. Indeed we have such VHS in our model, $\approx 35 meV$ away from the Fermi level (section 5.2).

With the knowledge gained above we can start computing an analytical formula for the

TEP in the case of constant lifetime τ and velocity v inside each patch, namely:

$$\lim_{w \to 0} TEP = -\frac{\pi^2}{3e} k_B^2 T \frac{v_c^2 \tau_c N_c'(\epsilon_f) + v_h^2 \tau_h N_h'(\epsilon_f)}{v_c^2 \tau_c N_c(\epsilon_f) + v_h^2 \tau_h N_h(\epsilon_f)}$$
(5.68)

In a more convenient form we obtain:

$$\lim_{w \to 0} TEP = -\frac{\pi^2}{3e} k_B^2 T \frac{N_c'(\epsilon_f) + \frac{v_h}{v_c} \frac{2\tau_h}{\tau_c} N_h'(\epsilon_f)}{N_c(\epsilon_f) + \frac{v_h}{v_c} \frac{2\tau_h}{\tau_c} N_h(\epsilon_f)} \approx -\frac{\pi^2}{3e} k_B^2 T \frac{N_c'(\epsilon_f)}{N_c(\epsilon_f)}$$
(5.69)

because we know from section 5.2 that $v_h \ll v_c$ and $\tau_h \ll \tau_c$. The small factor

$$R_{v,\tau} \equiv \left(\frac{v_h}{v_c}\right)^2 \cdot \frac{\tau_h}{\tau_c} \approx \frac{1}{36}$$

allows us to write the TEP in a more convenient form. A Taylor-expansion of the equation (5.68) to first order gives us:

$$\lim_{w \to 0} TEP = -\frac{\pi^2}{3e} k_B^2 T \frac{N_c'(\epsilon_f)}{N_c(\epsilon_f)} \left[1 + R_{v,\tau} \left(\frac{N_h'}{N_c'} - \frac{N_h}{N_c} \right) \right].$$
 (5.70)

We found out in our analysis that the TEP doesn't change with varying w thus the behavior of the TEP is given in this limit.

The linear temperature dependence of the TEP is in agreement with the results of Castellani et al. [8].

We know from experimental results (chapter 4), that the $TEP \propto T$ in the range T < 300K. In this region we can linearize it $TEP = \frac{\Delta TEP}{\Delta T} \cdot T + TEP_0$.

Inserting the physical constants in (5.70) gives us the leading, angle dependent contribution to the TEP as $TEP(\theta) = \left[-2.4 \cdot 10^{-8} \frac{N_c'(\theta)}{N_c(\theta)}\right] T$. So the angle θ determines mostly the TEP, as $N_c'(\theta)$ varies strongly with θ .

Table 5.3 shows the obtained slopes of the TEP's for different angles θ (obtained by inserting the physical constants and the values from table 5.2 into equation (5.70)).

The experimental result for the TEP, which is given in $[TEP] = \frac{V}{K}$, for Bi2212 is $\frac{\Delta TEP}{\Delta T} \approx -0.05 \frac{\mu V}{K^2}$. So we get a fairly good agreement with experiment for $\theta \approx 20^{\circ}$.

Kubo [30] noted that the negative TEP brings up that the transport mass perpendicular to the FS is electron like. On the other hand the Hall-angle is positive which is equivalent

 $^{^{37} \}text{In the case of } YBa_2Cu_3O_7 \text{ the ratio } \frac{\tau_c}{\tau_h} \approx 3.9 \text{ [5].} \text{We obtain a similar ratio for our model } \frac{\tau_c}{\tau_h} \approx 3.2 \text{ model}$

θ/°	2.6	6.5	12.9	19.0	24.6	34.6
$rac{\Delta TEP}{\Delta T} \ / \ rac{\mu V}{K^2}$	0.21	0.155	-0.335	-0.088	-0.053	-0.046

Table 5.3: The table shows the obtained slope of the TEP for different angles θ . The data are taken from table 5.2.

to the fact that the mass parallel to the FS is hole-like.

As we receive our best fit for $\theta \approx 20^\circ$ we obtain exactly his observations, namely negative TEP and positive Hall-angle. We are going to discuss this in more detail in chapter 7.

Chapter 6

The used Program

Our interest in the temperature dependence of transport properties of BSCCO forced us to write a Fortran77 program that is called "transport.f". This program allows us to get numerical values from the equations described in (5.33), (5.43), (5.53), (5.60), (5.63) and (5.65). These equations allow us to plot all quantities described in chapter 4 as a function of T.¹

In this chapter we want to explain and introduce the used variables and the syntax of the program. We use "gnuplot" to generate plots where the temperature dependence of the considered quantities can be extracted, as our program generates files of points that can be read by gnuplot.

The proceeding how to choose the values of our five parameters properly will be described in chapter 7.

6.1 The Input

Our interest in Bi2212 simplifies our studies because we don't have to consider the effect of chains in these materials. We are studying a purely 2D problem.

The FS of Bi2212 is shown in figure 2.4 which was generated by the tight binding fit given in (5.18). Subsection 6.1.1 repeats this briefly. In subsection 6.1.2 we define the geometry of our model by introducing some geometrical magnitudes. Finally we explain the external data of the program (in subsection 6.1.3) and the parameters (subsection 6.1.4) that have to be fitted.

¹The result obtained by the program is converted into units measured experimentally to be able to compare the results of the TPM with experiments.

6.1.1 The FS of Bi2212

The input of the program is the FS of Bi2212, given by a tight binding fit with up to fifth nearest neighbor hopping from (5.18), section 5.2. The Band-structure of Bi2212 is reproduced by this fit.

To be consistent with units the energy is always given in eV in the program. The numerical values of the parameters, c_i , i=1,...,6, are called ef, et1 ... et5 in our program. The functions given in the tight binding fit, η_i , i=1,...,6, are given by ek1 .. ek5. As shown in (5.18) the FS is reproduced by this functions weighted with parameters. Note that we can change the shape of the FS by changing the parameters c_i . So we can study the effect of the shape of the FS on the transport quantities.² Of course the lattice constant a (which is called "latt" in the program) is missing in formula (5.18). Thus each wavevector k_i , i=x,y has to be multiplied by a. The value for a is $a=3.76 \cdot 10^{-10} m=3.76 A^{\circ}$ in Bi2212 systems. Note that we write distances in Angstrom in the program, thus latt=3.76.

6.1.2 The geometry of the model

We parameterize the size of the cold area by the angle θ as usual. Figure (6.1) shows that four lines restrict the cold region. In reciprocal space these lines are given by

$$k_y = a \cdot k_x$$

$$k_y = b \cdot k_x$$

$$k_y = a \cdot k_x + d$$

$$k_y = b \cdot k_x + c$$

with $a = \cot(\theta) > 0$, $b = \tan(\theta) > 0$, a > b, $c = \pi(1 - \tan(\theta)) > 0$ and $d = \pi(1 - \cot(\theta)) < 0$ defined in section 5.1. A product of four functions describes the cold region. In the case of the smooth change between the cold and hot regions the cold region of the first BZ is described by:

$$\Phi_{\mathbf{k}} = \prod_{i=1}^{4} \Phi_i(\mathbf{k}) \tag{6.1}$$

²The shape of the FS has the biggest influence on the TEP and $\tan \theta_H$.

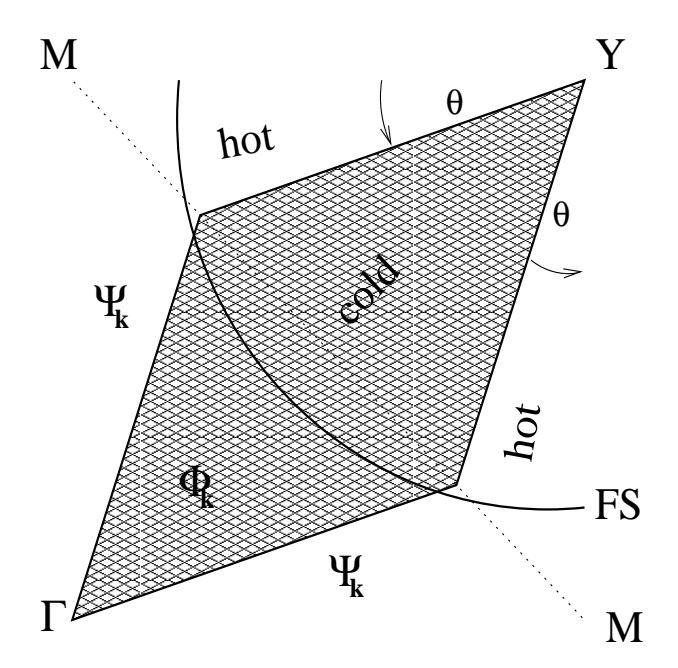


Figure 6.1: The size of the cold region is only parameterized by the angle θ .

with
$$\Phi_1(\mathbf{k}) = \frac{1}{2} \left[1 - \tanh\left(\frac{k_y - ak_x}{w}\right) \right]$$
, $\Phi_2(\mathbf{k}) = \frac{1}{2} \left[\tanh\left(\frac{k_y - bk_x}{w}\right) + 1 \right]$, $\Phi_3(\mathbf{k}) = \frac{1}{2} \left[1 - \tanh\left(\frac{k_y - bk_x - c}{w}\right) \right]$ and $\Phi_4(\mathbf{k}) = q\frac{1}{2} \left[\tanh\left(\frac{k_y - ak_x - d}{w}\right) + 1 \right]$ with the width of the transition region w introduced in section 5.1.

The parameters needed in the program are the angle θ , describing the size of the cold region, (program: theta) and the width w (program: w). The function $\Phi_{\mathbf{k}}$ is used in the subroutine "phipsi". This subroutine allows us to compute the size of the cold region, as it gives us the weight of Φ at every (discrete) point of the lattice. The functions $\Phi_1(\mathbf{k})$ etc. are called t1 etc. in this subroutine.

Summing over every point of the lattice with suitable weight Φ , which is done in the variable *sumphi* gives us the size, normalized to one, of the cold region (which we call α). The size of the hot region is given just by subtracting the cold region from 1.

6.1.3 External data

External data are data we insert in our program before we start computing the quantities of our interest. These data are the mash n_k^3 , the temperature-range (T_{min}, T_{max}) in

³The reciprocal space in the first quadrant of the first BZ is discretized!

eV), an external magnetic field B_{ext} and some converting-factors (like cfactor, sfactor, bh, mfactor and lofactor) that guarantee that the result has the same dimension as measured in experiments, which is important as we want to compare with experimental data.

The mash n_k is determined by the lowest temperature T_{min} as we decided to sum over the whole first quadrant of the first BZ and the function $\frac{\partial f^0}{\partial \epsilon}$ (it restricts transport processes around the FS!), that has a width of $\approx k_B \cdot T$, has to be modeled properly. We decided to study the transport data for temperatures $T \geq 60K$, thus a mash $n_k = 256$ is sufficient.

The temperature range is splitted into n_T equal temperature-slices. The studies were carried out in a temperature range T with $60K \le T \le 1100K$. We decided to chop this temperature-interval into hundred equal pieces, $n_T = 100$. This means we obtain temperature values every $\frac{T_{max} - T_{min}}{n_T}$ thus every $\approx 10K$.

Another external data is the value of the Fermi-function f (called fermi in the program). As $f = f(\epsilon)$ we have to compute $f(\epsilon)$ for every point of the lattice, i.e. for every pair (k_i, k_j) , i, j = 1, ..., 256 with the energy-dispersion given in (5.18).

When we want to get results for lower temperatures we might have to use more sophisticated methods like the "tetrahedron method" explained in the appendix.

6.1.4 Parameters of the model

The TPM was introduced in chapter 5. It included three parameters a, b and c that described the strength of the possible scattering mechanisms. These three parameters have to be chosen properly to give the correct results of the desired transport quantities. Two other parameters, explained in chapter 5, are also special importance, namely the angle θ that describes the size of the cold region and the width of the transition region w.

 θ has effects on every quantity of our interest (compare to chapter 5). So it has to be chosen very carefully. Note that for $\theta \approx 20^{\circ}$ the area of the cold region is approximately equal to the area of the hot region. The TEP suggests exactly this value for θ to be fitted well. This fifth parameter, the width of the transition region, is basically determined by

the magnetoresistance. Note that the MR contains factors with the second derivative of $\Phi_{\mathbf{k}}$. In the case of an discontinuous change between cold and hot regions we would get a divergence for the MR. That's why we originally introduced w.

6.2 Programming

As already pointed out we are interested in the temperature-dependence of transport properties of *BSCCO*. A temperature loop allows us to obtain transport properties as a function of temperature. We compute all transport properties of our interest for

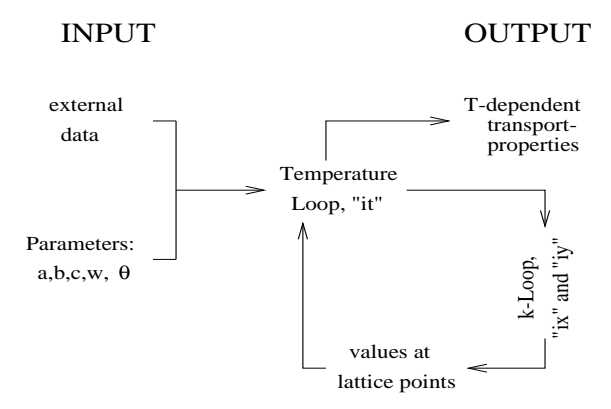


Figure 6.2: The picture shows the strategy of the program. A temperature loop computes the different transport properties, like ρ^{xx} , for discrete temperatures.

a given set of parameters a, b, c, w and θ and compare the result with experimental results. For a optimal set of parameters we can fit each data given in chapter 4 in a reasonable way.

6.2.1 Temperature-Loop

As already told we vary the temperature between T_{min} and T_{max} in steps of $\frac{T_{max}-T_{min}}{n_T}$. In a big temperature-loop (used variable "it") we are increasing T with steps of ΔT . We reset all transport data the beginning of every loop. The temperature dependent constants C_{Φ} and C_{Ψ} are computed like shown in section 5.4, which allows us to get transport properties of BSCCO for each (fixed) temperature in the considered range. To get these values we are summing over the first BZ with a discrete set of **k**-points. For symmetry reasons (the FS of the CuO_2 -planes has fourfold symmetry!) it is enough to sum only over the first quadrant of the first BZ.

As we are in a temperature range T>60K a mash of $n_k=256$ is big enough. So we have 256×256 contributions to transport in this quadrant. Because of the function $-\frac{\partial f}{\partial \epsilon}$ we are almost completely restricted on the FS which means that only **k**-points around the FS contribute to transport.

6.2.2 k-Loop

Inside the "k-Loop" we start to figure out the values of the functions $\Phi_{\mathbf{k}}$ and $\Psi_{\mathbf{k}}$ defined in (5.17) at every point of the lattice. These values are needed to be able to write down the relaxation time (5.8) that characterizes our model. Furthermore we compute the first and the second derivative of the functions that describe the hot / cold regions $\Phi_{\mathbf{k}}$ as they are needed in the formula for the (thermal) Hall-angle and the MR. These three jobs are done in the three subroutines "phipsi", "dphi" and "sdphi".

The next step is to compute the relaxation time, $\tau_{(k_x,k_y)} = \frac{1}{C_{\Phi}\Phi_{(k_x,k_y)} + C_{\Psi}\Psi_{(k_x,k_y)}}$, for a fixed **k**-point, as every transport quantity depends on this relaxation time.

From the energy-dispersion given in (5.18) we can derive velocities, e.g. $v_x = \frac{\partial \epsilon}{\partial k_x}$, masses, e.g. $m_{xx} = \frac{\partial^2 \epsilon}{\partial k_x^2}$, and third derivatives of the dispersion relation that will be of importance later (example for our notation: $dyxy = \frac{\partial^3 \epsilon}{\partial k_y \partial k_x \partial k_y}$). Note that we can use some symmetry relations, like $\frac{\partial^2 \epsilon}{\partial k_x \partial k_y} = \frac{\partial^2 \epsilon}{\partial k_y \partial k_x}$, to determine the transport properties of our model, as the FS of BSCCO has fourfold symmetry. From these analytical formulas we obtain numerical values for the velocity $\mathbf{v} = (v_x, v_y)$, mass etc. of a fixed \mathbf{k} -point.

Each transport quantity has the factor $\frac{\partial f}{\partial \epsilon}$, with the Fermi distribution f, in common. The energy dependence of $f(\epsilon)$ forces us to compute it at each lattice point (k_x, k_y) again. Also the derivative $\frac{\partial f}{\partial \epsilon}$ is computed for each point.

Now we can start computing transport properties just applying the formulas found in (5.33), (5.43), (5.53), (5.60), (5.63) and (5.65). The conductivity has a cold, "cc", and a hot, "ch", contribution in each point like it is shown in formula (5.33). The same splitting is done for the thermopower, where the "sc" labels the cold part of the

thermopower and "sh" the hot part of it. It can be seen in equation (5.43) that the Hall-conductivity σ^{xy} has three contributions (in the program we combined σ_2^{xy} and σ_3^{xy} to one contribution!). Note that we need the first derivative of $\Phi_{\mathbf{k}}$ to obtain σ^{xy} . This is why the subroutine "dphi" is important for this quantity. The thermal Hall-conductivity has the same constituents as σ^{xy} but an extra factor of $\epsilon_{(k_x,k_y)}^2$ due to the heat transport. The most complicated quantity is $\Delta\sigma^{xx}(\mathbf{B})$, which is called "magn" in the program. Like it is shown in section 5.4, equation (5.53) we get three contributions $(\propto \tau^3, \propto \tau^4 \text{ and } \propto \tau^5)$ to this quantity.

After we completed the loop over all **k**-points we have calculated all quantities of our interest we need to know to estimate the transport properties for a given temperature.

6.2.3 Converting in suitable quantities

One basic goal of our analysis is to compare the transport-results of our model with experimental data to find out whether this phenomenology describes experiments well. The quantities obtained from the **k**-Loop have to be converted into quantities measured in experiments. This is the reason why we inserted several factors, already mentioned above. Note that we are using units like eV and \hbar . When we convert these units in SI-units we have to multiply the obtained values by these factors. Another reason for some extra factors is how quantities are measured in experiments. For instance the resistivity is measured in $\mu\Omega cm$. Note that the relaxation time τ is given in units of $10^{-15}s$ and the length is given in $10^{-10}m$ in our program.

So we obtain the different quantities of our interest by multiplying them with the suitable values.

The values of the different transport quantities and the belonging temperature are written in different files. After this the same procedure starts with a temperature that is $\frac{T_{max}-T_{min}}{n_T}$ bigger.

6.3 subroutines

We are using three subroutines to compute values of $\Phi_{\mathbf{k}}$ and derivatives of this function. The relation $\frac{\partial \Phi_{\mathbf{k}}}{\partial k_x} = -\frac{\partial \Psi_{\mathbf{k}}}{\partial k_x}$ showed in the appendix allows us to consider only derivatives of Φ . Obviously the relation above is also true for derivatives with respect to k_y .

6.3.1 "phipsi"

The smooth change between the cold and the hot region, like it is described in (5.17), forces us to compute the value of Φ for every point of the lattice. Obviously we obtain values that are ≈ 0 far away from the cold region and values ≈ 1 inside the cold region. But anyway we need a knowledge of the values in the transition region. This subroutine allows us to get a numerical value of Φ for every **k**-point inside the first quadrant of the first BZ. Note that Ψ is achieved just by subtraction, $\Psi = 1 - \Phi$.

6.3.2 "dphi"

The computation of the Hall-conductivity σ^{xy} makes a derivative of the function Φ necessary. It follows from (5.17) that the derivatives $\frac{\partial \Phi}{\partial k_x}$ and $\frac{\partial \Phi}{\partial k_y}$ are not identical. The property mentioned above, $\frac{\partial \Phi_{\mathbf{k}}}{\partial k_x} = -\frac{\partial \Psi_{\mathbf{k}}}{\partial k_x}$, allows us to consider only the two different derivatives of Φ (with respect to k_x and k_y) and to neglect the derivatives of Ψ in this subroutine.

A analytical derivative of $\Phi_{\mathbf{k}}$ is done in the appendix. This formula is inserted in the subroutine.

6.3.3 "sdphi"

A second derivative of Φ becomes important when we want to compute $\Delta \sigma^{xx}(\mathbf{B})$. In this subroutine we obtain three different values, namely $\frac{\partial^2 \Phi}{\partial k_x^2}$, $\frac{\partial^2 \Phi}{\partial k_x \partial k_y}$ and $\frac{\partial^2 \Phi}{\partial k_y^2}$. Again we computed these derivatives analytically and inserted the solution into our program. The analytical derivatives are also shown in the appendix.

Chapter 7

Results and Discussion

A numerical solution of the TPM using the program described in chapter 6 is given in this chapter. The temperature dependence of the DC-resistivity ρ^{xx} , TEP, Hall-angle, MR and thermal Hall-conductivity are computed and compared with experiments (chapter 4). The influence of the fitting-parameters a, b, c, w and θ on the transport properties is studied.

Section 7.1 describes the influence of the fitting-parameters on the studied transport quantities. It shows in a numerical way the effect of the different fitting-parameters on the different transport quantities.

As we have to fit five parameters we suggest a possibility to fix these parameters in section 7.2. The problem is that we want to fit all considered transport quantities introduced in chapter 4 as good as possible. Thus we have to think of a way how to consider the effect of the five parameters on all quantities when fitting the data.

It turns out that the model has some problems in describing heat processes, like TEP and thermal Hall-angle. A Lorenz-plot doesn't show exactly the behavior we expect for instance. Electronic transport is described very well within the framework of the TPM. This is discussed in section 7.3.

The last section of this work, section 7.4, suggests some possibilities how to improve the model, like choosing a temperature dependent transition width w(T).

7.1 Parameters of the TPM

The size of the cold/hot region, so the angle θ , is the most important quantity in our approach as it effects every transport quantity of our interest. In the TPM the essential point is the construction of the scattering matrix $C_{\mathbf{k}\mathbf{k}'}$ which is determined by a,b and

 $c.^{1}$ Due to a divergence in the MR (second derivative of step function diverges!) we had to introduce a transition width w in the TPM. Finally we are up to fit five parameters given above.

We are studying the effect of these parameters on the transport quantities given in chapter 4 by keeping four parameters fixed and changing the fifth by $\pm \approx 33\%$ around its "best" value.² The "best" values are given here (compare to section 7.2) as: a = 60, b = 1.8, c = 6.5, w = 0.25 and $\theta = 20^{\circ}$.

7.1.1 DC-resistivity ρ^{xx}

The linearity of the resistivity up to $\sim 700K$ was found experimentally, e.g. [1]. Experiments show a temperature dependence of the resistivity $\rho^{xx}(T) \propto T^{\alpha}$, where [1] and [7] claim that α increases with doping (compare to figure 7.2). They observe a increasing α with increasing doping, $\alpha > 1$ for overdoped.

Figure 7.1 shows the effect on the resistivity of changing the different parameters. It can be seen that changing the cold region, the angle θ , has the biggest effect on ρ^{xx} . Figure 7.4 underlines this statement.

Note that the inter-patch scattering c changes the slope of ρ^{xx} , as predicted in (5.37). Increasing c results in a bigger slope of the resistivity. As the inter-patch scattering is important for ρ^{xx} a variation in w, which describes this transition region, has also a quite big effect on it. Furthermore it can be seen in figure 7.1 that a change in the scattering mechanism inside the cold a or the hot region b has only a minor effect on ρ^{xx} .

The offset in the resistivity shown in figure 7.1 was already explained in chapter 5. Remember that in the case of finite $w \tau_{\mathbf{k}}$ given in (5.7) doesn't diverge so we get some zero-temperature offset to the resistivity. In agreement to the predictions given in chapter 5 the offset increases with increasing $b(1-\alpha)$, so for increasing θ and b (figure

¹Note that we are talking about $\frac{\hbar \bar{a}}{k_B^2}$, $\hbar \bar{b}$ and $\frac{\hbar \bar{c}}{k_B}$ when we write a, b or c in this chapter. This idea was introduced in section 5.1. So the temperature dependence of a, b, c is eliminated from these parameters in this chapter.

²The word "best" doesn't mean the absolutely best value here - there might be a slightly better combination of the five parameters. As this set of parameters fits the data quite well we decided to choose this parameter set.

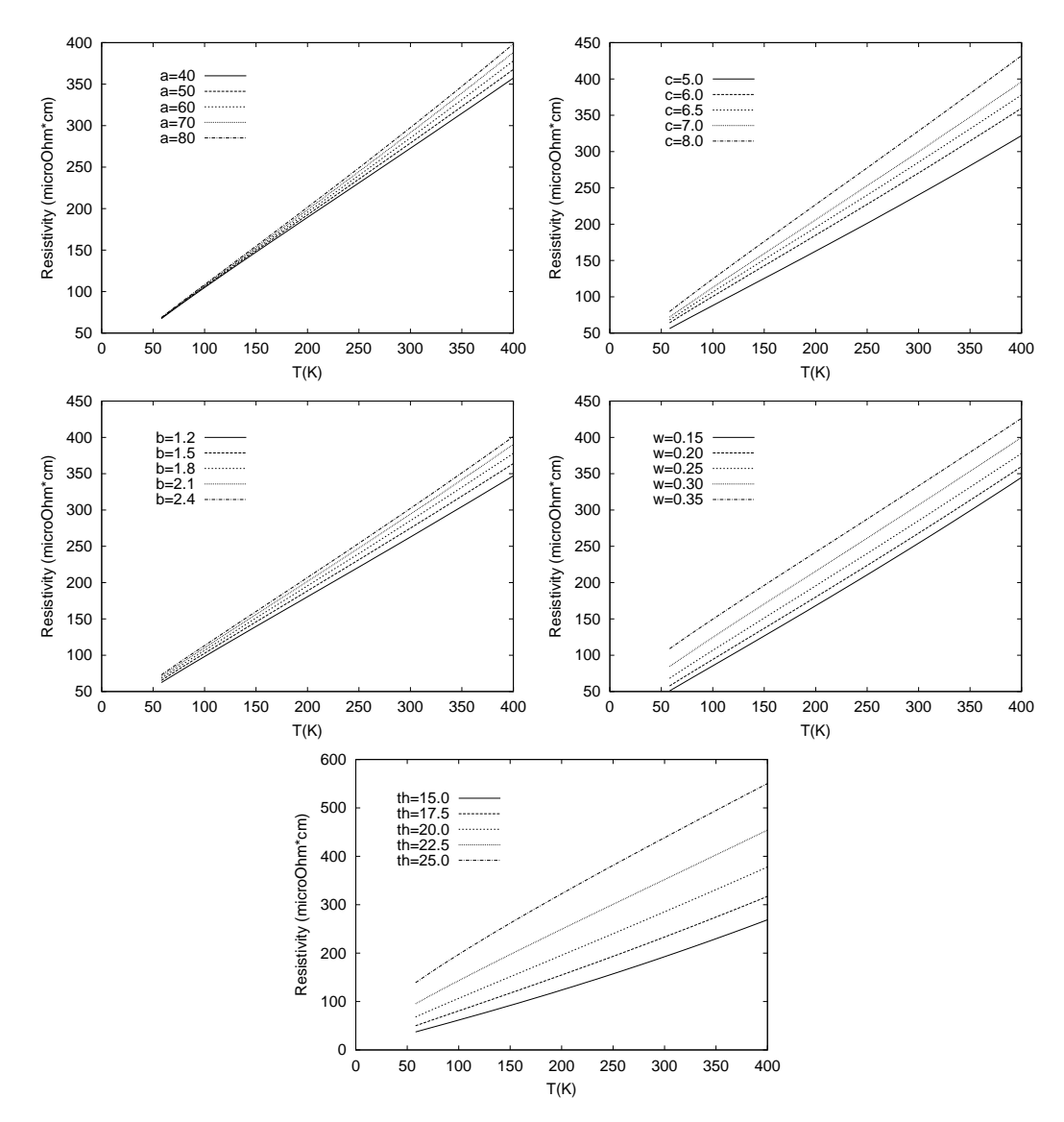


Figure 7.1: The plot shows the effect of changing the different parameters of the TPM (keeping the other parameters fixed) on the DC-resistivity ρ^{xx} as a function of T. The "optimal" parameter-values are set to: $a=60,\,b=1.8,\,c=6,5$, w=0.25 and $\theta=20^\circ$. The varied parameters and their values are written in each figure.

7.1). So the finite width and the temperature independent scattering in the hot regions might be thought as a contribution given by impurities. However the interpretation is difficult.

Furthermore a change in θ changes the exponent α of the T-dependence as mentioned in [1] and [7] (already pointed out above) (compare to figure 7.2).

Our TPM allows us to study the effect of doping by changing the area of the cold region (vary θ). Doping the material is like bringing more carriers into the cold region

(material is more FL-like!). So the cold region increases which is equivalent to decrease the angle θ (compare to figure 6.1). The lowest plot in figure (7.1) shows the effect of a change in θ thus the effect of doping on the TPM. The experimental result described above [1] and [7], namely that the exponent α , $\rho^{xx}(T) \propto T^{\alpha}$ increases with increasing doping (decreasing θ !) can be seen in figure (7.2).

Note that the coefficient α can be estimated from figure 7.2.

A problem of the TPM is that it is difficult to make statements about the residual resistivity with it, because the physical meaning of w and b is not very clear. It was found [1] that the residual resistivity increases with increasing doping in the optimally and overdoped regime.

For sure it is one problem of the TPM that it lacks this.

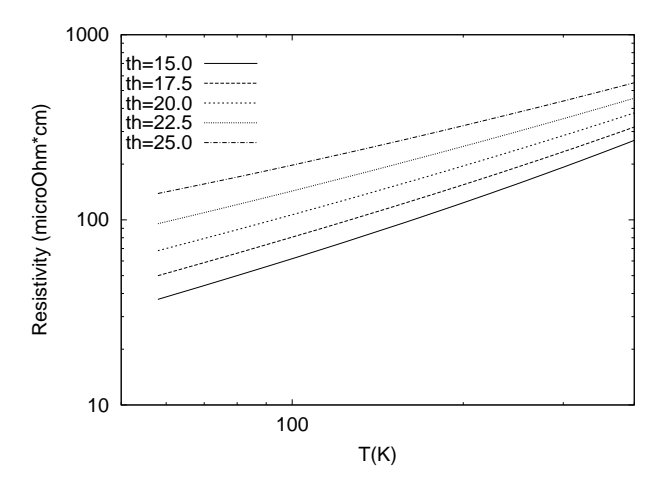


Figure 7.2: This log-log plot shows that the slope of the curves increases with decreasing θ (= increasing doping), as predicted in [1] and [7].

Furthermore we study the effect of a change in the FS on the resistivity. This is done by changing the parameters c_2 and c_3 in (5.18). The effect of these two parameters can be seen in figure 7.3. In this manner we can figure out which region of our model governs the different transport properties of our interest.

It turns out that c_2 has a big effect on the curvature of the FS, thus the change of the FS is biggest in the (π, π) -direction (cold region). c_3 is responsible to change the FS at the nodes, in $(0, \pi)$ and $(\pi, 0)$ -direction (hot regions).

Figure 7.4 shows that a change in c_2 has quite a big effect on ρ^{xx} . A change in c_3 doesn't affect ρ^{xx} . As the DC-resistivity is governed by the cold region this can be

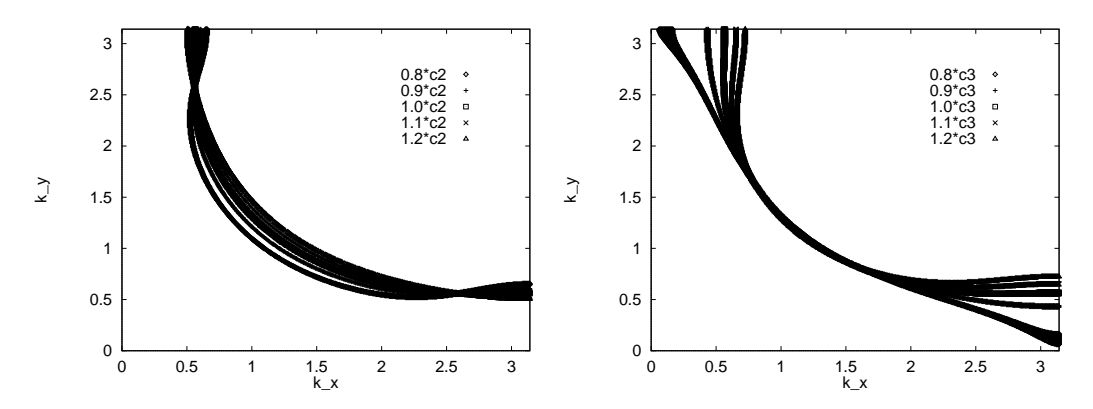


Figure 7.3: The effect of a change of c_2 and c_3 given in (5.18) can be seen in the two figures. c_2 affects the cold and c_3 the hot region.

understood. Changing c_3 only effects the hot regions that are not important for ρ^{xx} (compare to section 5.3).

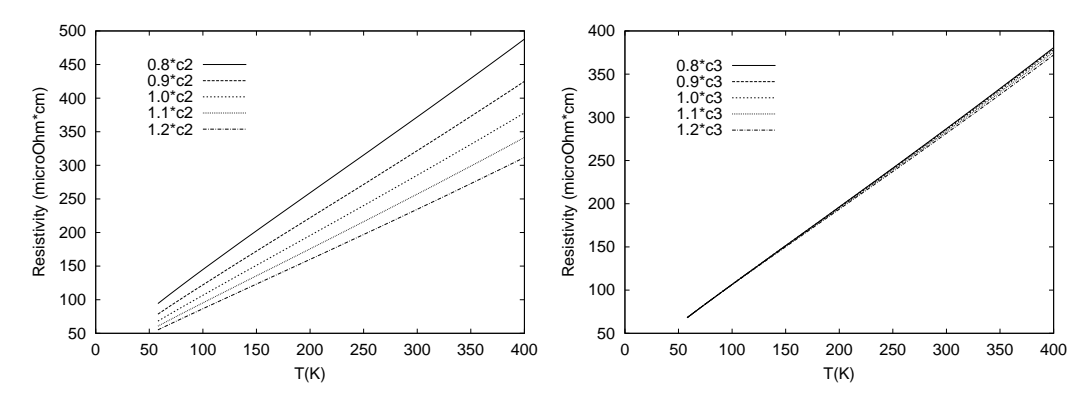


Figure 7.4: The left figure is due to a change in c_2 (cold region). The resistivity changes drastically whereas changing c_3 (hot region) doesn't change ρ^{xx} . The resistivity is governed by the cold region.

7.1.2 Thermoelectric power (TEP)

We know from (5.70) that the angle θ is the quantity that governs the TEP most [31]. So the ratio between the derivative in the density of states and the density of states in the cold region is the main quantity that determines the TEP. It was argued in section 5.6 that an angle $\theta \approx 20^{\circ}$ gives the best fit for the TEP.

Figure (7.5) shows that the TEP (obtained from the TPM) only changes slightly by changing a, b, c, w. We get the biggest effect on the TEP from the scattering in the hot region b. Thus we don't agree with Calyhold et al. [12] who argued that the TEP is

governed by the same relaxation rates that govern the magnetotransport.

In the range we are changing our parameters no big change is observable. Especially the offset (that is very sensitive to doping) doesn't change at all. The only parameter that really affects the TEP is the angle θ . The θ -dependent plot of the density of states $N(\epsilon)$ shows that we get always a negative TEP for $\theta \geq 10^{\circ}$, figure 5.7. Note that we don't expect a big change in $\frac{N'_c(\theta)}{N_c(\theta)}$ in the range we consider $(15^{\circ} \leq \theta \leq 25^{\circ})$, as $N'_c(\theta)$ doesn't change much in this range (compare to figure 5.7).

It has to be pointed out that the effect of CuO-chains affects the TEP strongly. We neglect this effect here, as we are considering BSCCO-materials.

Similar to [31] we find that the TEP is very sensitive to a variation of the electronic structure, reached by a change in c_2 and c_3 (figure 7.3). As McIntosh [31] already pointed out a change in the curvature of the FS has a big effect on the TEP. This is shown in the left figure in figure 7.6. A change of the curvature of the cold region (c_2) results in a big change in the TEP. Changing c_3 has also a quite big effect on the TEP. We remark finally that a change in the electronic structure has a much bigger effect on the TEP than a change in the parameters of our model.

7.1.3 Hall-angle

We expect a temperature dependence of this quantity $\cot \theta_H(T) \propto T^{\alpha}$, where $\alpha \leq 2$ as mentioned above. Experiments figured out that $1.65 \leq \alpha \leq 2$ [1] and [27]. A plot of $\sqrt{\cot(\theta_H)}$ vs. T shows that the Hall-angel has almost a temperature dependence $\propto T^2$. As shown in figure (7.7) we observe an almost straight line. Our TPM shows that a has a minor and especially b has almost no effect on the Hall-angle. It can also be seen in figure 7.7 that the inter-patch scattering c has a big effect on the Hall-angle and it changes the coefficient α slightly. As the inter-patch scattering c has a big effect on the Hall-angle also c0, describing the width of the transition region is important. Figure 7.9 shows that the transition region is important for the Hall-angle.

It is of interest, whether the slope α changes when we change the size of the cold region, i.e. when we dope. Experiments were carried out in [7], [22] and [27] and showed that

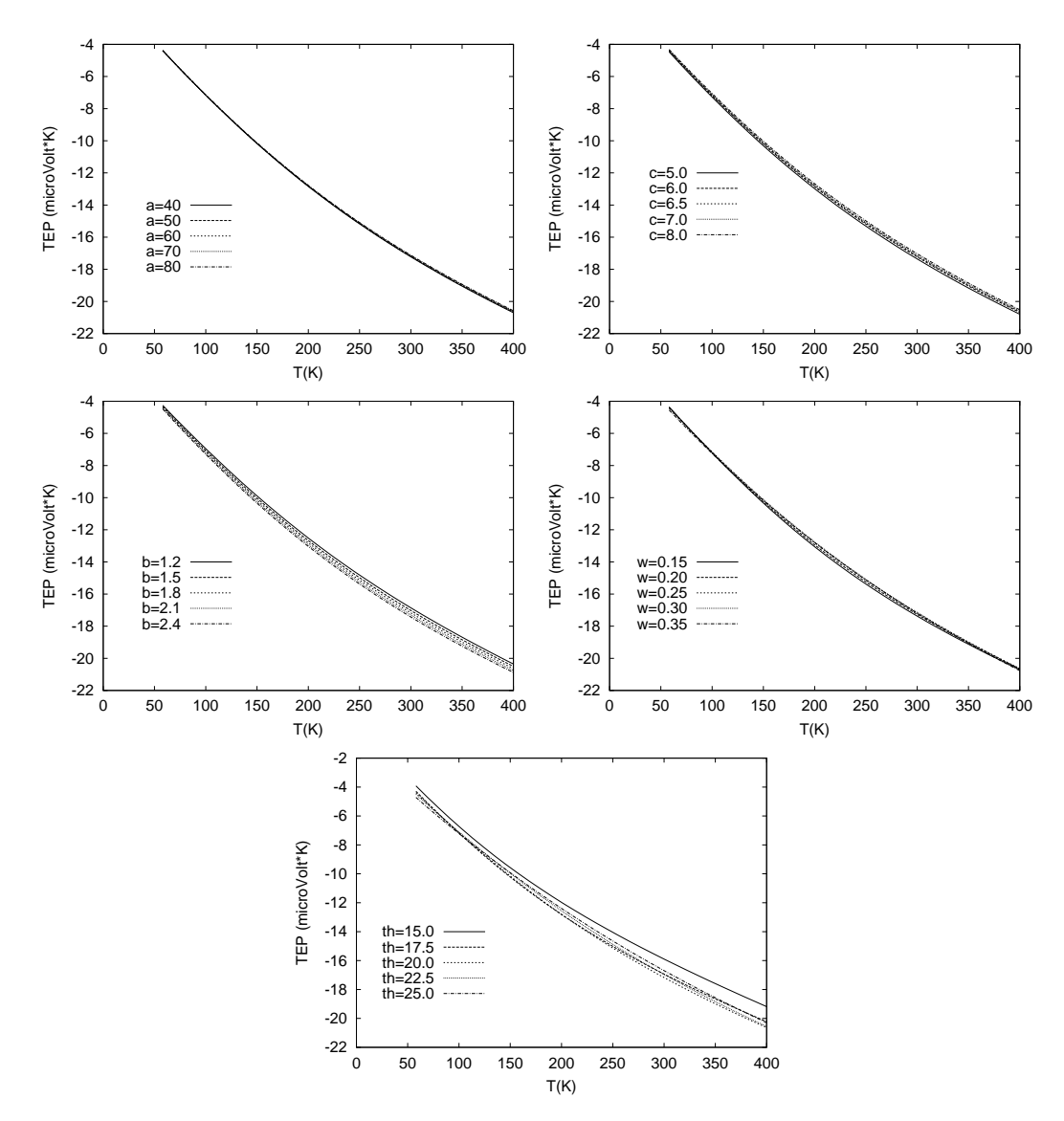


Figure 7.5: We can study the effect of the parameters on the TEP in this plots. It turns out that only the angle θ (and maybe b) has an effect on the TEP. Parameter values are: $a=60,\,b=1.8,\,c=6,5$, w=0.25 and $\theta=20^{\circ}$.

the slope α decreases when we increase doping. It is argued in these papers that the relation $\cot \theta_h \propto T^2$ is only valid in the strongly underdoped regime. The evolution of the slope with changing the angle θ can be studied in figure 7.8.

It can be seen in figure 7.8 that the value α increases slightly with increasing doping (decreasing θ) which is opposite to the experiments [27] and [1]. Anyway the change in the slope is only a very light one.

Note that doping also effects the offset of the Hall-angle [1]. This fact is difficult

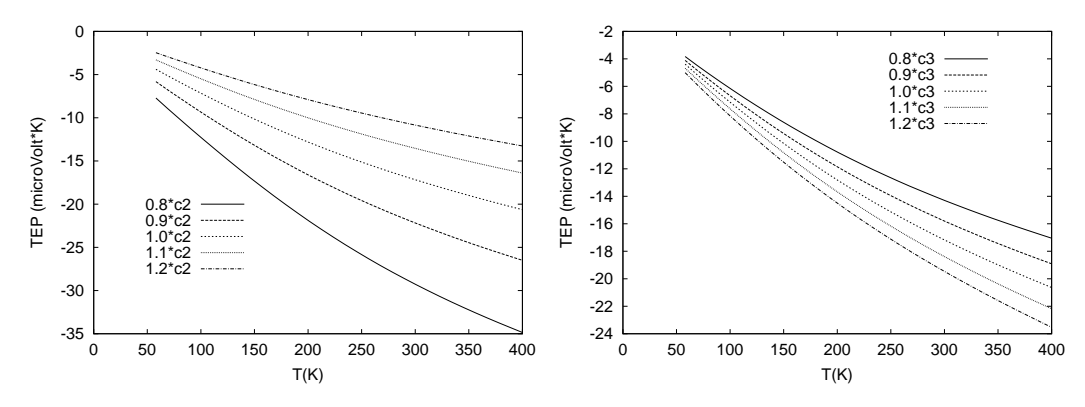


Figure 7.6: The TEP is mostly governed by the cold region, described by changing c_2 . However the influence of the hot region c_3 is not neglectable as the right figure shows.

to understand as $\cot \theta_H(T)$ is a ratio of two quantities (compare to (5.44)) σ^{xx} and σ^{xy} . Again, similar to before the offset is due to a finite transition width w and the hot scattering b. Konstantinovic [27] claimed that no model is able to describe this properties of the decreasing of α and the increasing of the offset with doping. Also the TPM is not able to reproduce this experimental results. Maybe a temperature and angle dependent width $w(T, \theta)$ could solve this problem.

Finally we study which region affects the Hall-angle most by changing the electronic structure (c_2 and c_3) of the system. Ong claimed [34] that the electronic structure of the system has a big effect on the Hall-angle. We agree with his conclusion, compare to figure 7.9, but want to point out that the electronic structure has even a bigger effect on the TEP (compare figure 7.6 and figure 7.9!).

The strong influence of the anisotropy of the electronic structure on the Hall-angle was also pointed out by Konstantinovic [27].

It turns out that the Hall-angle is very sensitive to a change in the transition region, whereas the TEP is sensitive to a change in the cold region. Thus the effect of changing the parameters c_2 and c_3 has the same magnitude (figure 7.9), as the transition region is changed slightly (compare to figure 7.3).

7.1.4 Magnetoresistance MR

Ando [1] reported measurements of the longitudinal and transverse MR of BSCCO-samples (chapter 4). This group also measured the MR for varying doping. Figure

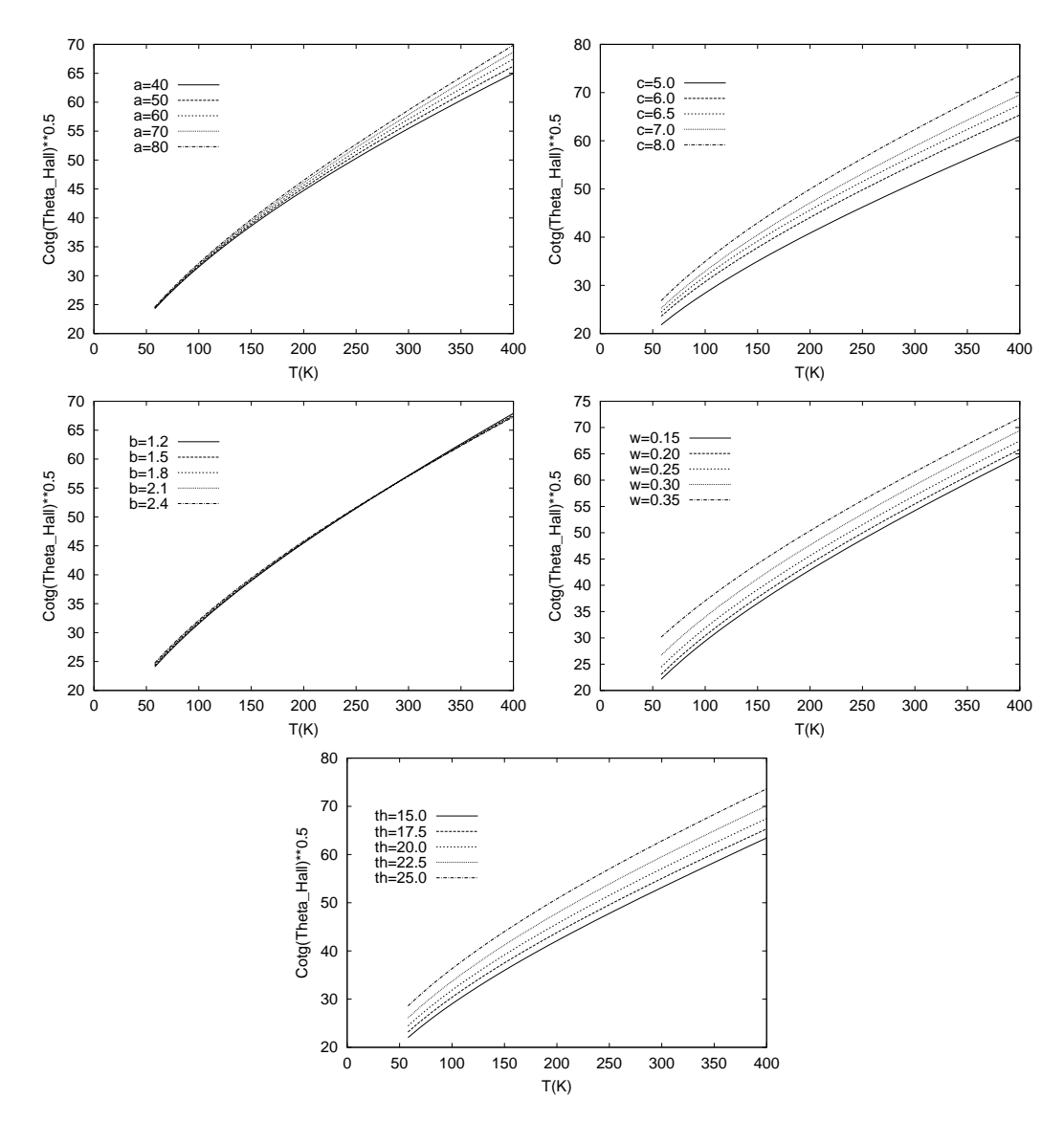


Figure 7.7: The Hall-angle is determined by the transition region between the cold and the hot region. So a change in c and w has quite big effects on this quantity. The plot is generated with a = 60, b = 1.8, c = 6, 5, w = 0.25 and $\theta = 20^{\circ}$.

(7.10) shows the effect of the different parameters of our model on the MR. Obviously a change in θ (i.e. doping) has a quite big effect on the MR in our model. Contrary to experiments the MR increases when increasing doping in the TPM.

It turns out that c, w and θ are the parameters that govern the MR. So it seems that also this quantity is governed by the transition region. However figure 7.12 shows that the MR is mostly governed by the hot region.

The effect of the transition width w can be studied figure (7.10). It can be seen

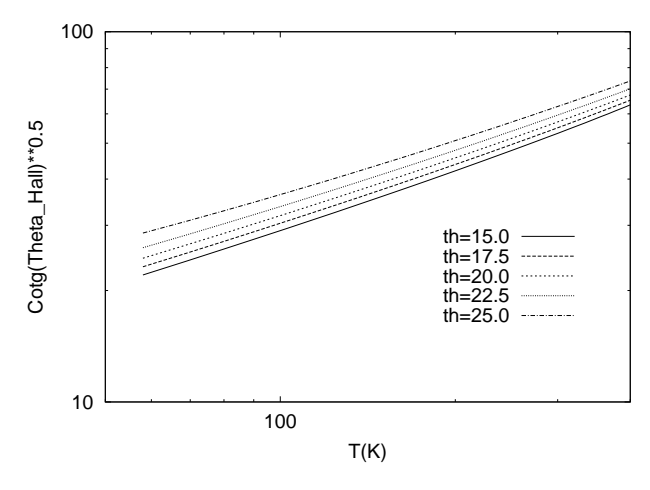


Figure 7.8: This plot shows how the slope α (for the Hall-angle) changes by changing θ (doping). α increases slightly with increasing doping (decreasing θ), opposite to [1] and [27].

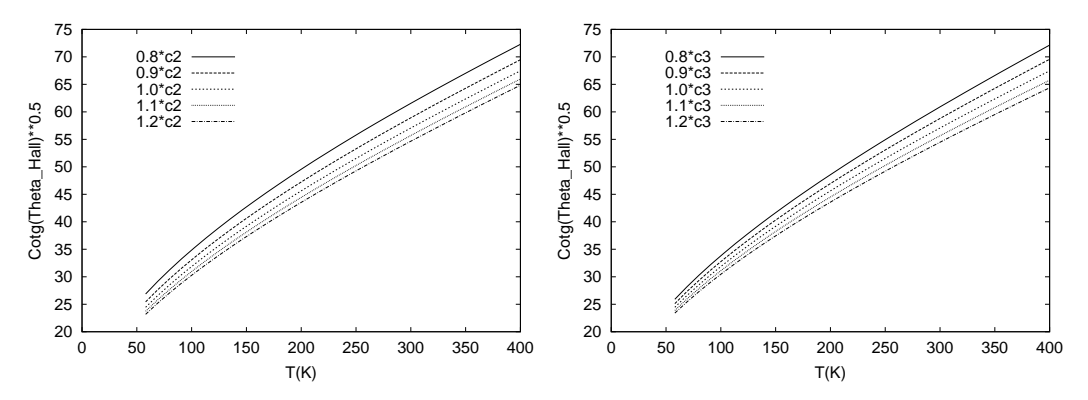


Figure 7.9: The effect of a change in c_2 and c_3 is of the same order for the Hall-angle, which tells us that this quantity is governed by the transition region. Note that a change of this parameters, especially c_2 , have a much bigger effect on the TEP (compare figure 7.6).

that this quantity becomes more and more important the smaller it becomes. A big difference in the MR can be observed between w = 0.15 and w = 0.35. So it seems that the MR diverges in the limit $w \to 0$ as predicted in 5.4. One improvement of our model would be to introduce a variable width $w(\theta, T)$ dependent on θ and T which seems to be a elementary idea as the MR is very sensitive to this quantities. One can expect that increasing the temperature broadens the width of the transition region.

We study the effect of doping on the slope α , $MR \propto T^{\alpha}$, in figure 7.11. The figure allows us to extract this slope from it and to compare it with the literature. Obviously doping (a variation of θ) doesn't change the slope α a lot.

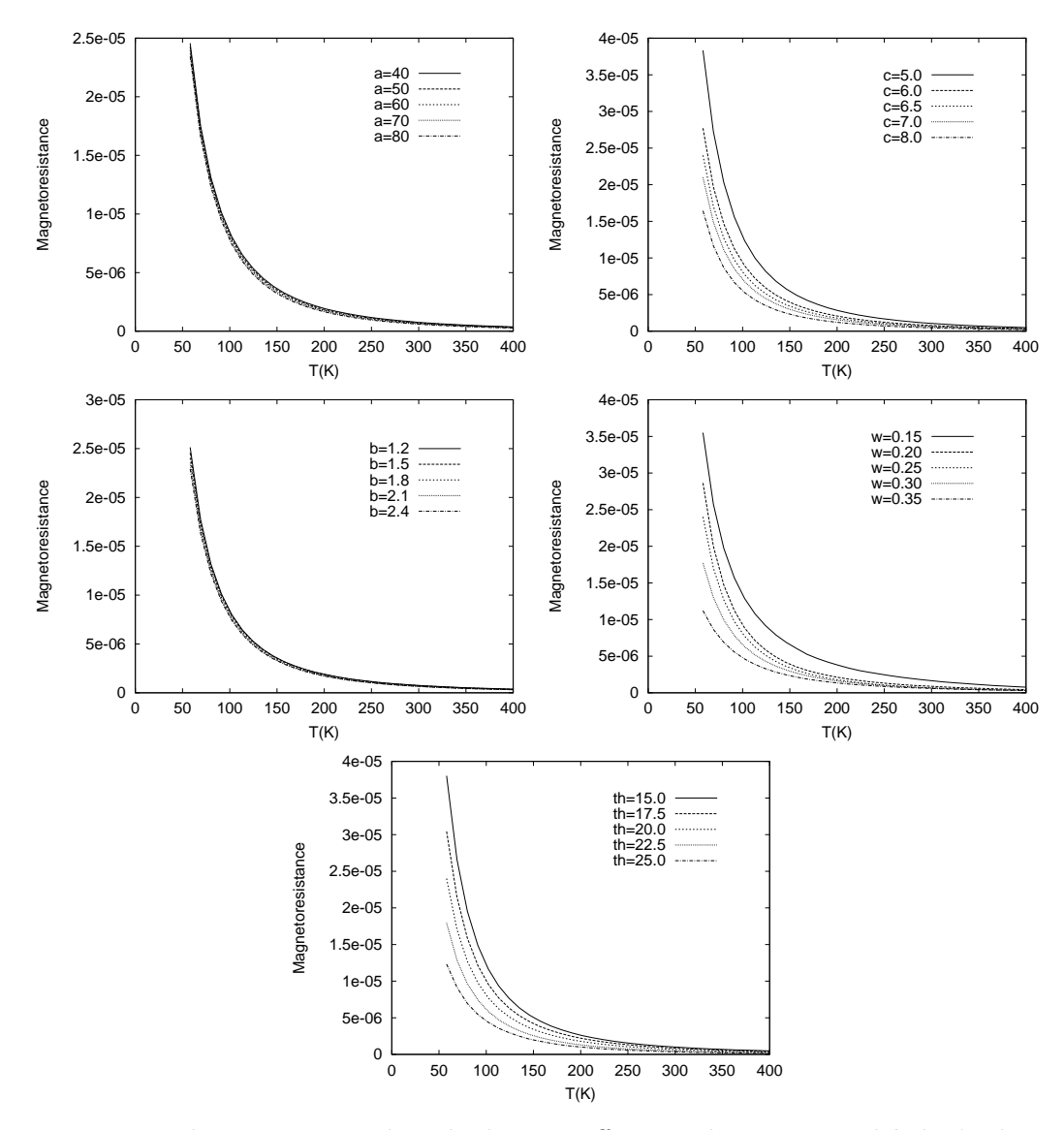


Figure 7.10: The parameter c has the biggest effect on the MR. a and b don't change the MR. Obviously the angle θ and transition width w are very important for the MR.

The region that determines the MR can be derived from figure 7.12. It turns out that the cold region has the biggest effect on the MR as predicted in the cold spot model [29].

7.1.5 Thermal Hall-conductivity

The last quantity we analyze is the thermal Hall conductivity κ^{xy} . For the thermal Hall-conductivity there is only an experimental value for α for a YBCO-sample available (chapter 4). It was found out that $\alpha \approx 1.19$ for YBCO. The influence of the different

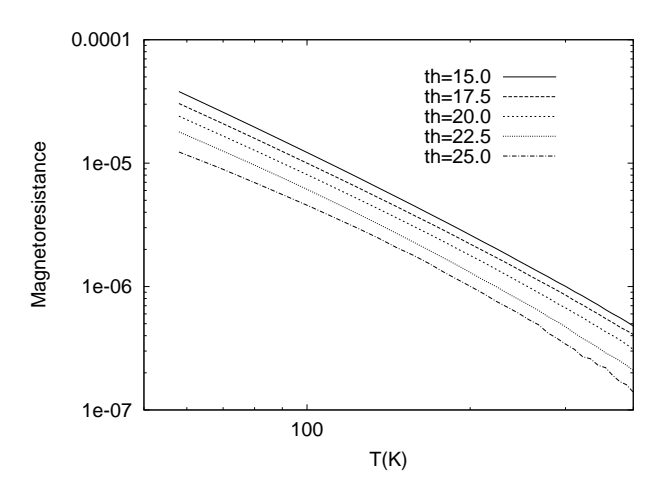


Figure 7.11: The slope changes only slightly.

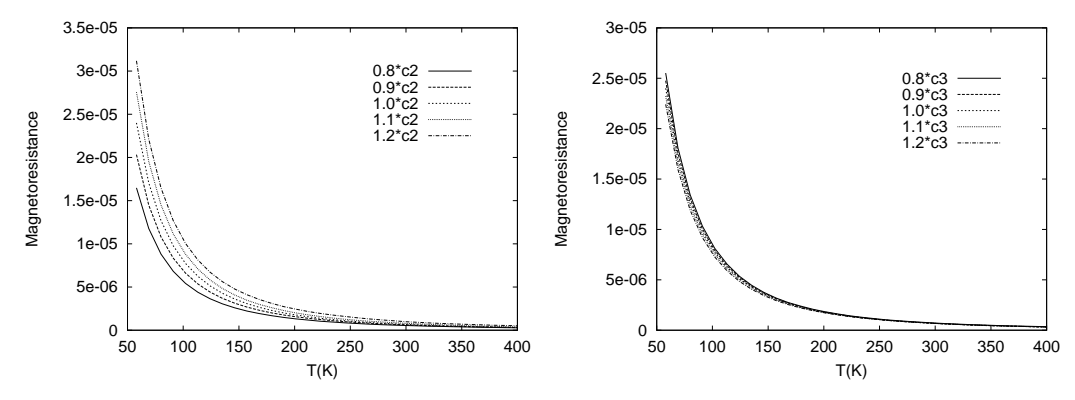


Figure 7.12: Changing the parameters c_2 and c_3 allows us to check the influence of the electronic structure on the MR.

parameters can be studies in figure 7.13

Figure 7.14 changes the change in the slope with doping. The result of the TPM is that α increases slightly with increasing doping.

We can extract from figure 7.15 that the thermal Hall-conductivity is governed by the cold region. However the effect of the hot region is not to be neglected.

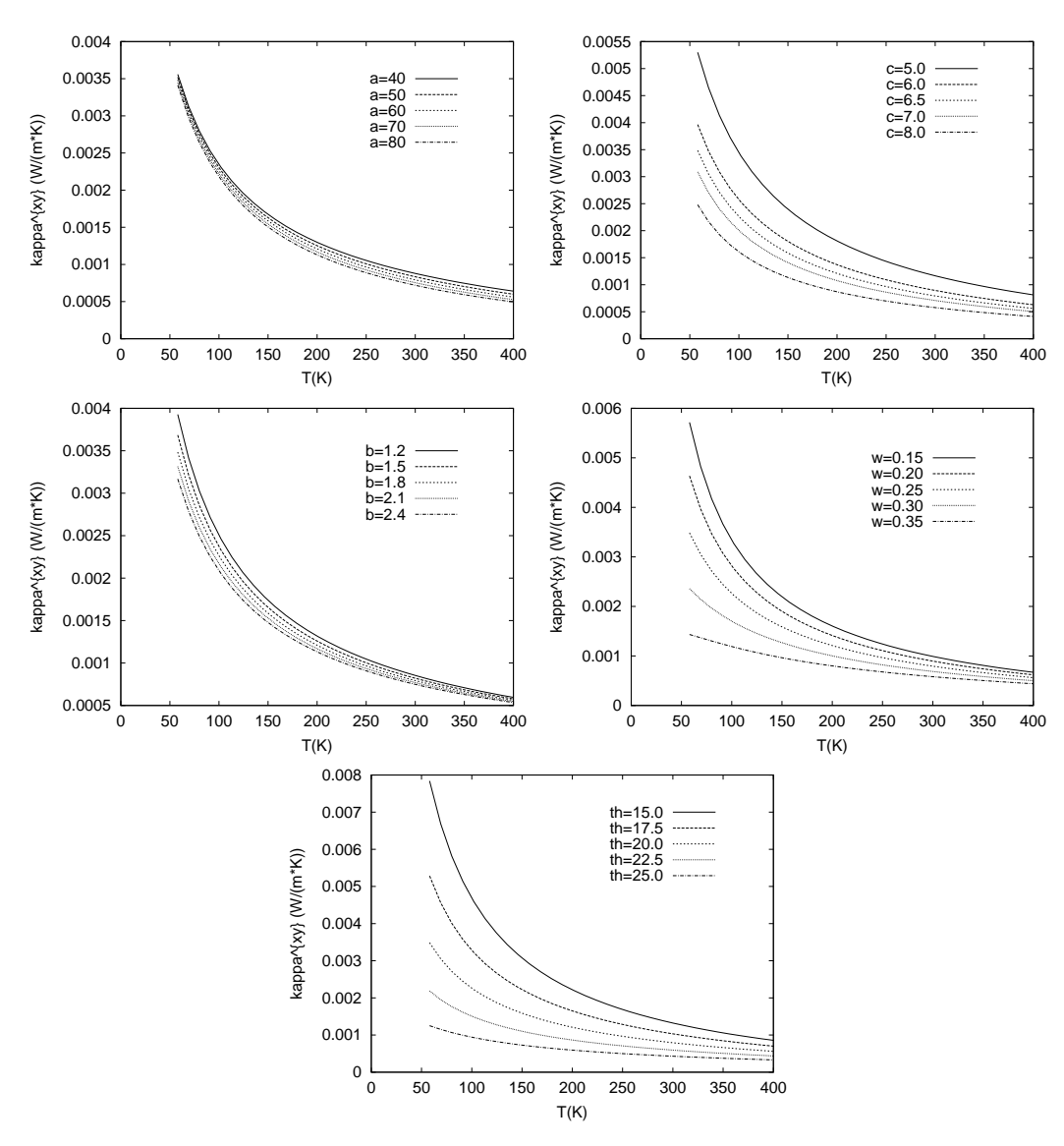


Figure 7.13: The figures show that the parameter b has some minor effect on κ^{xy} for small temperatures where a seems to become more important for big temperatures. The biggest effect on this quantity id due to c, θ and w.

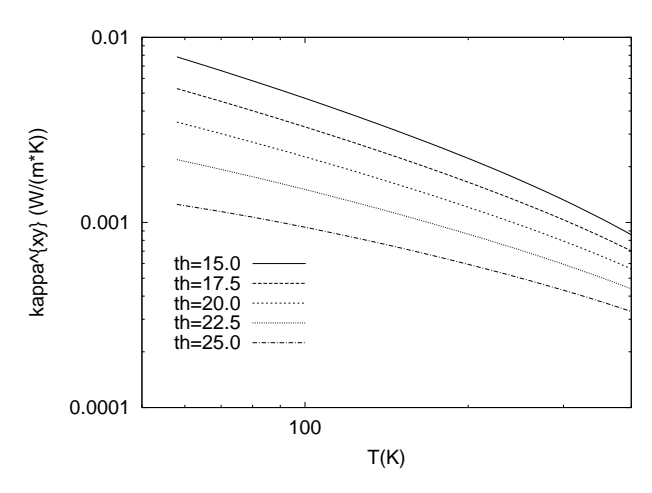


Figure 7.14: The slope changes only slightly.

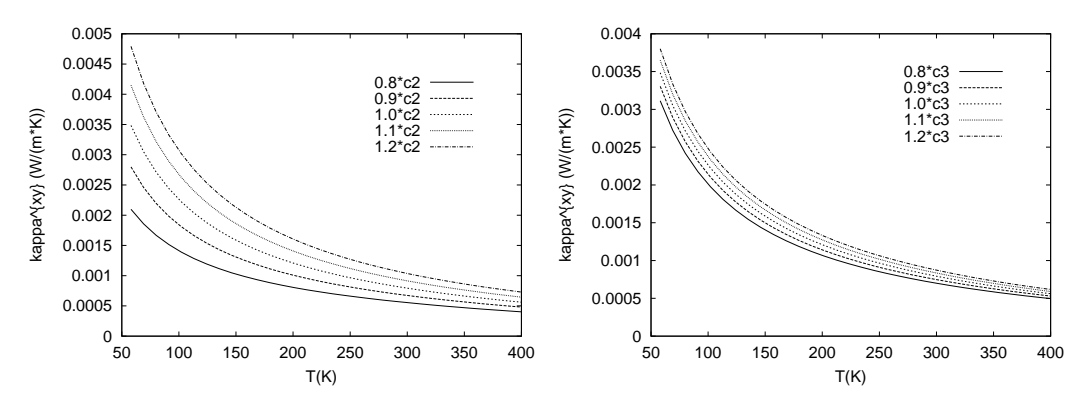


Figure 7.15: Changing the parameters c_2 and c_3 allows us to check the influence of the electronic structure on κ^{xy} .

7.2 Fitting experimental data

To be able to have some effect of a and b by a minor change of these quantities we are interested that the cold and the hot region have more or less of the same size. For $\theta = 20^{\circ} \approx 46\%$ of the BZ are cold. Thus a slight change in a or b has a quite big effect on the transport quantities studied in section 7.1. Another reason why to choose this angle is given by the TEP that is basically determined by the ration $\frac{N'_c(\theta)}{N_c(\theta)}$. In section 5.6 we argued that an angle $\approx 20^{\circ}$ reproduces the slope in the TEP very well. So the angle $\theta = 20^{\circ}$ seems to be a good starting point for the fitting process.

The strategy of the fitting of the data was the following. We introduce a temperature scale T_0 upon the T-linear term in the cold region dominates, compare to (5.8). This guarantees us that the resistivity is linear up to this temperature T_0 [1]. We can choose a temperature T_0 that has a typical value of $\sim 1000K \sim 0.1eV$. The relations $a = (1 - \alpha)c/(\alpha T_0)$ and $b = \alpha c T_0/(1 - \alpha)$ derived from (5.8) allow us to obtain certain values for a and b for given T_0 and c and a, where a is determined by the angle a0. Note that the width of the transition region is basically given by the MR.

Starting with different angles θ , thus with different sizes of the cold region α , we try to get a good fit of the Hall-angle data first. So we search for the optimal value of c, the inter-patch-scattering, for each given angle θ . We try to fit the Hall-angle and the slope of the resistivity for every given combination of θ and c well. It turns out that the angle $\theta \approx 20^{\circ}$ and $c \approx 6.5$ gives a pretty good fit of the Hall-angle and the slope of the resistivity. This angle was already predicted from TEP data given above. Once this is done we start changing the scattering in the hot region b by hand. Increasing b (= increasing the scattering in the hot region) increases the resistivity, compare to figure 7.1. The figures in section 7.1 allow us to predict the consequences of a change in the parameters. So we use this plots to change the parameters slightly in the "right way". The parameter b allows us to adjust the resistivity. Note that a has less effect on ρ^{xx} than b has (figure 7.1!). In this manner we can fix the parameters w, θ , c, b. The last parameter that is to be fixed is a. But the freedom for the parameter a is not so

big, because we have to obey the linearity of the resistivity. Thus the initial condition we have chosen for a, $a = (1 - \alpha)c/(\alpha T_0)$ has to remain valid. We can change a slightly in order to improve our fit.

After we have fixed the parameters of our model we start to compare the TPM with experimental data.

Looking the transport quantities given in chapter 4 we recognize that each quantity of the TPM fits experimental data quite well. The suggested TPM seems to be able to describe transport data on a phenomenological basis. We obtain a consistent picture of several transport quantities using the TPM starting with the linearized BE.

For the following parameter values we obtain the "best" fits for the different quantities shown below: w = 0.20, a = 60, b = 2.1, c = 7.0 and $\theta = 20^{\circ}$.

Note that the FS suggested in (5.18) is not changed to improve our fit.

Figure 7.16 shows our fit for the resistivity and compares it to the experimental data given in [14]. In agreement with experiments we obtain $\rho^{xx} \propto T$.

The TEP, shown in figure 7.17, is basically determined by the angle θ (compare to

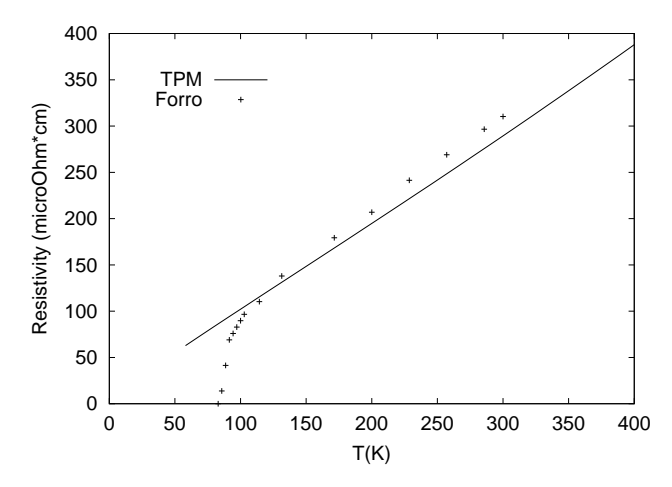


Figure 7.16: In spite of the fact that the points do not absolutely agree with the values obtained by the TPM, we get a pretty good fit of ρ^{xx} for the parameters given above. The experimental data of Bi2212 are taken from [14].

figure 7.5). As already mentioned in chapter 5 the electronic structure forces us to choose an angle $\theta \approx 20^{\circ}$. Note that the TEP is not exactly linear. But also the data seem not to be completely linear in temperature in the considered range. Unfortunately there were no data for Bi2212 available, so we fitted data of Bi2201.

It was pointed out by Obertelli [33] that the TEP is very sensitive to doping. Especially the offset of the TEP is changed very much by doping. On the other hand the slope doesn't change much when changing doping, Choi argued [4]. A change in θ doesn't affect the TEP very much. So it is very likely that a changing angle doesn't model doping very well. Again we have the problem to obtain an offset from our model.

As pointed out in chapter 4 the different T-dependence between the Hall-angle and

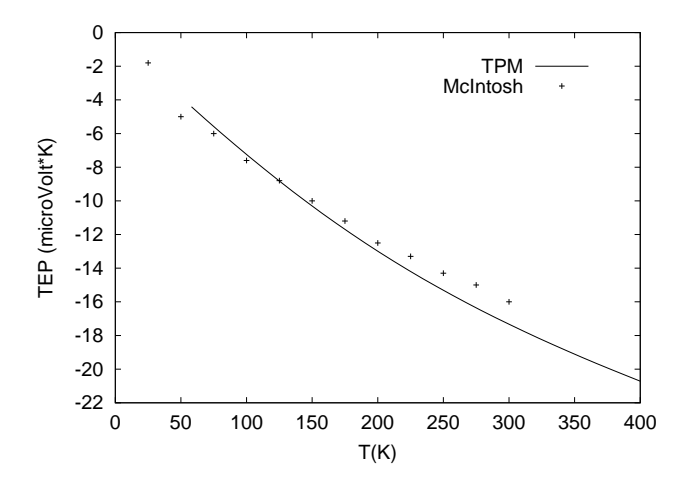


Figure 7.17: Thermoelectric data for Bi2201 given by McIntosh [31] are fitted very good in our model (with the given parameters). The TEP is not very sensitive to the parameters of our model (compare to figure 7.5). The most important parameter is, as already told, θ .

the resistivity can't be explained in a Drude model. The TPM gives us a T-dependence of the Hall-angle that is $\approx T^2$. Actually the exponent of the T-dependence is slightly smaller than 2. Note that $\sqrt{\cot \theta_H(T)}$ is plotted vs. T in figure 7.18.

As already pointed out the MR in very sensitive to the width of the transition region w. Within small errors we can reproduce the experimental measured values of the MR with our given parameter set. Similar to the case of the TEP we only found MR-data for Bi2201. Figure 7.19 shows the obtained fit and the experimentally obtained values.

A plot of the thermal Hall-conductivity vs. temperature is shown in figure 7.20. As we don't have experimental values for κ^{xy} for Bi-based cuprates we only plot the result obtained by the TPM. Experimental data for YBCO show exactly the behavior showed in the plot. So the magnitude and the shape of κ^{xy} seems to be described very good by the TPM.

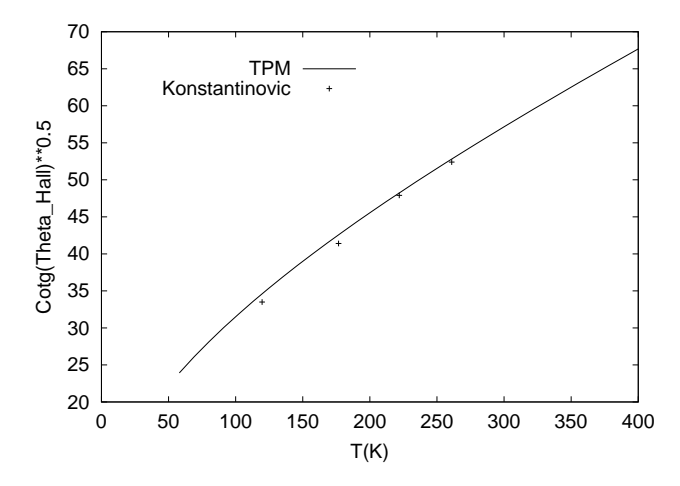


Figure 7.18: We can also fit the experimental data for the Hall-angle using our parameters. We get good agreement with experimental data for Bi2212 [27]. It can be seen from the plot that we get a temperature dependence $\sqrt{\cot \theta_H} \propto T^{\alpha}$, with $\alpha < 2$.

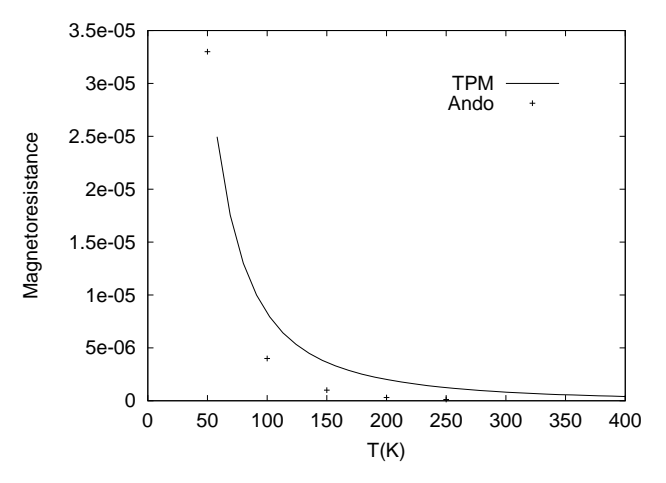


Figure 7.19: The figure shows the magnetoresistance obtained from our model. The points shown in the plot are taken from [1] for a Bi2201 sample with (optimally) doping $\delta = 0.44$.

In agreement with Kubo [30] the TPM gives us a Hall-mass parallel to the FS which is holelike (Hall-angle > 0) and a transport mass perpendicular to the FS which is electron-like (TEP < 0).

Another check of the TPM can be obtained when we generate a Kohler- and a Lorenz-plot introduced in chapter 4.

These plots are a ratio of two transport quantities so it is difficult to interpret them. But anyway these plots, shown in figure 7.21 and 7.22, can give us another hint whether

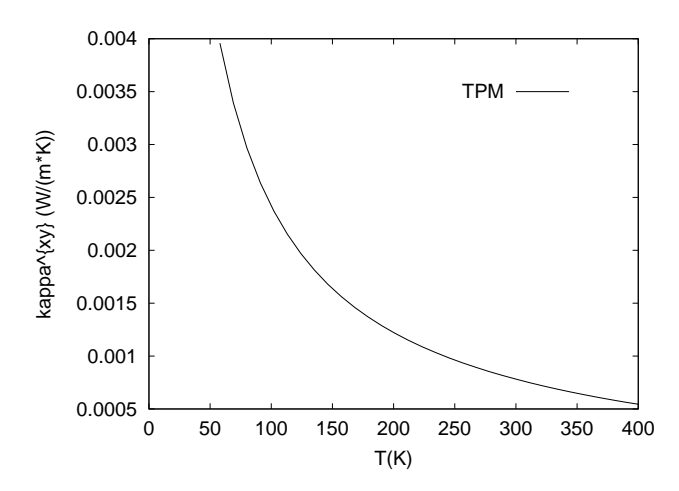


Figure 7.20: We plot the thermal Hall conductivity κ^{xy} vs. temperature. The data shown in the plot agree very good with YBCO data [24]. The experimental data for Bi2212 shouldn't change much.

the TPM generates quantities of the right magnitude.

7.2.1 Lorenz-number and Kohler-plot

We generate this figures to have another check of our model.

Experiments show that the Kohler number varies between 1.6 (for YBCO) and 13.6 (for LaSCO). Within the framework of the TPM we obtain a Kohler-number ≈ 8.5 which is in a very good range! Zheleznyak et al. [6] claim that the saturation should be at a value ≈ 6 . Figure 7.21 shows our result.

As already mentioned before the TPM has some difficulties to describe heat transport. The Lorenz-number seems to be constant and ≈ 3.3 which is close to the theoretical value for metals. The bigger the cold region is (small θ !) the better we obtain a straight line. A saturation of the Lorenz number to this value is expected but it seems a problem of the TPM that the Lorenz number has always the same value.

Anyway again the magnitude of the number (figure 7.22) agrees very good with experimental results for cuprates. Note that the Lorenz number was obtained by the ratio $\kappa^{xy}/(T\sigma^{xy})$ thus has no phononic contributions. So the plot shows indeed only the contributions from the electrons!

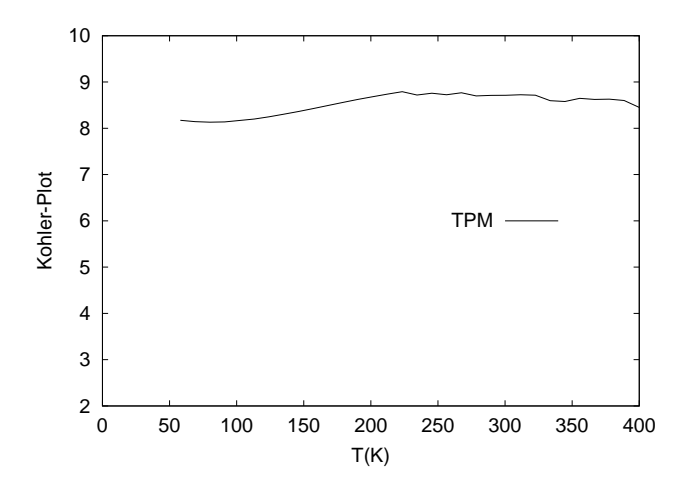


Figure 7.21: Using the parameters we obtain a good result for the Kohler plot. A Kohler-plot is obtained by multiplying the magnetoresistance with $(\cot \theta_H)^2$. The result is in good agreement with the experimentally obtained one. Unfortunately there are no data for Bi2212 available.

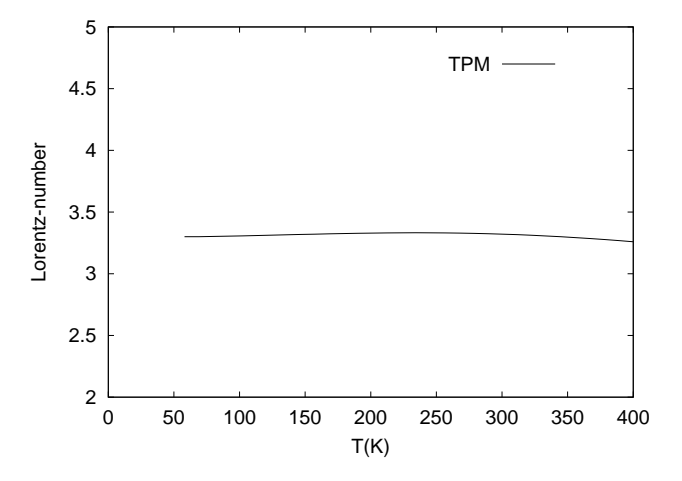


Figure 7.22: It can be seen that the value for a metal, $\pi^2/3$ is achieved very fast. The Lorenz-number describes the ratio between heat and electrical transport. The temperature dependence of this number is very weak.

7.3 Problems of the model

The associated temperature dependences of the different scattering mechanisms (cold-cold, cold-hot, hot-hot), seem to describe the considered transport quantities very well. But a microscopic derivation of the assigned T-dependence is missing. Especially the linearity in temperature of the interpatch-scattering should be derived from a more microscopic theory.

Furthermore the model is not able to describe transport processes at very low temperatures as it doesn't contain quantum mechanics. This semiclassical approach is for sure reasonable in the temperature range we considered, but it will fail when lowering the temperature. So it should be nice to combine the idea of different patches with a more microscopic theory. In the limit of big temperatures this "new theory" should come back to the suggested TPM.

Almost every considered transport quantity is determined by the cold regions of our model, as predicted by Ioffe and Millis [29]. However the hot regions are important to get a complete picture of transport (e.g. they have a big effect on the TEP). The influence of the hot region can be recognized when we consider the fitting procedure. It was important to choose b properly. Anyway the effect of the hot regions is not completely clear. It seems that in the case of heat transport we can't neglect this regions any more. So a complete picture of transport in cuprates should include the effect of the hot regions. So it seems that the hot regions have to be included in a microscopic theory.

Another problem arises from the effect of doping. The TPM is not able to describe the effects of doping on the different quantities in a reliable manner. For instance the TEP changes a lot with doping. It is quite difficult, even impossible, to obtain this shift of the TEP in the TPM. So the idea of modeling doping by changing θ has to be seen very critically.

Offsets, like the residual resistivity, of transport quantities are very difficult to realize in the TPM. As our model lacks the existence of impurities completely we have to be very careful with offsets obtained from the model.

7.4 How to go on?

The introduced TPM can be improved in various ways. We only mention some possible improvements that might allow us some deeper insight into the transport process.

A temperature and angle dependent transition width $w(T,\theta)$ could be introduced. For sure the width w changes with increasing temperature. So it seems natural to introduce a width that depends on the temperature. As the FS is very flat at the nodes and very curved in (π,π) -direction the influence of the temperature on w should also depend on the position on the FS, thus $w(T,\theta)$.

Furthermore one can try to expand this model to the case of AC transport. It was already mentioned in chapter 3 that we have to consider FL-corrections in the AC-case. So the interaction, described by $f_{\mathbf{k}\mathbf{k}'}^{\sigma\sigma'}$, has to be introduced into the geometry of the TPM. This could be done by introducing a interaction $f_{\mathbf{k}\mathbf{k}'}^{\sigma\sigma'}$ that changes in the different patches. In this manner we would get some extra parameter.

It is not obvious whether we can put frequency dependence in the TPM by just substituting $\tau^{-1} \to \tau^{-1} - i\omega$. But it seems to be the next step to find out what result we would get with the TPM in the frequency dependent case. To test the temperature dependence of the AC-case would be a good test whether the TPM is also able to describe this case.

The final step seems to be to try to translate this phenomenological model in a microscopic one. A microscopic TPM can be realized by applying the idea of different patches on dynamical mean field theory (cluster DMFT). The gained parameters and the insight in the transport process might be a good starting point for the application of this theory.

Appendix A

Abbreviations

The following abbreviations are used in the text:

FS	Fermi-surface		
BE	Boltzmann-equation		
NS	normal state		
BZ	Brillouin-zone		
HTSC	high temperature superconductor		
FL	Fermi-liquid		
MFL	marginal Fermi-liquid		
ARPES	angle resolved photoemission		
TPM	two patch model		
TEP	thermoelectric power		
MR	magnetoresistance		
VHS	van Hove-singularity		

Appendix B

Constants

The values we obtain for the Boltzmann-constant k_B and for the Planck-constant \hbar are given in atomic units [32]:

$$k_B = 8.617 \cdot 10^{-5} \frac{eV}{K}$$
 (B.1)

$$\hbar = 6.5821 \cdot 10^{-16} eV \cdot s \tag{B.2}$$

Their ratio is given by $\frac{\hbar}{k_B} = 7.6315 \cdot 10^{-12} Ks$ which is a number that we use several times (e.g. to multiply \bar{c} with).

Other physical constant like the elementary charge e were taken from [3].

Appendix C

Properties of $\frac{\partial \Phi_{\mathbf{k}}}{\partial k_x}$ and $\frac{\partial \Psi_{\mathbf{k}}}{\partial k_x}$

The connection between the derivatives of $\Phi_{\mathbf{k}}$ and $\Psi_{\mathbf{k}}$ with respect to k_x or k_y can be understood in the following way.

Let's concentrate on the case where $\Phi_{\mathbf{k}}$ and $\Psi_{\mathbf{k}}$ are step functions. The upper figure in figure 5.5 represents the cold region in the first BZ.

A derivative with respect to k_x has only contributions at points where we switch between the cold and hot regions, shown in figure C.1.

As the cold and the hot region are complementary, i.e. $\Phi_{\mathbf{k}} + \Psi_{\mathbf{k}} = 1$, the relation $\frac{\partial \Phi_{\mathbf{k}}}{\partial k_x} = -\frac{\partial \Psi_{\mathbf{k}}}{\partial k_x}$ is valid. When we enter the cold region we leave the hot region or vice versa.

The same reasoning works for a derivative with respect to k_y in the case of the stepfunctions.

In the case of the smooth change between hot and cold regions, given in section 5.1, the things are a little bit more complicated. Figure C.2 shows the smooth change between hot and cold regions.

The question is whether the derivative in the points A and B are the negative of each other? As the change between the two patches is a tanh-function it is symmetrical around its center S. So the derivatives in A and D are the same. With the same argument used above (entering one region = leaving the other region) we follow that the derivatives in A and C are equal up to a "minus". Thus the derivatives in A and B are its negative, which shows that the relation discovered for the case where we have a discontinuous change is also valid for the smooth change between the two regions.

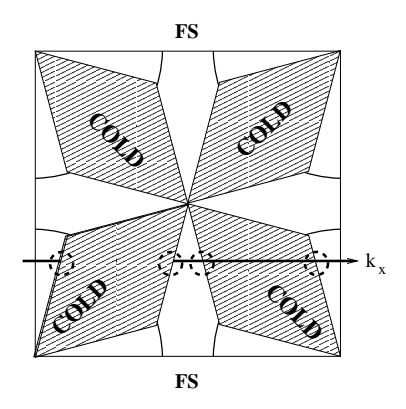


Figure C.1: The points that contribute to $\frac{\partial \Phi_{\mathbf{k}}}{\partial k_x}$ are marked in the figure. The antisymmetry of the derivative can be recognized in the figure.

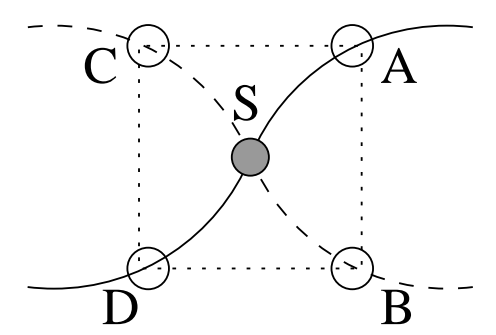


Figure C.2: In the case of the smooth change between the two regions the derivative in point A has the negative value of the derivative in point B.

Our conclusion is that all the functions $\frac{\partial \Psi_{\mathbf{k}}}{\partial k_y}$, $\frac{\partial \Psi_{\mathbf{k}}}{\partial k_x}$, $\frac{\partial \Phi_{\mathbf{k}}}{\partial k_y}$ and $\frac{\partial \Phi_{\mathbf{k}}}{\partial k_x}$ are antisymmetric functions (compare to figure C.1) and furthermore the general formula

$$\frac{\partial \Phi_{\mathbf{k}}}{\partial k_x} = -\frac{\partial \Psi_{\mathbf{k}}}{\partial k_x} \tag{C.1}$$

$$\frac{\partial \Phi_{\mathbf{k}}}{\partial k_x} = -\frac{\partial \Psi_{\mathbf{k}}}{\partial k_x}$$

$$\frac{\partial \Phi_{\mathbf{k}}}{\partial k_y} = -\frac{\partial \Psi_{\mathbf{k}}}{\partial k_y}$$
(C.1)
(C.2)

is valid.

Appendix D

Derivatives of the smooth function $\Phi_{\mathbf{k}}$

Formulas for the derivatives of $\Phi_{\mathbf{k}}$ are important for the computation of σ^{xy} and $\Delta \sigma^{xx}(\mathbf{B})$ as seen in chapter 5.

Note that it is not necessary to write down explicitly the hot region, as their derivatives obey the condition given in (C.1). Thus one set of derivatives is enough!

The first derivatives of $\Phi_{\mathbf{k}}$ become:

$$\frac{\partial \Phi_{\mathbf{k}}}{\partial k_{x}} = \frac{1}{16w} \left[\frac{a}{\left(\cosh\left(\frac{k_{y} - ak_{x}}{w}\right)\right)^{2}} \cdot \Phi_{2}(\mathbf{k}) \cdot \Phi_{3}(\mathbf{k}) \cdot \Phi_{4}(\mathbf{k}) \right. \\
\left. - \frac{b}{\left(\cosh\left(\frac{k_{y} - bk_{x}}{w}\right)\right)^{2}} \cdot \Phi_{1}(\mathbf{k}) \cdot \Phi_{3}(\mathbf{k}) \cdot \Phi_{4}(\mathbf{k}) \right. \\
\left. + \frac{b}{\left(\cosh\left(\frac{k_{y} - bk_{x} - c}{w}\right)\right)^{2}} \cdot \Phi_{1}(\mathbf{k}) \cdot \Phi_{2}(\mathbf{k}) \cdot \Phi_{4}(\mathbf{k}) \right. \\
\left. - \frac{a}{\left(\cosh\left(\frac{k_{y} - ak_{x} - d}{w}\right)\right)^{2}} \cdot \Phi_{1}(\mathbf{k}) \cdot \Phi_{2}(\mathbf{k}) \cdot \Phi_{3}(\mathbf{k}) \right] \right. \\
\frac{\partial \Phi_{\mathbf{k}}}{\partial k_{y}} = \frac{1}{16w} \left[- \frac{1}{\left(\cosh\left(\frac{k_{y} - ak_{x}}{w}\right)\right)^{2}} \cdot \Phi_{1}(\mathbf{k}) \cdot \Phi_{3}(\mathbf{k}) \cdot \Phi_{4}(\mathbf{k}) \right. \\
\left. + \frac{1}{\left(\cosh\left(\frac{k_{y} - bk_{x}}{w}\right)\right)^{2}} \cdot \Phi_{1}(\mathbf{k}) \cdot \Phi_{3}(\mathbf{k}) \cdot \Phi_{4}(\mathbf{k}) \right. \\
\left. - \frac{1}{\left(\cosh\left(\frac{k_{y} - bk_{x} - c}{w}\right)\right)^{2}} \cdot \Phi_{1}(\mathbf{k}) \cdot \Phi_{2}(\mathbf{k}) \cdot \Phi_{4}(\mathbf{k}) \right. \\
\left. + \frac{1}{\left(\cosh\left(\frac{k_{y} - bk_{x} - c}{w}\right)\right)^{2}} \cdot \Phi_{1}(\mathbf{k}) \cdot \Phi_{2}(\mathbf{k}) \cdot \Phi_{3}(\mathbf{k}) \right] \right.$$

The magneto-resistance is a quantity that is also sensible to the second derivative of $\Phi_{\mathbf{k}}$. The three second derivatives are given by:

$$\begin{split} \frac{\partial^2 \Phi_{\mathbf{k}}}{\partial k_x^2} &= \frac{1}{16w^2} \left\{ \frac{a}{\left(\cosh\left(\frac{k_y - ak_x}{w}\right) \right)^2} \\ &\cdot \left[2a \tanh\left(\frac{k_y - ak_x}{w}\right) \cdot \Phi_2(\mathbf{k}) \cdot \Phi_3(\mathbf{k}) \cdot \Phi_4(\mathbf{k}) \right. \\ &- \frac{b}{\left(\cosh\left(\frac{k_y - bk_x}{w}\right) \right)^2} \cdot \Phi_3(\mathbf{k}) \cdot \Phi_4(\mathbf{k}) + \frac{b}{\left(\cosh\left(\frac{k_y - bk_x - c}{w}\right) \right)^2} \cdot \Phi_2(\mathbf{k}) \cdot \Phi_4(\mathbf{k}) \\ &- \frac{a}{\left(\cosh\left(\frac{k_y - bk_x}{w}\right) \right)^2} \cdot \Phi_2(\mathbf{k}) \cdot \Phi_3(\mathbf{k}) \right] \\ &- \frac{b}{\left(\cosh\left(\frac{k_y - bk_x}{w}\right) \right)^2} \left[2b \tanh\left(\frac{k_y - bk_x}{w}\right) \cdot \Phi_1(\mathbf{k}) \cdot \Phi_3(\mathbf{k}) \cdot \Phi_4(\mathbf{k}) \right. \\ &+ \frac{a}{\left(\cosh\left(\frac{k_y - bk_x - c}{w}\right) \right)^2} \cdot \Phi_3(\mathbf{k}) \cdot \Phi_4(\mathbf{k}) + \frac{b}{\left(\cosh\left(\frac{k_y - bk_x - c}{w}\right) \right)^2} \cdot \Phi_1(\mathbf{k}) \cdot \Phi_4(\mathbf{k}) \\ &- \frac{a}{\left(\cosh\left(\frac{k_y - bk_x - c}{w}\right) \right)^2} \left[2b \tanh\left(\frac{k_y - bk_x - c}{w}\right) \cdot \Phi_1(\mathbf{k}) \cdot \Phi_2(\mathbf{k}) \cdot \Phi_4(\mathbf{k}) \right. \\ &+ \frac{a}{\left(\cosh\left(\frac{k_y - bk_x - c}{w}\right) \right)^2} \cdot \Phi_1(\mathbf{k}) \cdot \Phi_2(\mathbf{k}) - \frac{b}{\left(\cosh\left(\frac{k_y - bk_x - d}{w}\right) \right)^2} \cdot \Phi_1(\mathbf{k}) \cdot \Phi_4(\mathbf{k}) \\ &- \frac{a}{\left(\cosh\left(\frac{k_y - ak_x - d}{w}\right) \right)^2} \cdot \Phi_1(\mathbf{k}) \cdot \Phi_2(\mathbf{k}) \right] \\ &- \frac{a}{\left(\cosh\left(\frac{k_y - ak_x - d}{w}\right) \right)^2} \left[2a \tanh\left(\frac{k_y - ak_x - d}{w}\right) \cdot \Phi_1(\mathbf{k}) \cdot \Phi_2(\mathbf{k}) \cdot \Phi_3(\mathbf{k}) \right. \\ &+ \frac{b}{\left(\cosh\left(\frac{k_y - ak_x}{w}\right) \right)^2} \cdot \Phi_1(\mathbf{k}) \cdot \Phi_2(\mathbf{k}) \right] \\ &+ \frac{b}{\left(\cosh\left(\frac{k_y - ak_x}{w}\right) \right)^2} \cdot \Phi_1(\mathbf{k}) \cdot \Phi_2(\mathbf{k}) \right] \\ &+ \frac{\partial^2 \Phi_{\mathbf{k}}}{\partial k_y^2} &= \frac{1}{16w^2} \left\{ \frac{-1}{\left(\cosh\left(\frac{k_y - ak_x}{w}\right) \right)^2} \cdot \Phi_2(\mathbf{k}) \cdot \Phi_3(\mathbf{k}) \cdot \Phi_4(\mathbf{k}) \right. \\ &+ \left[-2 \tanh\left(\frac{k_y - ak_x}{w}\right) \right)^2 \cdot \Phi_2(\mathbf{k}) \cdot \Phi_3(\mathbf{k}) \cdot \Phi_4(\mathbf{k}) \right] \\ &+ \left[-2 \tanh\left(\frac{k_y - ak_x}{w}\right) \right] \cdot \Phi_2(\mathbf{k}) \cdot \Phi_3(\mathbf{k}) \cdot \Phi_4(\mathbf{k}) \right] \\ &+ \left[-2 \tanh\left(\frac{k_y - ak_x}{w}\right) \cdot \Phi_2(\mathbf{k}) \cdot \Phi_3(\mathbf{k}) \cdot \Phi_4(\mathbf{k}) \right] \\ &+ \left[-2 \tanh\left(\frac{k_y - ak_x}{w}\right) \right] \cdot \Phi_2(\mathbf{k}) \cdot \Phi_3(\mathbf{k}) \cdot \Phi_4(\mathbf{k}) \\ &+ \left[-2 \tanh\left(\frac{k_y - ak_x}{w}\right) \right] \cdot \Phi_2(\mathbf{k}) \cdot \Phi_3(\mathbf{k}) \cdot \Phi_4(\mathbf{k}) \right] \\ &+ \left[-2 \tanh\left(\frac{k_y - ak_x}{w}\right) \right] \cdot \Phi_2(\mathbf{k}) \cdot \Phi_3(\mathbf{k}) \cdot \Phi_4(\mathbf{k})$$

$$+\frac{1}{\left(\cosh\left(\frac{k_{y}-bk_{x}}{w}\right)\right)^{2}}\cdot\Phi_{3}(\mathbf{k})\cdot\Phi_{4}(\mathbf{k}) - \frac{1}{\left(\cosh\left(\frac{k_{y}-bk_{x}-c}{w}\right)\right)^{2}}\cdot\Phi_{2}(\mathbf{k})\cdot\Phi_{4}(\mathbf{k})$$

$$+\frac{1}{\left(\cosh\left(\frac{k_{y}-bk_{x}}{w}\right)\right)^{2}}\cdot\Phi_{2}(\mathbf{k})\cdot\Phi_{3}(\mathbf{k})$$

$$+\frac{1}{\left(\cosh\left(\frac{k_{y}-bk_{x}}{w}\right)\right)^{2}}\left[-2\tanh\left(\frac{k_{y}-bk_{x}}{w}\right)\cdot\Phi_{1}(\mathbf{k})\cdot\Phi_{3}(\mathbf{k})\cdot\Phi_{4}(\mathbf{k})\right]$$

$$-\frac{1}{\left(\cosh\left(\frac{k_{y}-ak_{x}-d}{w}\right)\right)^{2}}\cdot\Phi_{3}(\mathbf{k})\cdot\Phi_{4}(\mathbf{k}) - \frac{1}{\left(\cosh\left(\frac{k_{y}-bk_{x}-c}{w}\right)\right)^{2}}\cdot\Phi_{1}(\mathbf{k})\cdot\Phi_{4}(\mathbf{k})$$

$$+\frac{1}{\left(\cosh\left(\frac{k_{y}-bk_{x}-c}{w}\right)\right)^{2}}\left[-2\tanh\left(\frac{k_{y}-bk_{x}-c}{w}\right)\cdot\Phi_{1}(\mathbf{k})\cdot\Phi_{2}(\mathbf{k})\cdot\Phi_{4}(\mathbf{k})\right]$$

$$-\frac{1}{\left(\cosh\left(\frac{k_{y}-ak_{x}-d}{w}\right)\right)^{2}}\cdot\Phi_{2}(\mathbf{k})\cdot\Phi_{4}(\mathbf{k}) + \frac{1}{\left(\cosh\left(\frac{k_{y}-bk_{x}}{w}\right)\right)^{2}}\cdot\Phi_{1}(\mathbf{k})\cdot\Phi_{4}(\mathbf{k})$$

$$+\frac{1}{\left(\cosh\left(\frac{k_{y}-ak_{x}-d}{w}\right)\right)^{2}}\cdot\Phi_{1}(\mathbf{k})\cdot\Phi_{2}(\mathbf{k})\right]$$

$$+\frac{1}{\left(\cosh\left(\frac{k_{y}-ak_{x}-d}{w}\right)\right)^{2}}\left[-2\tanh\left(\frac{k_{y}-ak_{x}-d}{w}\right)\cdot\Phi_{1}(\mathbf{k})\cdot\Phi_{2}(\mathbf{k})\cdot\Phi_{3}(\mathbf{k})\right]$$

$$-\frac{1}{\left(\cosh\left(\frac{k_{y}-ak_{x}-d}{w}\right)\right)^{2}}\cdot\Phi_{2}(\mathbf{k})\cdot\Phi_{3}(\mathbf{k}) + \frac{1}{\left(\cosh\left(\frac{k_{y}-bk_{x}}{w}\right)\right)^{2}}\cdot\Phi_{1}(\mathbf{k})\cdot\Phi_{3}(\mathbf{k})\right]$$

$$-\frac{1}{\left(\cosh\left(\frac{k_{y}-ak_{x}-d}{w}\right)\right)^{2}}\cdot\Phi_{1}(\mathbf{k})\cdot\Phi_{2}(\mathbf{k})\right]$$

The last derivative we need is the mixed derivative $\frac{\partial^2 \Phi_{\mathbf{k}}}{\partial k_x \partial k_y}$. It is very similar to the other second derivatives. Only some factors change.

$$\frac{\partial^{2} \Phi_{\mathbf{k}}}{\partial k_{x} \partial k_{y}} = \frac{1}{16w^{2}} \left\{ \frac{a}{\left(\cosh\left(\frac{k_{y} - ak_{x}}{w}\right)\right)^{2}} \cdot \left[-2 \tanh\left(\frac{k_{y} - ak_{x}}{w}\right) \cdot \Phi_{2}(\mathbf{k}) \cdot \Phi_{3}(\mathbf{k}) \cdot \Phi_{4}(\mathbf{k}) \right. \\
\left. + \frac{1}{\left(\cosh\left(\frac{k_{y} - bk_{x}}{w}\right)\right)^{2}} \cdot \Phi_{3}(\mathbf{k}) \cdot \Phi_{4}(\mathbf{k}) - \frac{1}{\left(\cosh\left(\frac{k_{y} - bk_{x} - c}{w}\right)\right)^{2}} \cdot \Phi_{2}(\mathbf{k}) \cdot \Phi_{4}(\mathbf{k}) \right. \\
\left. + \frac{1}{\left(\cosh\left(\frac{k_{y} - ak_{x} - d}{w}\right)\right)^{2}} \cdot \Phi_{2}(\mathbf{k}) \cdot \Phi_{3}(\mathbf{k}) \right]$$

$$-\frac{b}{\left(\cosh\left(\frac{k_y-bk_x}{w}\right)\right)^2}\left[-2\tanh\left(\frac{k_y-bk_x}{w}\right)\cdot\Phi_1(\mathbf{k})\cdot\Phi_3(\mathbf{k})\cdot\Phi_4(\mathbf{k})\right.\\ -\frac{1}{\left(\cosh\left(\frac{k_y-ak_x}{w}\right)\right)^2}\cdot\Phi_3(\mathbf{k})\cdot\Phi_4(\mathbf{k}) - \frac{1}{\left(\cosh\left(\frac{k_y-bk_x-c}{w}\right)\right)^2}\cdot\Phi_1(\mathbf{k})\cdot\Phi_4(\mathbf{k}) \\ +\frac{1}{\left(\cosh\left(\frac{k_y-ak_x-d}{w}\right)\right)^2}\cdot\Phi_1(\mathbf{k})\cdot\Phi_3(\mathbf{k})\right] \\ +\frac{b}{\left(\cosh\left(\frac{k_y-bk_x-c}{w}\right)\right)^2}\left[-2\tanh\left(\frac{k_y-bk_x-c}{w}\right)\cdot\Phi_1(\mathbf{k})\cdot\Phi_2(\mathbf{k})\cdot\Phi_4(\mathbf{k}) \\ -\frac{1}{\left(\cosh\left(\frac{k_y-ak_x}{w}\right)\right)^2}\cdot\Phi_2(\mathbf{k})\cdot\Phi_4(\mathbf{k}) + \frac{1}{\left(\cosh\left(\frac{k_y-bk_x}{w}\right)\right)^2}\cdot\Phi_1(\mathbf{k})\cdot\Phi_4(\mathbf{k}) \\ +\frac{1}{\left(\cosh\left(\frac{k_y-ak_x-d}{w}\right)\right)^2}\cdot\Phi_1(\mathbf{k})\cdot\Phi_2(\mathbf{k})\right] \\ -\frac{a}{\left(\cosh\left(\frac{k_y-ak_x-d}{w}\right)\right)^2}\left[-2\tanh\left(\frac{k_y-ak_x-d}{w}\right)\cdot\Phi_1(\mathbf{k})\cdot\Phi_2(\mathbf{k})\cdot\Phi_3(\mathbf{k}) \\ -\frac{1}{\left(\cosh\left(\frac{k_y-ak_x}{w}\right)\right)^2}\cdot\Phi_2(\mathbf{k})\cdot\Phi_3(\mathbf{k}) + \frac{1}{\left(\cosh\left(\frac{k_y-bk_x}{w}\right)\right)^2}\cdot\Phi_1(\mathbf{k})\cdot\Phi_3(\mathbf{k}) \\ -\frac{1}{\left(\cosh\left(\frac{k_y-ak_x}{w}\right)\right)^2}\cdot\Phi_1(\mathbf{k})\cdot\Phi_2(\mathbf{k})\right]\right\}$$

Appendix E

The tetrahedron method

Solving integral equations is in most cases a very difficult even unsolvable problem. The Tetrahedron method provides a method that allows the computation of integrals that are non-trivial to integrate, because of possible singularities.

Dealing with a function that doesn't allow us to obtain an explicit function in an analytic way, we have to use numerical methods to compute the integral. Especially in solid state physics, where a lot of properties of a system can be measured by experiment, there is a big interest in computing some integral equations numerically to get values for transport parameters of the system we are interested in.

We are most interested in transport properties of solids (especially HTSC) that can be obtained from solving a transport equation. In all the formulas we get for those properties we have to sum over an area next to the FS in order to obtain the value of the special transport coefficient we want to find out. In a more sophisticated approach (using techniques of Greens functions) we get for instance the longitudinal conductivity from the equation¹

$$\sigma_{xx} = \frac{1}{\omega} \sum_{k} \left[\frac{\partial \epsilon_{\mathbf{k}+1/2}}{\partial k_x} \right]^2 \left[\frac{f(\epsilon_{\mathbf{k}+\mathbf{q},\uparrow}) - f(\epsilon_{\mathbf{k},\downarrow})}{\epsilon_{\mathbf{k}+\mathbf{q},\uparrow} - \epsilon_{\mathbf{k},\downarrow} - \omega + i\delta} \right]$$
(E.1)

where the functions f represent the Fermi-function.

As it can be seen in equation (E.1) we only have to integrate over a small area next to the Fermi surface. But we get only contributions to the integral from a small area next to the FS, because of the Fermi-function f in the numerator of the considered integral

¹The first term in the sum, $\frac{\partial \epsilon_{\mathbf{k}+1/2}}{\partial k_x}^2$ is given by the vertices, where the second part of this equation comes from the bubble. We can get this result when we calculate the Greens-function for different momenta (q+k) and k which are given in the bubble. We don't consider corrections because of vertices or higher order bubble-terms so far.

(figure E.1).

The formula we use for changing summation and integration (continuum-limit) is, as usual:

$$\sum_{k} \to V \int_{0}^{k_f} \frac{d^3k}{(2\pi)^3} \tag{E.2}$$

But still the problem of solving an integral over an area at the FS remains.

To get a better understanding we look at an arbitrary FS, showed in figure E.1.

We divide this chapter into several pieces to show how the method works and to

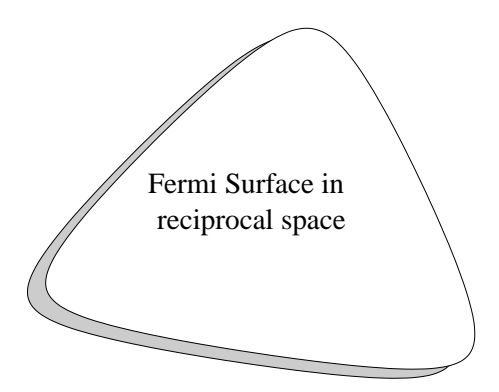


Figure E.1: A possible FS in reciprocal space without a spherical symmetry. Only the shaded area contributes to the integral given in (E.1). Our strategy is that we first check whether a triangle is outside the first Fermi surface (FS1) then we check whether it is inside the second (moved) Fermi surface (FS2)

explain how it can be **computed**.

E.1 Numerical integration in 2D

Our problem is to solve an integral (e.g. equation (E.1) over a certain area, which is determined by $f(\epsilon_{\mathbf{k}+\mathbf{q}})$ and $f(\epsilon_{\mathbf{k}})$. So let's consider an area (first BZ), a square, in which the original and the moved FS is completely inside.

We divide the square into small sub-squares. If the function we want to integrate (e.g. equation (E.1)) is smooth enough, it doesn't change rapidly in this smaller sub-squares. Figure E.2 shows the first BZ containing the two FS that are given by $f(\epsilon_{\mathbf{k}})$ (FS1) and $f(\epsilon_{\mathbf{k+q}})$ (FS2).

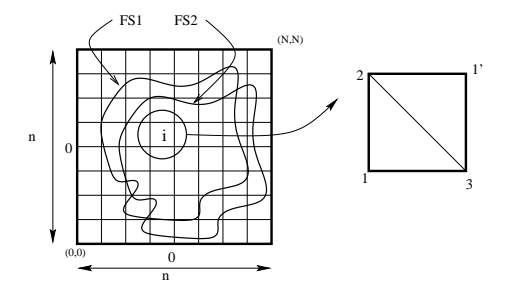


Figure E.2: The lattice in the first BZ. The i-th square is taken out and divided into two triangles. In this case this square is completely inside FS1 and FS2.

This new coordinate system (square-lattice) has its origin in the center of the initial square and has an amount of discrete values $(N \times N)$. The advantage is that we can compute the value of a function F (e.g. $\left(\frac{\partial \epsilon_{\mathbf{k}+1/2}}{\partial k_x}\right)^2 \frac{1}{\epsilon_{\mathbf{k}+\mathbf{q},\uparrow}-\epsilon_{\mathbf{k},\downarrow}-\omega+i\delta}$) at each discrete point. Finally we integrate over each small square to obtain the contribution to equation (E.1). Dependent whether we are inside or outside FS1 and FS2 we get a contribution (which is given by F) to the integral or not.

It exists the possibility that the FS1 and FS2 divides one sub-square into a piece that contributes to the integral and one that doesn't, shown in figure E.3. The sub-squares at the boundary of the region of interest have a part which is inside and a part that is outside the important region showed in figure E.1.

The important trick, in order to get a good result, is, to divide each sub-square into two triangles and compute that part of the triangle that is in the area of our interest. Figure (E.3) shows this strategy.

E.1.1 Possible situations for the triangle

We can imagine four possibilities for each triangle. The easiest possibilities are if the triangles are completely inside or outside the region of interest. In this case the integral over the BZ gets just a contribution of the whole triangle or no contribution at all. So in this two cases we don't have to worry much.

But there is also the possibility that there is only a part of such a triangle inside the

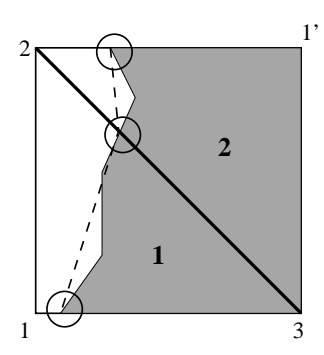


Figure E.3: A sub-square at the boundary of the FS1 or FS2. The cases 1 and 2 are different as described in the text.

interesting region and another part of the triangle is outside this region, which are the cases where we have to be more careful and are shown in figure (E.3).

We have to identify that part of the triangle that is inside the region that contributes to the integral in (E.1). We get the part inside this region either by taking one new triangle (which is represented by **case 1** in figure (E.3)) or by dividing the part that is inside the region into two parts (**case 2** in figure (E.3)). In this case we get two triangles respectively.

After this we compute the contribution of each (new) triangle to (E.1). The problem that arises is of course to find the positions where the energy is zero (thus the position where we get from inside the region to its outside). This positions has to be found by a root-finder.

So far we only approximated the area contributing to (E.1) by triangles.

E.1.2 An easy root-finder and an easy integration

The values of F, given in (E.1), at the corners of each triangles, shown in figure (E.3), are known. Energy values ϵ at this points are as well positive as negative as we consider triangles at the boundary of the contributing area here. The energy values at each corner allows us to decide at which side we expect the energy to become zero at least for one time. In the easiest case we assume the energy to be linear at the sides of each triangle. This simple assumption gives us reasonable values for the intersection-points.

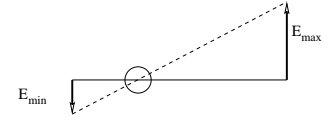


Figure E.4: In the case of linear energy variation we obtain this geometry. The ration between E_{max} and E_{min} estimates the intersection point.

The approximation of a linear behavior of the energy at each side allows us to get an easy formula for the intersection point. Figure E.4 shows the geometry in this case. But this version is only good if we deal with a dispersion relation that changes very slow. More sophisticated methods to estimate the intersection-point are bisection etc..

Once we have found all triangles in the interesting area (or to be more clear: once we have described the contributing region by triangles) we can integrate this by integrating each triangle.

So far we is just took a square, the BZ, that contains the FS1 and FS2 completely, divided it in a large number of sub-squares $(N \times N)$, divide each sub-square into two triangles and decided whether the triangle is inside outside or at the boundary of the important region, shown in figure E.2 and E.3.

Now we have to integrate over each triangle that is in the contributing area. The easiest way to integrate over a triangle is to take the three values of F at the three corners of the triangle F_i , i = 1, 2, 3, average it $\frac{F_1 + F_2 + F_3}{3}$ and to multiply this with the area of the triangle:

$$\int_{\triangle} F dx = A_{\triangle} \frac{F_1 + F_2 + F_3}{3} \tag{E.3}$$

This is surely a good method if F is smooth enough.

In our special case we have to be careful with this integration as we lose a lot of information when we use this kind of integration. Thus more general way will be described below.

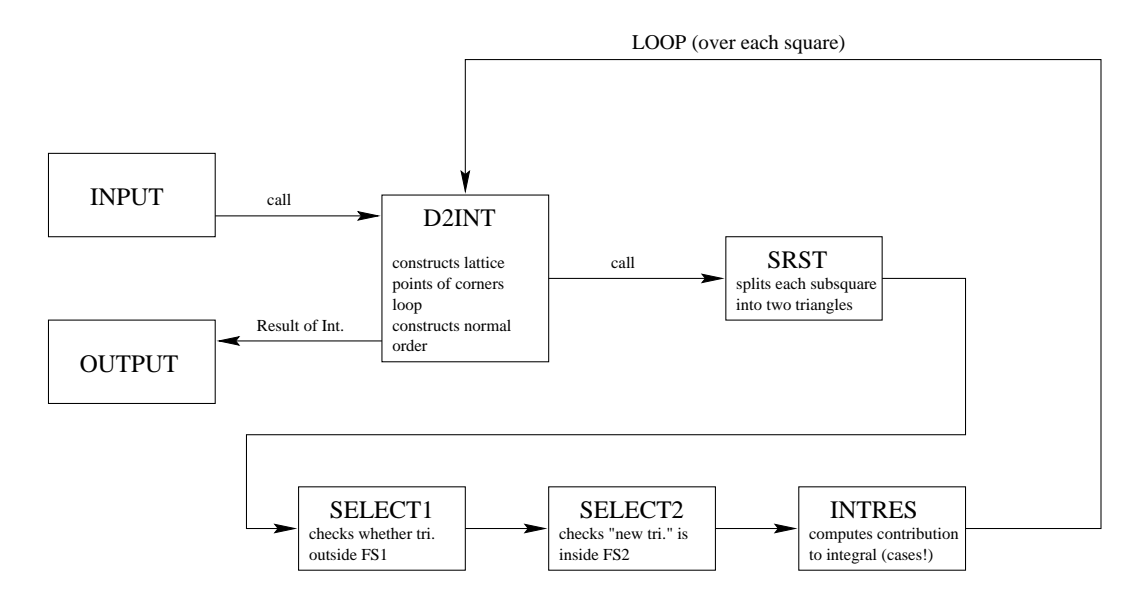


Figure E.5: The different subroutines and what they do.

E.2 The algorithm

Equation (E.1) tells us that only an area around the original FS can contribute, between FS1 and FS2. In the program we use different subroutines that can be seen in figure E.5 to compute the integral (E.1).

Different subroutines interact via common blocks which allow to submit coordinates of the considered triangles to other subroutines. Only those triangles that lie in the important area are integrated!

The next section is going to explain the mathematical background of this method.

E.3 The mathematical background - formulas for the program

At first, of course, we have to decide what function we choose to describe the FS. One possibility is the parameterization of the FS, like it is done in the Hubbard model, $\epsilon(x,y) = \cos x + \cos y$. To compute a integral of the type described in equation (E.1)

²Note that we are in reciprocal space. Thus we should use k_x instead of x to avoid confusion. The lattice parameter a has also to be inserted in the cos-terms. We neglect all this for convenience.

we have also to know the energy value $\epsilon^{\mathbf{q}}(x,y)$ which is given by

$$\epsilon^{\mathbf{q}}(x,y) = \cos[x+x_0] + \cos[y+y_0] \tag{E.4}$$

with the vector \mathbf{q} given by $\mathbf{q} = (x_0, y_0)$.

So typical integrals we have to integrate are, similar to (E.1), of the form:

$$I_{ij}(\mathbf{q}) = \int_{square} d^2x \frac{f(\epsilon_{\mathbf{k}+\mathbf{q}}) \left[f(\epsilon_{\mathbf{k}+\mathbf{q}}) - f(\epsilon_{\mathbf{k}}) \right]}{\epsilon^{\mathbf{q}}(x,y) - \epsilon(x,y)}$$
(E.5)

with i, j = 1, ..., N, the Fermi-function f and the vector \mathbf{q} that represents the perturbation of the system.

Only triangles outside the "first", undisturbed, FS, FS1, and inside the "second", with wave vector **q** moved FS, FS2, contribute to (E.5). We divide our proceeding into two steps to solve this integration.

In the first step we want to estimate the region that contributes to the integral, thus outside FS1 and inside FS2 and describe this region by small triangles.

In the second step we integrate a function, in our example $\frac{1}{\epsilon^{\mathbf{q}}(x,y)-\epsilon(x,y)}$, over each contributing triangle. This is done by linearizing the energy for each triangle separately. So we get a contribution to the integral from every triangle that is in the interesting area. The difficult part of the second step is that we have to be very careful avoiding singularities.

E.4 Estimating the contributing region

We split the search of the contributing area into two pieces. In a first subroutine (SELECT1) we separate triangles that are outside FS1. Only these triangles are passed to the second subroutine (SELECT2) which estimates what part of the passed triangle is inside FS2 (compare to figure (E.5)).

E.4.1 Triangles outside FS1 - SELECT1

It is easy to estimate the triangles outside FS1 when we remember that all energy values with $\epsilon < \mu$, where μ is the chemical potential, are occupied. Renormalizing the energy $\epsilon(x,y)$ in the way $\epsilon(x,y) - \mu \to \epsilon(x,y)$ shows us that we are only interested in triangles

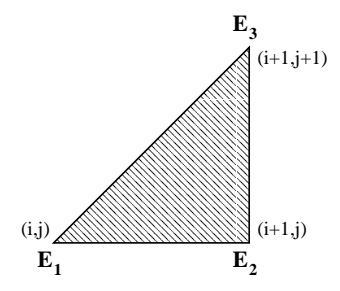


Figure E.6: One of the 2 N^2 triangles we get from dividing the first BZ. The normal order in energies is already performed.

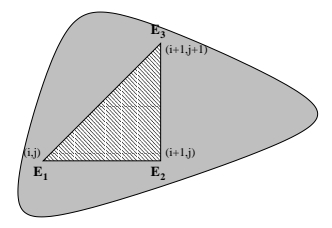


Figure E.7: The triangle is completely inside the FS1. Therefore we get no contribution to the Integral. $I_{ij}(\mathbf{q}) = 0!$

that have energies $\epsilon(x,y)$ with $\epsilon(x,y) > 0$.

Because of the discretization of the BZ in a lattice we know the energy values at the corners of each triangle ϵ_i , i = 1, 2, 3.

First we arrange the energy values at the corners of a triangle to normal order what means: $\epsilon_1 \leq \epsilon_2 \leq \epsilon_3$. This is shown in figure E.6.

When organized the normal order, what is done in the subroutine D2INT, it is easy to find out what part of the considered triangle is outside FS1. Three different cases are possible:

1. case $\epsilon_1 \leq \epsilon_2 \leq \epsilon_3 \leq \mu$

The triangle is complete inside the Fermi surface, given the energy dispersion is not too curious (figure E.7). As we can raise the number of lattice points N it should become reasonable for big enough N that the triangle is completely inside the FS.

2. case $\epsilon_1 \leq \epsilon_2 \leq \mu \leq \epsilon_3$

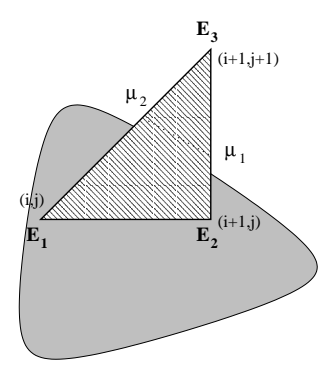


Figure E.8: The triangle is partly inside the FS1. We get only a contribution to the Integral. $I_{ij}(\mathbf{q})$ from the triangle $\mu_1 \epsilon_3 \mu_2$.

In this case one corner is outside of FS1 (figure E.8). Only a small triangle around this corner contributes to the integral. But still we don't know the coordinates of the corners (μ_1 and μ_2 and ϵ_3) of the "new" triangle that is outside FS1. Therefore we have to think of a method that allows us to estimate the two unknown points ν_1 and ν_2 .

We linearize the energy around the corner ϵ_3 and get for the linearized energy in the form

$$\epsilon(x,y) = \epsilon_3 + A(x - x_3) + B(y - y_3)$$
 (E.6)

with the coordinates of the corner with the energy value ϵ_3 (x_3, y_3) and the constants A and B.

Equation (E.6) allows us to describe the two sides of the triangle $\epsilon_1 \epsilon_2 \epsilon_3$ that cross the FS. These two lines are described by the equation:

$$\epsilon_1(x,y) - \epsilon_3 = A(x_1 - x_3) + B(y_1 - y_3)$$

$$\epsilon_2(x,y) - \epsilon_3 = A(x_2 - x_3) + B(y_2 - y_3)$$

The constants A and B are determined by these equations. The constants are needed to obtain the intersection points μ_1 and μ_2 .

Applying Cramers-Rule we solve the equation-system above and obtain:

$$Det = (x_1 - x_3)(y_2 - y_3) - (y_1 - y_3)(x_2 - x_3)$$

$$Det A = (\epsilon_1 - \epsilon_3)(y_2 - y_3) - (y_1 - y_3)(\epsilon_2 - \epsilon_3)$$

$$DetB = (x_1 - x_3)(\epsilon_2 - \epsilon_3) - (\epsilon_1 - \epsilon_3)(x_2 - x_3)$$

So we obtain the values for A and B, using $A = \frac{DetA}{Det}$ and $B = \frac{DetB}{Det}$.

$$A = \frac{(\epsilon_1 - \epsilon_3)(y_2 - y_3) - (y_1 - y_3)(\epsilon_2 - \epsilon_3)}{(x_1 - x_3)(y_2 - y_3) - (y_1 - y_3)(x_2 - x_3)}$$
$$B = \frac{(x_1 - x_3)(\epsilon_2 - \epsilon_3) - (\epsilon_1 - \epsilon_3)(x_2 - x_3)}{(x_1 - x_3)(y_2 - y_3) - (y_1 - y_3)(x_2 - x_3)}$$

We can describe the lines that connects the two corners ϵ_1 or ϵ_2 with ϵ_3 now. This lines have the equation:

$$y - y_3 = \frac{y_1 - y_3}{x_1 - x_3}(x - x_3)$$
$$y - y_3 = \frac{y_2 - y_3}{x_2 - x_3}(x - x_3)$$

The crossing points μ_i , i=1,2, are obtained when we compute $\mu_i - \epsilon_3 = A(x_\mu - x_3) + B(y_\mu - y_3)$, where μ_i is the energy this point. When we insert this in the equation above we get $\mu - \epsilon_3 = \left[A + B\frac{y_1 - y_3}{x_1 - x_3}\right](x_\mu - x_3)$. We solve this equation to get the coordinates of the intersection points assuming a linear energy. The coordinates of μ_1 are determined by the equations:

$$y_{\mu_1} - y_3 = \frac{(\mu_1 - \epsilon_3)(y_1 - y_3)}{A(x_1 - x_3) + B(y_1 - y_3)}$$
$$x_{\mu_1} - x_3 = \frac{(\mu_1 - \epsilon_3)(x_1 - x_3)}{A(x_1 - x_3) + B(y_1 - y_3)}$$

with the constants A, B and the coordinates of the corners x_i, y_i .

The coordinates of the other intersection point μ_2 are obtained in the same way.

$$\begin{pmatrix} x_{\mu_2} \\ y_{\mu_2} \end{pmatrix} - \begin{pmatrix} x_3 \\ y_3 \end{pmatrix} = \begin{pmatrix} \frac{(\mu_2 - \epsilon_3)(x_2 - x_3)}{A(x_2 - x_3) + B(y_2 - y_3)} \\ \frac{(\mu_2 - \epsilon_3)(y_2 - y_3)}{A(x_2 - x_3) + B(y_2 - y_3)} \end{pmatrix}$$
(E.7)

Finally we obtained a triangle $\mu_1\mu_2\epsilon_3$ that is completely outside FS1, like it is shown in figure E.8.

We make small mistakes due to the approximation of linear energy dispersion. But a dispersion-relation that is not too fancy and with the first BZ divided in a big number of sub-squares N^2 the error remains small.

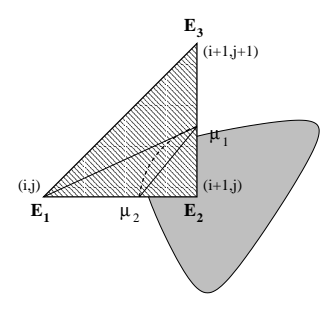


Figure E.9: The two triangles $\epsilon_2\mu_1\mu_2$ and $\epsilon_2\epsilon_3\mu_1$ contribute to the integral. The intersection points are computed in the same way as in case 2.

3. case $\epsilon_1 \leq \mu \leq \epsilon_2 \leq \epsilon_3$

This case is very similar to case 2. But here we have to divide the area that contributes to the integral into two triangles, as it can be seen in figure E.9. We get the intersection points like we get them in case 2. The difference here is that we linearize the energy around ϵ_1 in this case.

We get the following values for A and B similar to case 2.

$$A = \frac{(\epsilon_2 - \epsilon_3)(y_3 - y_1) - (y_2 - y_1)(\epsilon_3 - \epsilon_1)}{(x_2 - x_1)(y_3 - y_1) - (y_2 - y_1)(x_3 - x_1)}$$
$$B = \frac{(x_2 - x_1)(\epsilon_3 - \epsilon_1) - (\epsilon_2 - \epsilon_1)(x_3 - x_1)}{(x_2 - x_1)(y_3 - y_1) - (y_2 - y_1)(x_3 - x_1)}$$

Thus we obtain the intersection points are:

$$\begin{pmatrix} x_{\mu_i} \\ y_{\mu_i} \end{pmatrix} - \begin{pmatrix} x_1 \\ y_1 \end{pmatrix} = \begin{pmatrix} \frac{(\mu_i - \epsilon_1)(x_{i+1} - x_1)}{A(x_{i+1} - x_1) + B(y_{i+1} - y_1)} \\ \frac{(\mu_i - \epsilon_1)(y_{i+1} - y_1)}{A(x_{i+1} - x_1) + B(y_{i+1} - y_1)} \end{pmatrix}$$
(E.8)

with i = 1, 2.

4. case $\mu \le \epsilon_1 \le \epsilon_2 \le \epsilon_3$

Figure E.10 shows the situation of this case. The triangle $\epsilon_1\epsilon_2\epsilon_3$ is completely outside FS1. Therefore the whole triangle is passed to the next subroutine that checks whether the triangle is inside FS2.

We estimated all triangles outside FS1 until now. We store the (new) coordinates of the corners of each triangle outside FS1 and pass this "new" triangle to a subroutine that checks whether the new triangle lies inside the "moved" Fermi surface, FS2.

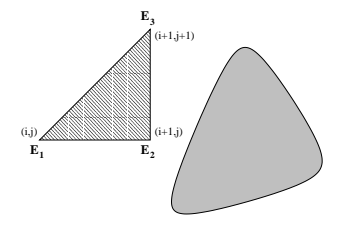


Figure E.10: The triangle is completely outside the FS1. We don't have to change the coordinates of the corners.

E.4.2 Triangles inside FS2

This step is very similar to the previous section, where we looked for triangles outside FS1. Here we are only interested in those triangles that are outside FS1 and additional inside FS2.

Because we moved the Fermi surface by some arbitrary vector \mathbf{q} we can describe the inner region of the "moved" FS by the equation $\epsilon^{\mathbf{q}}(x,y) \leq \mu$, where the vector \mathbf{q} with $\epsilon^{\mathbf{q}}(x,y) = \epsilon(x+q_x,y+q_y)$. Because we know the energy dispersion relation we can compute this energies easily. Again we have to consider four cases.

1. case
$$\mu \le \epsilon_1^{\mathbf{q}} \le \epsilon_2^{\mathbf{q}} \le \epsilon_3^{\mathbf{q}}$$

The considered triangle is completely outside FS2. We get no contribution to the integral, $I_{ij}(\mathbf{q}) = 0$, from this triangle. The picture we get is the same as in case 4 of the previous section (Of course the drawn Fermi surface in this case has to be FS2!).

2. case
$$\epsilon_1^{\mathbf{q}} \le \mu \le \epsilon_2^{\mathbf{q}} \le \epsilon_3^{\mathbf{q}}$$

Again we first arrange the three energy values to normal order. When this is done this case is very similar to case 2 of the previous section. We compute the intersection points μ_1 and μ_2 . The only difference now is that we have to linearize the new energy $\epsilon^{\mathbf{q}}(x,y)$ (of course again around the lowest energy value $\epsilon_1^{\mathbf{q}}!$), $\epsilon^{\mathbf{q}}(x,y) - \epsilon_1^{\mathbf{q}} = A^{\mathbf{q}}(x-x_1) + B^{\mathbf{q}}(y-y_1)$ with the values for $A^{\mathbf{q}}$ and $B^{\mathbf{q}}$:

$$A^{\mathbf{q}} = \frac{(\epsilon_2^{\mathbf{q}} - \epsilon_1^{\mathbf{q}})(y_3 - y_1) - (y_2 - y_1)(\epsilon_3^{\mathbf{q}} - \epsilon_1^{\mathbf{q}})}{(x_2 - x_1)(y_3 - y_1) - (y_2 - y_1)(x_3 - x_1)}$$
$$B^{\mathbf{q}} = \frac{(x_2 - x_1)(\epsilon_3^{\mathbf{q}} - \epsilon_1^{\mathbf{q}}) - (\epsilon_2^{\mathbf{q}} - \epsilon_1^{\mathbf{q}})(x_3 - x_1)}{(x_2 - x_1)(y_3 - y_1) - (y_2 - y_1)(x_3 - x_1)}$$

Thus the two intersection points are given (similar to previous section) by:

$$\begin{pmatrix} x_{\mu_i} \\ y_{\mu_i} \end{pmatrix} - \begin{pmatrix} x_1 \\ y_1 \end{pmatrix} = \begin{pmatrix} \frac{(\mu_i - \epsilon_1^{\mathbf{q}})(x_{i+1} - x_1)}{\overline{A^{\mathbf{q}}(x_{i+1} - x_1) + B^{\mathbf{q}}(y_{i+1} - y_1)}} \\ \frac{(\mu_i - \epsilon_1^{\mathbf{q}})(y_{i+1} - y_1)}{\overline{A^{\mathbf{q}}(x_{i+1} - x_1) + B^{\mathbf{q}}(y_{i+1} - y_1)}} \end{pmatrix}$$
 (E.9)

with i=1,2. Substituting $A\to A^{\mathbf{q}}$ etc. gives us the same result as before.

The obtained triangle is a triangle that lies in the area that contributes to $I_{ij}(\mathbf{q})$. It is passed to a subroutine that integrates over this triangle.

3. case
$$\epsilon_1^{\mathbf{q}} \le \epsilon_2^{\mathbf{q}} \le \mu \le \epsilon_3^{\mathbf{q}}$$

In this case we linearize the energy $\epsilon^{\mathbf{q}}$ around the corner that has the energy value $\epsilon_3^{\mathbf{q}}$, $\epsilon^{\mathbf{q}}(x,y) - \epsilon_3^{\mathbf{q}} = A^{\mathbf{q}}(x-x_3) + B^{\mathbf{q}}(y-y_3)$. The picture we obtain is similar to the picture we got in case 3 of the previous section. Again using Cramers rule we obtain the crossing points of the two sides. $A^{\mathbf{q}}$ and $B^{\mathbf{q}}$ are given as, $A^{\mathbf{q}} = \frac{(\epsilon_1^{\mathbf{q}} - \epsilon_3^{\mathbf{q}})(y_2 - y_3) - (y_1 - y_3)(\epsilon_2^{\mathbf{q}} - \epsilon_3^{\mathbf{q}})}{(x_1 - x_3)(y_2 - y_3) - (y_1 - y_3)(x_2 - x_3)}$ and $B^{\mathbf{q}} = \frac{(x_1 - x_3)(\epsilon_2^{\mathbf{q}} - \epsilon_3^{\mathbf{q}}) - (\epsilon_1^{\mathbf{q}} - \epsilon_3^{\mathbf{q}})(x_2 - x_3)}{(x_1 - x_3)(y_2 - y_3) - (y_1 - y_3)(x_2 - x_3)}$. The intersection points can be computed with this values as done before. Note that we have to split this area into two triangles, like it is done in case 3 of the previous section.

4. case
$$\epsilon_1^{\mathbf{q}} \le \epsilon_2^{\mathbf{q}} \le \epsilon_3^{\mathbf{q}} \le \mu$$

This is the case where the whole triangle considered is inside FS2. Thus we get a contribution to the integral from the whole triangle. The picture that describes this is similar to the picture we got in case 4 of the previous section. So the coordinates of the triangle are not changed in this case.

Now we have approximated the area that contributes to $I_{ij}(\mathbf{q})$ by small triangles. We have approximated the shaded area of figure E.1 by triangles using the subroutines SELECT1 and SELECT2.

In the next step we integrate each of these remaining triangles over the function described in (E.5).

E.4.3 Integration over a triangle

Only triangles that passed the two subroutines SELECT1 and SELECT2 are passed to this subroutine (INTRES). So every remaining triangle contributes to this integral.

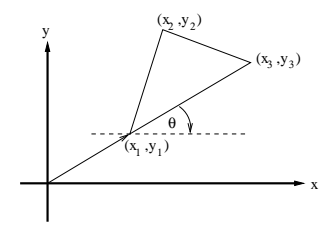


Figure E.11: An arbitrary triangle with the corners already arranged to the order $x_1 \le x_2 \le x_3$. Also the angle of the rotation θ is drawn.

We write down the integral for an arbitrary triangle.

$$I_{ij}(\mathbf{q}) = \int_{\triangle} \frac{dxdy}{\epsilon^{\mathbf{q}}(x,y) - \epsilon(x,y)}$$
 (E.10)

To obtain a reasonable result we linearize the two energies $\epsilon^{\mathbf{q}}$ and ϵ like it is done before. Linearizing around the corner ϵ_1 gives:

$$\epsilon(x,y) = \epsilon_1 + A(x - x_1) + B(y - y_1)$$

$$\epsilon^{\mathbf{q}}(x,y) = \epsilon_1^{\mathbf{q}} + A^{\mathbf{q}}(x-x_1) + B^{\mathbf{q}}(y-y_1)$$

We are interested in the magnitude $\epsilon^{\mathbf{q}}(x,y) - \epsilon(x,y)$ what can be seen in (E.10), so

$$\epsilon^{\mathbf{q}}(x,y) - \epsilon(x,y) = C_1 + C_2(x-x_1) + C_3(y-y_1)$$
 (E.11)

where $C_1 = \epsilon_1^{\mathbf{q}} - E_1$, $C_2 = A^{\mathbf{q}} - A$ and $C_3 = B^{\mathbf{q}} - B$.

It is convenient to arrange the coordinates of the corners so that we obtain for the x-coordinates of the corners $x_1 \leq x_2 \leq x_3$, like it is shown in figure E.11. We have to rotate the triangle with by angle θ (compare to figure E.11) that is given by

$$\tan \theta = \frac{y_3 - y_1}{x_3 - x_1} \tag{E.12}$$

The rotation around the horizontal axis is described by

$$\mathbf{x}' = \begin{pmatrix} \cos \theta & \sin \theta \\ -\sin \theta & \cos \theta \end{pmatrix} \begin{pmatrix} x - x_1 \\ y - y_1 \end{pmatrix}$$

Because of the angle we have chosen above we get the new coordinates of the rotated and translated (by $(-x_1, -y_1)$) triangle as:

$$\mathbf{x}_1' = \begin{pmatrix} 0 \\ 0 \end{pmatrix}$$

$$\mathbf{x}_2' = \begin{pmatrix} x_2' \\ y_2' \end{pmatrix}$$

$$\mathbf{x}_3' = \begin{pmatrix} x_3' \\ 0 \end{pmatrix}$$

with values x'_2, x'_3, y'_2 determined by the rotation and translation. we can write the integral introduced above just by using trigonometric functions $\sin \theta$ and $\cos \theta$. So the linearized energy has the form:

$$\epsilon^{\mathbf{q}}(x,y) - \epsilon(x,y) = A + Bx + Cy \tag{E.13}$$

because x_1 and y_1 are chosen to be 0. Of course we should write x' and y' in the linearized energy above, because we are now integrating over the transformed triangle. Again we can easily compute the energy values at the corners of the triangle. We name the differences in the energy values v_i , i = 1, 2, 3. Equation (E.13) allows us to write:

$$v_1 = \epsilon_1^{\mathbf{q}} - \epsilon_1 = A$$

$$v_2 = \epsilon_2^{\mathbf{q}} - \epsilon_2 = A + Bx_2 + Cy_2$$

$$v_3 = \epsilon_3^{\mathbf{q}} - \epsilon_3 = A + Bx_3$$

with the solution of this equation system:

$$A = v_1$$

$$B = \frac{v_3 - v_1}{x_3}$$

$$C = \frac{(v_2 - v_1) - \frac{x_2}{x_3}(v_3 - v_1)}{v_2}$$

The knowledge of these constants allows us to integrate each triangle. Figure E.12 shows the "new" integral. Now the final integral has the form:

$$I_{ij}(\mathbf{q}) = \int_{\triangle} \frac{dxdy}{A + Bx + Cy}$$
 (E.14)

with the constants A, B, C as described above.

When we divide the triangle into two triangles (triangle 1 and 2 in figure E.12) we get an easy expression for the integral:

$$I_{ij}(\mathbf{q}) = \int_0^{x_2} dx \int_0^{\frac{y_2}{x_2}x} dy \frac{1}{A + Bx + Cy} + \int_{x_2}^{x_3} dx \int_0^{\frac{y_2}{x_2 - x_3}(x - x_3)} dy \frac{1}{A + Bx + Cy}$$
(E.15)

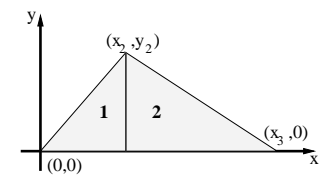


Figure E.12: The rotated and translated triangle. Of course it has the same area as before. We can integrate this triangle easy by dividing it in two triangles, marked as 1 and 2 in the picture.

At this point we have to be careful, because we can obtain singularities when the denominator is equal to zero. Therefore we have to consider different cases.

1. case $v_1 = v_2 = v_3 = v \neq 0$

In this case we get in the denominator only v, because B=C=0 what can be seen in (E.15). The integral becomes:

$$I_{ij}(\mathbf{q}) = \int_0^{x_2} dx \int_0^{\frac{y_2}{x_2}x} dy \frac{1}{v} + \int_{x_2}^{x_3} dx \int_0^{\frac{y_2}{x_2 - x_3}(x - x_3)} dy \frac{1}{v} = \frac{y_2 x_2}{2v} + \frac{y_2}{2v(x_3 - x_2)}(x_3 - x_2)^2 = \frac{y_2 x_3}{2v}$$

2. case $v_1 \neq v_2, v_2 \neq v_3, v_1 \neq v_3, v_1 \neq 0, v_2 \neq 0, v_3 \neq 0$

We consider this case know, because we will use it to consider the next cases. In this case we don't have to fear any singularities in the integrand. Doing the y-integration of (E.15) gives:

$$I_{ij}(\mathbf{q}) = \int_0^{x_2} dx \frac{1}{C} \ln \left| \frac{A + Bx + C\frac{y_2}{x_2}x}{A + Bx} \right| + \int_{x_2}^{x_3} dx \frac{1}{C} \ln \left| \frac{A + C\frac{y_2y_3}{x_3 - x_2} + \left[B - C\frac{y_2}{x_3 - x_2} \right] x}{A + Bx} \right|$$
(E.16)

with A, B, C as showed before. We simplify some terms in the integral using the value of these constants:

 $B+C\frac{y_2}{x_2}=\frac{v_2-v_1}{x_2},\,A+C\frac{y_3x_3}{x_3-x_2}=\frac{x_3v_2-x_2v_3}{x_3-x_2}$ and $B-C\frac{y_2}{x_3-x_2}=\frac{v_3-v_2}{x_3-x_2}$ what simplifies (E.16). It is convenient to split (E.16) into three pieces:

$$I_{1}(\mathbf{q}) = \int_{0}^{x_{2}} dx \frac{1}{C} \ln \left| A + \frac{v_{2} - v_{1}}{x_{2}} x \right|$$

$$I_{2}(\mathbf{q}) = \int_{x_{2}}^{x_{3}} dx \frac{1}{C} \ln \left| \frac{x_{3}v_{2} - x_{2}v_{3}}{x_{3} - x_{2}} + \frac{v_{3} - v_{2}}{x_{3} - x_{2}} \right|$$

$$I_{3}(\mathbf{q}) = \int_{0}^{x_{3}} dx \frac{1}{C} \ln \left| v_{1} + \frac{v_{3} - v_{1}}{x_{3}} x \right|$$

The total integral is thus given by:

$$I_{ij}(\mathbf{q}) = I_1(\mathbf{q}) + I_2(\mathbf{q}) - I_3(\mathbf{q}) \tag{E.17}$$

Be aware of the minus-sign in this equation!

The solution of this integrals leads us to the expression:³

$$I_{1}(\mathbf{q}) = \frac{x_{2}}{v_{2} - v_{1}} (v_{2} \ln|v_{2}| - v_{1} \ln|v_{1}| - (v_{2} - v_{1}))$$

$$I_{2}(\mathbf{q}) = \frac{x_{3} - x_{2}}{v_{3} - v_{2}} (v_{3} \ln|v_{3}| - v_{2} \ln|v_{2}| - (v_{3} - v_{2}))$$

$$I_{3}(\mathbf{q}) = \frac{x_{3}}{v_{3} - v_{1}} (v_{3} \ln|v_{3}| - v_{1} \ln|v_{1}| - (v_{3} - v_{1}))$$

Inserting these three integrals into (E.17) we obtain the final result. Some algebraic calculation gives us:

$$I_{ij}(\mathbf{q}) = x_3 y_2 \left(\frac{v_1 \ln|v_1|}{(v_1 - v_3)(v_1 - v_2)} + \frac{v_2 \ln|v_2|}{(v_2 - v_1)(v_2 - v_3)} + \frac{v_3 \ln|v_3|}{(v_3 - v_1)(v_3 - v_2)} \right)$$
(E.18)

The knowledge of the values of I_1, I_2, I_3 allows us to discuss other cases now.

3. case $v_1 = v_2 = v, v \neq 0, v \neq v_3$

The term $\epsilon^{\mathbf{q}} - \epsilon$ simplifies in the following manner when we insert the values for A, B, C from above:

$$\epsilon^{\mathbf{q}}(x,y) - \epsilon(x,y) = v + \frac{v_3 - v}{x_3} x - \frac{x_2 y_2}{x_3} (v_3 - v) y$$
(E.19)

A integration of the term in (E.19) gives:

$$I_{ij}(\mathbf{q}) = \int_0^{x_2} dx \int_0^{\frac{y_2}{x_2}x} \frac{dy}{v + \frac{v_3 - v}{x_3}x - \frac{x_2 y_2}{x_3}(v_3 - v)y} + \int_{x_2}^{x_3} dx \int_0^{\frac{y_2}{x_2 - x_3}(x - x_3)} \frac{dy}{v + \frac{v_3 - v}{x_2}x - \frac{x_2 y_2}{x_2}(v_3 - v)y}$$

Instead of doing this integrals we insert the values of the v's in the integrals I_1, I_2, I_3 calculated above. Equation (E.17) gives us the value of $I_{ij}(\mathbf{q})$ in this case:

$$I_{ij}(\mathbf{q}) = \frac{y_2 x_3}{v_3 - v} \left[\frac{1}{v_3 - v} \left(v_3 \ln|v_3| - v \ln|v| \right) - \ln|v| - 1 \right]$$
 (E.20)

³The important integral is an integral of the type $\int \ln |A+Bx| dx$. Making the substitution z=A+Bx we obtain: $\int \ln |A+Bx| dx = \frac{1}{B}z \ln z - z = \frac{1}{B}(A+Bx) \ln (A+Bx) - (A+Bx)$

4. case $v_1 = v_3 = v, v \neq 0, v \neq v_2$

We write the difference in energy in the same manner as before. Again we use the three integrals I_1, I_2, I_3 to obtain the correct result for this integral. We obtain the integral:

$$I_{ij}(\mathbf{q}) = \frac{y_2 x_3}{v_2 - v} \left[\frac{1}{v_2 - v} \left(v_2 \ln|v_2| - v \ln|v| \right) - \ln|v| - 1 \right]$$
 (E.21)

5. case $v_2 = v_3 = v, v \neq 0, v \neq v_1$

The last case gives the following integral, written in a more compact way than the integrals before:

$$I_{ij}(\mathbf{q}) = \frac{y_2 x_3}{v_1 - v} \left[\frac{v_1}{v_1 - v} \ln \left| \frac{v_1}{v} \right| - 1 \right]$$
 (E.22)

So we finally computed all integrals we need to get the result of the integral.

References

- [1] Y. Ando and T. Murayama. Nonuniversal power law of the Hall scattering rate in a single-layer cuprate $Bi_2Sr_{2-x}La_xCuO_6$. Phys. Rev. B, 60:6991–6994, 1999.
- [2] N.W. Ashcroft and N.D. Mermin. Solid State Physics. Saunders College, Philadelphia, 1976.
- [3] B.H. Bransden and C.J. Joachain. *Physics Of Atoms And Molecules*. Longman, New York, N.Y., 1983.
- [4] M.-Y. Choi and J.S. Kim. Thermopower of high T_c cuprates. *Electronic Archive*, xxx.lanl.gov, cond-mat/9810101, 1998.
- [5] A.T. Zheleznyak et al. Phenomenological interpretations of the ac Hall effect in the normal state of $YBa_2Cu_3O_7$. Phys. Rev. B, 57:3089–3098, 1998.
- [6] A.T. Zheleznyak et al. Magnetoresistance of $YBaCu_3O_7$ in the "cold spots" model. Phys. Rev. B, 59:207–210, 1999.
- [7] B.Q. Cao et al. Doping dependence of the in-plane resistivity and Hall effect of cuprate superconductors. *Phys. Rev. B*, 62:15237–15240, 2000.
- [8] C. Castellani et al. Thermoelectric power in disordered electronic systems near the Anderson transition. *Phys. Rev. B*, 37:6663–6666, 1988.
- [9] Ding et al. Electronic Excitations in $Bi_2Sr_2Ca_Cu_2O_8$: Fermi Surface, Dispersion, and Absence of Bilayer Splitting. *Phys. Rev. Lett.*, 76:1533–1536, 1996.
- [10] F. Rullier-Albenque et al. Effect of electron irradiation on $Bi_2Sr_2CaCu_2O_8$ and $Bi_2Sr_2CuO_6$ superconductors. Physica C, 254:88–92, 1995.
- [11] G. Kotliar et al. Hall effect and magnetoresistance in copper oxide metals. *Phys. Rev. B*, 53:3573–3577, 1996.
- [12] J.A. Clayhold et al. Two lifetimes in the thermopower of the cuprate metals. Electronic Archive, xxx.lanl.gov, cond-mat/9708125, 1997.
- [13] J.C. Campuzano et al. Direct observation of particle-hole mixing in the superconducting state by angle-resolved photoemission. *Phys. Rev. B*, 53:14737–14740, 1996.
- [14] L. Forro et al. Hall-effect measurements on superconducting and nonsuperconducting copper-ocide-based metals. Phys. Rev. B, 42:8704–8706, 1990.
- [15] M.A. Quijada et al. ab-plane anisotropy in single-domain $Bi_2Sr_2CaCu_2O_8$ high-temperature superconductors. *Physica C*, 235-240:1123–1124, 1994.

- [16] M.R. Norman et al. Phenomenological models for the gap anisotropy of Bi2Sr2CaCu2O8 as measured by angle-resolved photoemission spectroscopy. Phys. Rev. B, 52:615–622, 1995.
- [17] N.L. Wang et al. Crystal growth and anisotropic resistivity of $Bi_2Sr_{2-x}La_xCuO_y$ thin films at various oxygen contents. *Phys. Rev. B*, 54:7449–7454, 1996.
- [18] O.K. Andersen et al. Plane dimpling and saddle-point bifurcation in the band structures of optimally doped high-temperature superconductors: A tight-binding model. *Phys. Rev. B*, 49:4145–4157, 1994.
- [19] R.Jin et al. Normal-state resistivity of superconducting $Bi_{1.95}Sr_{1.65}La_{0.4}CuO_{6+\delta}$ single crystals. *Physica C*, 250:395–402, 1995.
- [20] S. Martin et al. Anisotropic critical current density in superconducting $Bi_2Sr_2CaCu_2O_8$ crystals. Appl. Phys. Lett., 54:72–74, 1989.
- [21] S.A. Sunshine et al. Structure and physical properites of single crystals of the 84-K superconductor $Bi_{2.2}Sr_2Ca_{0.8}Cu_2O_{8+\delta}$. Phys. Rev. B, 38:893–896, 1988.
- [22] T.R.Chien et al. Scaling of the temperature dependent Hall effect in $La_{2-x}Sr_xCuO_4$. Phys. Rev. Lett., 72:2636–2639, 1994.
- [23] Y. Ando et al. Carrier concentrations in $Bi_2Sr_{2-z}La_zCuO_{6+\delta}$ single crystals and their relation to Hall coefficient and thermpower. *Phys. Rev. B*, 61:14956–14959, 2000.
- [24] Y. Zhang et al. Determining the Wiedemann-Franz ratio from the thermal Hall conductivity: Application to Cu and $YBa_2Cu_3O_{6.95}$. Electronic Archive, xxx.lanl.qov, cond-mat/0001037, 2000.
- [25] Y.D. Chuang et al. Reexamination of the Electronic Structure of $Bi_2Sr_2CaCu_2O_{8+\delta}$ and $Bi_2Sr_2Cu_1O_{6+\delta}$: Electronlike Portions of the Fermi Surface and Depletion of the Spectral Weight near \bar{M} . Phys. Rev. Lett., 83:3717–3720, 1999.
- [26] Yoichi Ando et al. Systematic Evolution of the Magnetotransport Properties of $Bi_2Sr_{2-x}La_xCuO_6$ with Carrier Concentration . Jour. Low Temp. Phys., 117:1117–1121, 1999.
- [27] Z. Konstantinovic et al. Temperature dependence of the Hall effect in single-layer and bilayer $Bi_2Sr_2Ca_{n-1}Cu_nO_y$ thin films at various oxygen contents. *Phys. Rev.* B, 62:11989–11992, 2000.
- [28] R. Hlubina and T.M. Rice. Resistivity as a function of temperature for models with hot spots on the Fermi surface. *Phys. Rev. B*, 51:9253–9260, 1995.
- [29] L.B. Ioffe and A.J. Millis. Zone-diagonal-dominated transport in high- T_c cuprates. *Phys. Rev. B*, 58:11631–11637, 1998.
- [30] Y. Kubo. Doping dependence of the thermopower of high- T_c cuprates: Tight-binding band model. *Phys. Rev. B*, 50:3181–3188, 1994.

- [31] G.C. McIntosh and A.B. Kaiser. van Hove scenario and thermopower behavior of the high- T_c cuprates. *Phys. Rev. B*, 54:12569–12575, 1996.
- [32] P.J. Mohr and B.N. Taylor. CODATA recommended values of the fundamental physical constants: 1998. Rev. Mod. Phys., 72:351–495, 2000.
- [33] S.D. Obertelli and J.R. Cooper. Systematics in the thermopower of high- T_c oxides. Phys. Rev. B, 46:14928–14931, 1992.
- [34] N.P. Ong. Geometric interpretation of the weak-field Hall conductivity in twodimensional metals with arbitrary Fermi surface. *Phys. Rev. B*, 43:193–202, 1991.
- [35] D. Pines and P. Noziéres. The Theory Of Quantum liquids, Vol I. W.A. Benjamin, Inc., New York, N.Y., 1966.
- [36] K.G. Sandeman and A.J. Schofield. Measuring anisotropic scattering in the cuprates. *Electronic Archive*, xxx.lanl.gov, cond-mat/0007299 v2, 2000.
- [37] C.M. Varma. Pseudogap Phase and the Quantum-Critical Point in Copper-Oxide Metals. *Phys. Rev. Lett.*, 83:3538–3541, 1999.
- [38] C.M. Varma and E. Abrahams. Effective Lorentz Force due to Small-angle Impurity Scattering: Magnetotransport in High- T_c Superconductors. *Electronic Archive*, xxx.lanl.gov, cond-mat/0011020 v2, 2000.
- [39] Rainer Wesche. High-Temperature Superconductors. Kluwer Academic Publishers, Norwell, Massachusetts, 1998.